UNIVERSITÄT HAMBURG
DEPARTMENT PHYSIK

Interaction of antimicrobial peptides with lipid membranes.

Dissertation zur Erlangung
des Doktorgrades
des Departments Physik
der Universität Hamburg

vorgelegt von
Mária Hanulová
aus
Bratislava

Hamburg
2008

Gutachter der Dissertation:	Prof. Dr. E. Weckert Prof. Dr. R. L. Johnson
Gutachter der Disputation:	Prof. Dr. E. Weckert Prof. Dr. K. Brandenburg
Datum der Disputation:	5. September 2008
Vorsitzender des Prüffungsausschusses:	Dr. Georg Steinbrück
Vorsitzender des Promotionsausschusses:	Prof. Dr. Jochen Bartels
MIN-Dekan des Departments Physik:	Prof. Dr. Arno Frühwald

Abstract

Antimicrobial peptides are part of the immune system of most living creatures. They are able to kill invading bacteria and at the same time, they do not attack the host cells. Such selectivity in the peptide action is usually explained by the difference in the lipid composition of the cell membranes. In studies on the mechanism of action of antimicrobial peptides, the bacterial membranes are usually represented by negatively charged lipids like phosphatidylglycerols while the mammalian membranes by zwitterionic lipids like phosphatidylcholines. However, cell membranes contain a wide variety of lipid species which certainly contribute to the lipid-peptide interaction.
This study aims to investigate the difference in the interaction of antimicrobial peptides with two classes of zwitterionic peptides, phosphatidylethanolamines (PE) and phosphatidylcholines (PC). The structural difference between them is in the headgroup, with PE having three hydrogens bound to the nitrogen while PC three methyl groups. Phosphatidylethanolamines have been used in very few lipid-peptide studies up to date. They are an important component of bacterial membranes and unlike PC, they form non-lamellar hexagonal phases. Further experiments were performed on model membranes prepared from specific bacterial lipids, lipopolysaccharides (LPS) isolated from *Salmonella minnesota*. Lipopolysaccharides form the outer layer of the asymmetric outer membrane of Gram negative bacteria.
Two widely studied peptides were chosen for this study, alamethicin isolated from the fungus *Trichoderma viridae* and melittin isolated from bee venom. Both exhibit antimicrobial and hemolytic activity and their crystal and membrane-associated structure is an α-helix with a bend around Pro14. Alamethicin forms voltage-dependent membrane channels. Melittin causes vesicle leaking and in some cases forms transmembrane channels.
The structure of the lipid-peptide aqueous dispersions was studied by small- and wide-angle X-ray diffraction during heating and cooling from 5 to 85°C. The lipids and peptides were mixed at lipid-to-peptide ratios 10-10000 (POPE and POPC) or 2-50 (LPS). All experiments were performed at synchrotron soft condensed matter beamline A2 in Hasylab at Desy in Hamburg, Germany. The phases were identified and the lattice parameters were calculated.
Alamethicin and melittin interact in similar ways with the lipids. Both insert between the lipid headgroups in the polar-apolar interface and consequently change the average headgroup to chains cross section ratio. Insertion in the polar-apolar interface is favoured by the amphipathic structure of both pep-

tide helices. The structures induced in the lipid membranes by the insertion of the peptide are the outcome of the competition between the curvature elastic energy and packing frustration. Pure POPC forms only lamellar phases. The insertion of a peptide between the headgroups increases the curvature stress although not enough to break up the lamellar structure. To relieve the stress, bilayers become undulated and the mean bilayer spacing increases. POPE forms lamellar phases at low temperatures that upon heating tranform into a highly curved inverse hexagonal phase. Insertion of the peptide induced inverse bicontinuous cubic phases which are an ideal compromise between the curvature stress and the packing frustration.
Melittin usually induced a mixture of two cubic phases, Im3m and Pn3m, with a ratio of lattice parameters close to 1.279, related to the underlying minimal surfaces. They formed during the lamellar to hexagonal phase transition and persisted during cooling till the onset of the gel phase. The phases formed at different lipid-to-peptide ratios had very similar lattice parameters. Epitaxial relationships existed between coexisting cubic phases and hexagonal or lamellar phases due to confinement of all phases to an onion vesicle, a vesicle with several layers consisting of different lipid phases. Alamethicin induced the same cubic phases, although their formation and lattice parameters were dependent on the peptide concentration. The cubic phases formed during heating from the lamellar phase and their onset temperature decreased with increasing peptide concentration. At low alamethicin concentrations, both Im3m and Pn3m formed and coexisted with the hexagonal phase. As the concentration of the peptide increased, the amount of hexagonal phase and Im3m decreased, until only Pn3m remained. Same epitaxial relationships were observed as for POPE with melittin.
Lipopolysaccharides (LPS), strains R595 and R60 and their "endotoxic principle" lipid A, were studied. Longer sugar-chain LPS R60 and lipid A form cubic phases and LPS R595 lamellar phases at the employed water content around 95%. Melittin induced several lamellar phases and a hexagonal phase in all LPS varieties. Further experiments are necessary to understand the mechanism of interaction of LPS and melittin.

Zusammenfassung

Antibakterielle Peptide sind ein Baustein des Immunsystems. Diese Peptide können Bakterien abtöten, ohne dabei die Zellen des Organismus zu beschädigen. Die Selektivität ihrer Wirkung beruht auf den verschiedenen Lipidzusammensetzungen der Zellmembranen. Für experimentelle Zwecke werden tierische Membranen am häufigsten mit neutralen Lipiden (wie Phosphatidylcholin) und bakterielle Membranen mit negativen Lipiden (wie Phosphatidylglycerol) eingesetzt. Die Zellmembranen bestehen jedoch aus vielen verschiedenen Lipidtypen, wobei alle zur Lipid-Peptid Wechselwirkung beitragen.
In dieser Arbeit wurden die unterschiedlichen Wechselwirkungen von antibakteriellen Peptiden mit zwei neutralen Lipidgruppen, Phosphatidylcholinen (PC) und Phosphatidylethanolaminen (PE), untersucht. Diese beiden Lipidgruppen unterscheiden sich strukturell durch ihre Kopfgruppe. Bei PC sind drei Methylgruppen und bei PE drei Wasserstoffe an den Stickstoff gebunden. An PE wurden bisher nur wenige Experimente zur Lipid-Peptid Wechselwirkung durchgeführt. PE sind ein wichtiger Bestandteil von bakteriellen Zellmembranen. Im Gegenteil zu PC bilden sie nichtlamellare hexagonale Phasen. Weitere Experimente wurden mit Lipopolysacchariden (LPS) durchgeführt, die aus der Membran von *Salmonella minnesota* isoliert wurden. Lipopolysaccharide bilden die Aussenseite der äusseren Membran gramnegativer Bakterien.
Für diese Arbeit wurden zwei bereits gut charakterisierte Peptide ausgewählt, Alamethicin aus dem Pilz *Trichoderma viridae* und Melittin aus Bienengift. Beide wirken antibakteriell und hämolytisch. Im kristallinen Zustand liegen beide Substanzen in einer gebeugten α-Helix vor. Alamethicin bildet spannungsabhängige Kanäle in Lipidmembranen. Melittin erhöht die Permeabilität der Membranen und bildet nur in manchen Fällen Kanäle.
Die Struktur der Lipid-Peptid Membranen wurde mit Hilfe der Kleinwinkelstreuung im Temperaturbereich von 5 bis 85°C bestimmt. Das Peptid-Lipid Verhältnis wurde von 1/10 bis 1/10000 (für POPC - palmitoyloleoyl phosphatidylcholin und POPE - palmitoyloleoyl phosphatidylethanolamin) und von 1/2 bis 1/50 (für LPS) variiert. Die Experimente wurden am Messplatz A2 am Hasylab, Desy in Hamburg durchgeführt. Aus den Beugungsbildern wurden die vorliegenden Lipidphasen und Gitterparameter bestimmt und im Anschluss Phasendiagramme konstruiert.
Die Wechselwirkungen von Alamethicin und Melittin mit Lipiden sind gle-

ichartig. Beide lagern an den Kopfgruppenbereich der Membran an, der Grenze zwischen dem polaren und apolaren Membranbereich, was der amphiphilen Struktur der Peptidhelices entspricht. Der Einbau der Peptide in die Membran verändert deren Struktur. Diese ist bestimmt durch die elastische Krümmungsenergie (curvature elastic energy) und die entgegenwirkende Packungsfrustration (packing frustration) der Moleküle. POPC bildet nur lamellare Phasen. Der Einbau der Peptide erhöht die elastische Spannung, jedoch nicht stark genug, um die lamellare Struktur aufzubrechen. Um die elastische Spannung zu verringern, nehmen die Membranen eine wellenförmige Deformation an. POPE bildet bei niedrigen Temperaturen lamellare Phasen, die sich durch Erwärmen in nichtlamellare hexagonale Phasen mit einer hohen Krümmung umwandeln. Das Einfügen der Peptide führt zur Bildung von zwei bikontinuierlichen kubischen Phasen, welche einen optimalen Ausgleich zwischen Krümmungsspannung und Packungsfrustration darstellen.
Normalerweise bilden die Lipidmembranen mit Melittin zwei verschiedene kubische Phasen, Pn3m und Im3m. Das Verhältnis ihrer Gitterparameter beträgt annähernd 1.279. Dieser Wert ergibt sich aus den zu Grunde liegenden Minimalflächen. Die kubischen Phasen traten während des lamellar-hexagonalen Phasenübergangs auf und blieben beim Abkühlen bis zum Einsetzen der Gelphase bestehen. Trotz verschiedener Peptidkonzentrationen weisen die kubischen Phasen sehr ähnliche Gitterparameter auf. Zwischen den koexistierenden kubischen, hexagonalen und lamellaren Phasen treten mehrere Epitaxien auf. Diese wurden ebenfalls bei Membranen mit Alamethicin beobachtet. Der Grund hierfür ist der Einschluss aller Phasen in demselben Liposom, dem sogenannten Zwiebelliposom (onion vesicle). Dieses enthält mehrere Schichten aus unterschiedlichen Phasen.
Lipidmembranen mit Alamethicin bilden dieselben kubischen Phasen, deren Gitterparameter jedoch von der Peptidkonzentration abhängig sind. Die kubischen Phasen bilden sich hier aus der lamellaren Phase. Die Temperatur des Phasenübergangs und der relative Anteil jeder Phase ist ebenfalls von der Peptidkonzentration abhängig.
Zudem wurden Lipopolysaccharide aus den bakteriellen Stämmen R595 und R60 und der Lipidanker Lipid A untersucht. LPS R60 und Lipid A bilden kubische Phasen und LPS R595 lamellare Phasen. Melittin hat die Bildung von verschiedenen lamellaren und einer hexagonalen Phase bewirkt. Weitere Untersuchungen sind nötig, um den Mechanismus der Wechselwirkung zu verstehen.

Contents

List of Figures

Chapter 1

Introduction

The first antimicrobial and cell lytic peptides were isolated about 40 years ago [1]. Now, hundreds of natural or "designer" sequences are known, listed in the Antimicrobial Sequences Database of the University of Trieste. Natural antimicrobial or lytic peptides form part of the immune system of organisms where they act against invader cells by perturbing the integrity of their cell membranes. Many attempts have been made to unravel the mechanism of action of these peptides. The goal is to understand the details of the interaction and to design peptides that could replace conventional antibiotics. A perfect antimicrobial peptide drug should act selectively on bacterial cell membranes, and not attack the host cell membranes.
Antibacterial peptides destroy the integrity of bacterial cell membranes. Their action is not bound to a specific protein receptor in the membrane, as with conventional antibiotics, but rather depends on the lipid composition of the cell membrane. This makes it difficult for the bacteria to develop resistance, because mutating the membrane composition is an immensely complicated task compared to the mutation of a single membrane protein receptor. On the other hand, the antibacterial peptides attack only the intruder bacterial membranes and not the host animal or plant membranes. This selectivity lies in the differences in the membrane lipid composition of different species. To understand the basis of the selectivity of the antibacterial activity, we need to study the interaction of antibacterial peptides with a variety of lipid species. The usual lipids that researchers have previously used to highlight the differences between bacterial and animal membranes are charged lipids like phosphatidylglycerols (PG) and neutral lipids like phosphatidylcholines (PC). In this study, two neutral lipids were

chosen, palmitoyl-oleoyl phosphatidylcholine (POPC) and palmitoyl-oleoyl phosphatidylethanolamine (POPE), to investigate the differences in the interaction with antimicrobial peptides inside this lipid category. A specific bacterial lipid isolated from the bacterium *Salmonella minnesota* was also studied.

POPE is representative for bacterial membrane lipids and POPC for mammalian membrane lipids. A large part of the thermal phase diagram of POPE can be studied between 0 and 100°C. Although the measurements were performed at non-physiological temperatures, the results are applicable to real cell membranes. POPE is a member of the category of monounsaturated phosphatidylethanolamines. The lipids in this class have the same headgroup and go through the same phases, but have different phase transition temperatures depending on the composition of their hydrocarbon chains. The mechanism of interaction of the peptides with this class of lipids should be the same. POPC was chosen as a complementary lipid to POPE. The whole phase diagram could not be recorded because measurements below 0°C, where the POPC gel-fluid transition occurs, were not possible. However, the differences in the lipid-peptide interaction between the two lipid classes, the phosphatidylethanolamines and the phosphatidylcholines, could be identified.

The peptides melittin and alamethicin used in this study are commercially available and have been extensively investigated. The positions and conformations of the peptides in the membranes and their action on different kinds of lipids are described in the literature. Melittin is a model for amphipathic helical antimicrobial peptides and for the membrane penetrating and curvature inducing peptides. The results from the interaction of melittin and alamethicin with POPE and POPC in this study form the basis for comparison with studies on newly synthesized peptides with similar characteristics.

Lipid membranes, the factors that determine their shape, peptides, peptide-membrane interactions and sample preparation are described in Chapter 2. The measurements are presented in Chapter 3 with particular emphasis on the influence of the peptides on the lipid phase diagrams. The conclusions and an outlook are summarized in Chapter 4.

Chapter 2

Membranes and peptides

2.1 Lipid membranes

2.1.1 Lipid molecules

Lipid molecules come in many kinds and shapes; nevertheless, they all share an important property, amphiphilicity. Every lipid is composed of a hydrophilic (polar, liking water) head and a hydrophobic (apolar, not liking water) chain. This structure governs the interaction of lipids with water and proteins and promotes the formation of lipid membranes of various shapes. In this thesis, three phospholipids and three lipopolysaccharides are investigated. In general, phospholipids have two hydrocarbon chains and one headgroup joined by a glycerol backbone. Three monounsaturated phospholipids were chosen for the present work. Palmitoyl-oleoyl phosphatidylcholine (POPC) is typical for animal cell membranes, and palmitoyl-oleoyl phosphatidylethanolamine (POPE) and palmitoyl-oleoyl phosphatidylglycerol (POPG) are found mainly in bacterial cell membranes (Fig. 2.1, 2.2, 2.3). They have the same chains, one 16 carbons long saturated and one 18 carbons long unsaturated between the carbon positions 9 and 10, but the headgroups differ. The only difference between POPC and POPE is that POPC has three methyl groups attached to the nitrogen while POPE has three hydrogens. POPG does not have an amino group in the head, but two OH groups and therefore bears a negative charge at physiological pH.
Lipopolysaccharides (LPS) form the outer layer of the asymmetric outer membrane of the Gram-negative bacteria, a class of bacteria with two cell membranes [2]. The inner layer is formed by phospholipids [3]. Melittin ex-

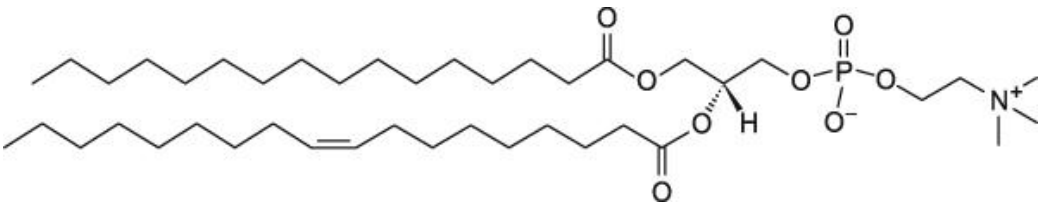

Figure 2.1: 1-Palmitoyl-2-Oleoyl-sn-Glycero-3-Phosphocholine (POPC).

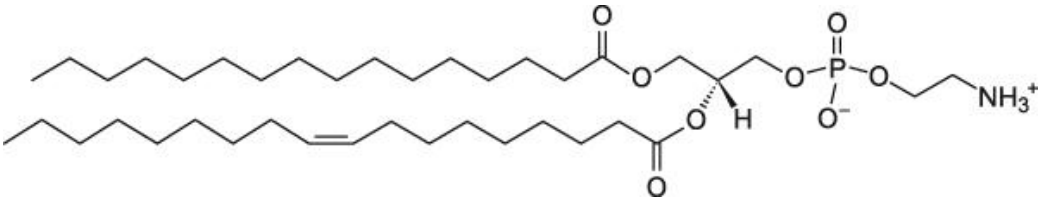

Figure 2.2: 1-Palmitoyl-2-Oleoyl-sn-Glycero-3-Phosphoethanolamine (POPE).

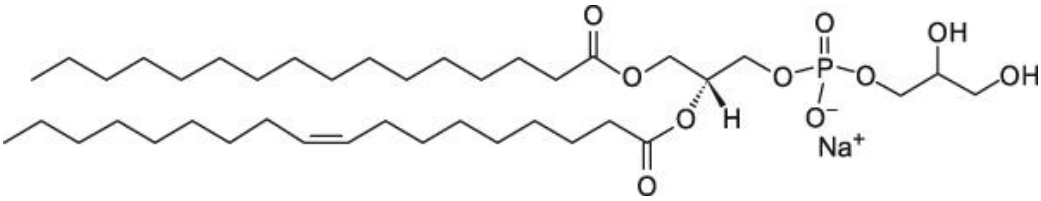

Figure 2.3: 1-Palmitoyl-2-Oleoyl-sn-Glycero-3-[Phospho-rac-(1-glycerol)] (Sodium Salt) (POPG).

hibits antibacterial activity against these bacteria. The bactericidal activity is the result of the lysis of the inner cytoplasmic membrane, so melittin must overcome the LPS membrane first. In general, a lipopolysaccharide consists of 5 to 7 hydrocarbon chains and a large sugar headgroup. The size of the head depends on the microbial strain.
Two different lipopolysaccharides from *Salmonella minnesota*, strains R60 and R595 and their "endotoxic principle" lipid A, were studied. The structure is shown in Fig. 2.4. All molecules have seven hydrocarbon chains and the size of the sugar headgroup grows from lipid A to LPS R60.

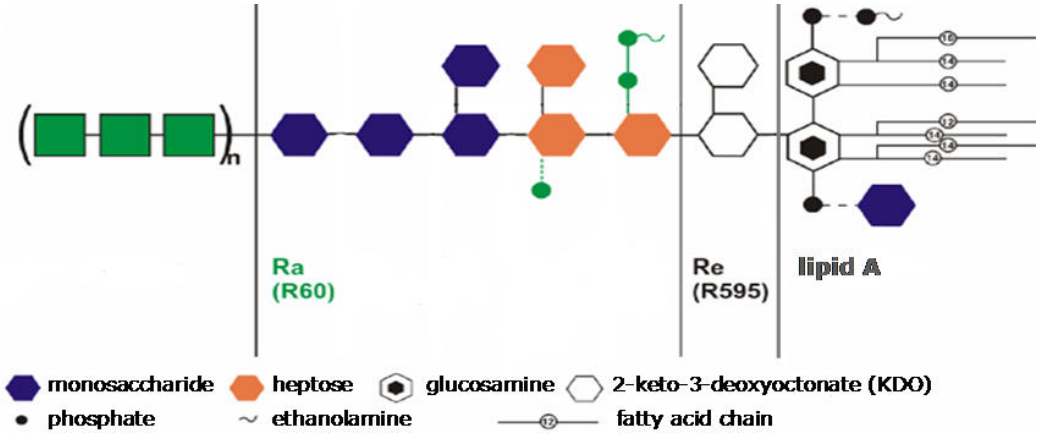

Figure 2.4: Structure of LPS. Modified from [4].

2.1.2 Forces that shape lipid membranes

Lipids dispersed in water form membranes - supramolecular structures in which the polar parts of the lipids are in contact with water while the apolar parts are hidden from it. This process, called self-assembly, is driven by the hydrophobic interaction. The shape of the membranes is given by the geometric packing properties of the molecules and resulting intramembrane forces. The spatial arrangement of membranes is influenced by the intermembrane forces - the attractive van der Waals force and repulsive hydration, fluctuation and, in case of charged lipids, also electrostatic forces.
The shape of one bilayer membrane can be described by the membrane curvature of the two monolayers forming it, or rather by the curvature of the polar-apolar interface of each monolayer. This surface is close to the neutral

surface, a surface whose area does not change upon bending the monolayer. We distinguish two types of curvatures, mean and Gaussian:

- mean curvature $H = (c_1 + c_2)/2$
- Gaussian curvature $K = c_1 c_2$

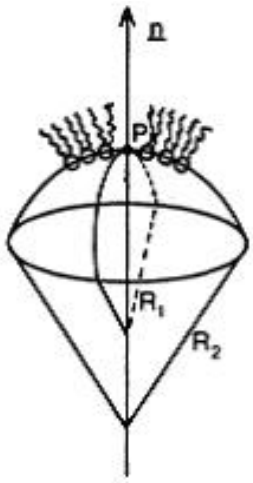

Figure 2.5: Principal radii of curvature [5].

where $c_1 = 1/R_1$ and $c_2 = 1/R_2$ are two principal curvatures of the interface (Fig. 2.5). By convention, a monolayer with positive mean curvature is curved towards the lipid chains. Surfaces with positive Gaussian curvature or elliptic surfaces are closed shells. In the lipid world, these are micelles. Surfaces with zero Gaussian curvature are called parabolic. Lamellar and 2D hexagonal phases belong to this family. Finally, the hyperbolic surfaces possess a negative Gaussian curvature. The saddle surfaces which construct the bicontinuous cubic phases have this property. To change the mean curvature of a monolayer, it is necessary to bend it, but no stretching is required. To change the Gaussian curvature, stretching of the surface is required. The curvature of the membrane polar-apolar interface arises from intramembrane forces (Fig. 2.6). The thermal *cis-trans* rotation of the C-C bonds of the lipid chains imparts momentum to neighbouring molecules and results in chain pressure. The interfacial pressure arises from the close packing of the lipids in an effort to minimize the hydrocarbon-water contact area. The headgroup pressure is the sum of outward pressures due to steric,

hydration and electrostatic interactions and inward pressure from hydrogen bonding. The final shape of a lipid bilayer is the result of the balance between the curvature elastic energy and the packing frustration [6]. A general

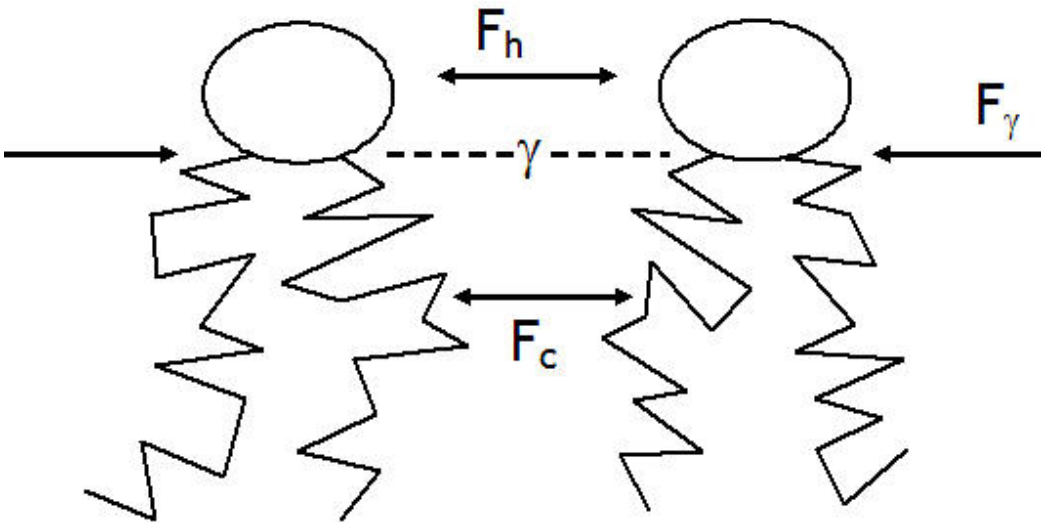

Figure 2.6: Lateral pressure in a lipid monolayer. F_c - chain pressure, F_h - headgroup pressure, F_γ - interfacial pressure [5].

lytropic phase diagram is shown in Fig. 2.7. A thermotropic phase diagram may contain the phases depicted here depending on the lipid type. Lamellar phases divide into several subtypes (subgel, gel, fluid, ripple) according to the temperature-dependent conformation of the lipid chains. In general, PC form only lamellar phases, while phosphatidylethanolamines (PE) lamellar phases at low and hexagonal phases at higher temperatures.

2.1.3 Lamellar phases

Lamellar structures are an arrangement of evenly spaced plane lipid bilayers separated by water layers. The most common are multilamellar liposomes, a series of closed membrane shells. The diameter of the liposomes is much larger than the thickness of one bilayer (micrometers vs. a few nanometers), so locally the bilayers can be considered flat. A special case is a unilamellar liposome with only one bilayer. We distinguish between gel and fluid lamellar phases. Gel phases occupy the low temperature region of the phase diagram.

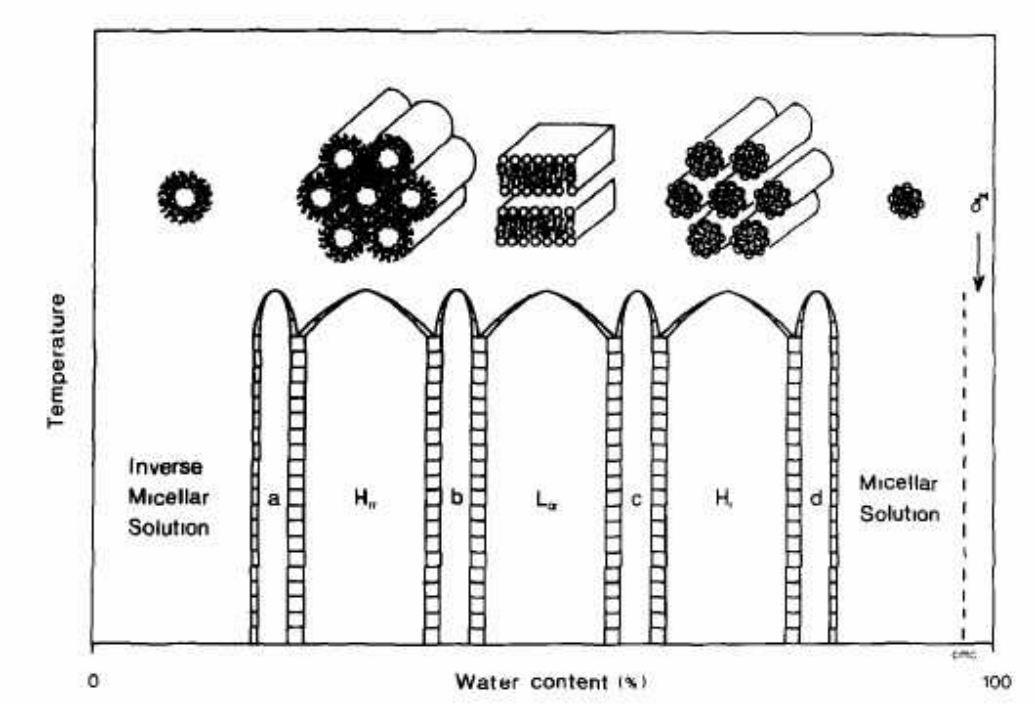

Figure 2.7: Hypothetical lipid/water binary phase diagram. Regions denoted a, b, c and d contain intermediate phases, many of which are cubic. Reproduced from [6].

The C-C bonds of the lipid chains are in the *trans* conformation and consequently the chains are extended and quite rigid. They are arranged on a hexagonal lattice while the headgroups are disordered. Molecules cannot freely diffuse within the plane of the bilayer and chain rotation is hindered, occuring at a timescale of about 100 μsec. In the L_β gel phase, the chains are parallel to each other, with a mean cross-sectional area of $\sim$20 Å^2.
At higher temperatures, the lipid chains melt, the number of *gauche* isomers increases and the bilayer turns into the fluid lamellar state, the L_α phase. A single g^+tg^- (*trans-gauche-trans*) kink reduces the chain length by 0.125 nm, the projected length of one CH_2 group [7]. The chain cross section increases to $\sim$21 Å^2 and the molecular interfacial area expands by 15-30%. Consequently, the bilayer gets thinner. At the same time, more water penetrates in between the bilayers. Whichever of these two processes prevails, determines the bilayer spacing. Usually, it becomes smaller compared to the gel phase. The 2D ordering of lipid chains within one bilayer is lost and lipid molecules diffuse rapidly within the plane of the bilayer (diffusion coefficient $D_{trans} = 10^{-11}$ m^2/s).

2.1.4 The inverse hexagonal phase

Packing of lipid molecules into a lamellar phase requires similar cross sections of headgroups and chains. With rising temperature, the number of *gauche* isomers in the lipid chains rises and the chain mobility increases. This increases the mean chain cross section, creates lateral stress in the chain region and forces the molecules to move farther apart, so increasing the chance of unfavourable contacts of the hydrophobic membrane interior with water. After reaching a critical point, both monolayers constituting the bilayer curve towards the water in order to reduce the effective cross section for headgroups and create more space for the chains. The curvature is incompatible with bilayer packing, as it creates energetically unfavourable voids in the membrane interior, and the membranes transform into non-lamellar phases. This never happens in POPC, whose overall molecular shape is cylindrical. Moreover, POPC headgroups form hydrogen bonds with water, which increases the overall phase hydration, lowers the temperature of the gel-fluid transition and prevents the formation of non-lamellar phases. At very high temperatures, the bilayers start to undulate and the interlamellar correlations become weaker. On the other hand, POPE has an intrinsically smaller headgroup cross section than POPC, making the molecular shape similar to

a truncated cone, and the heads form hydrogen bonds directly to each other. An inverse hexagonal phase (H_{II}) evolves in POPE at high temperatures - cylindrical micelles arranged on a hexagonal lattice. The micelles are not of equal length, so the phase has only a 2D symmetry. Considering a circular cross section of the micelles, a hexagonal phase still has some frustration in the chain packing, as some chains have to be stretched more than others to fill the voids. To relieve this tension, the polar-apolar interface might deform from a circle to a hexagon [6].

2.1.5 Bicontinuous cubic phases

Other non-lamellar phases able to relieve the curvature stress created in the bilayers upon heating are bicontinuous cubic phases (bc phases). They can be viewed as a continuous network of membrane tubes filled with water (or vice versa). Taking into account the similarity of the dimensions of the tube diameters and the tube lengths, it can be seen that the tube network is indeed constructed from saddle surfaces (tube junctions) (Fig. 2.8). These "saddle membranes" are drapped on minimal surfaces, surfaces with a zero mean and a negative Gaussian curvature, as $c_1 = -c_2$. The Gaussian curvature is most negative at the saddle point and increases smoothly to zero at the apices. In the inverse bc phases, the centre of the bilayer coincides with the minimal surface. In the normal bc phases, it is the centre of the water channel.
In the inverse phases, the head-chain and lipid-water interfaces can lie on planes parallel to the minimal surfaces or on planes with the same curvature as the minimal surface. In the former case, the bilayer has equal thickness everywhere, but the cross-sectional area per molecule changes along the bilayer normal. For cubic phases with a large lattice parameter compared to the bilayer thickness, these two surfaces are practically identical. The area of a minimal surface is always greater than the area of planes parallel to it. Consequently, the monolayers drapped on it have net negative curvature. Cubic phases are therefore adopted by systems with headgroup cross section smaller than chain cross section [5].
Unlike the lamellar or hexagonal phases, bc phases are optically isotropic and very viscous. Three bc phases have been found until now in lipid or surfactant mixtures: Ia3d, Pn3m and Im3m, also known as Q^{230}, Q^{224} and Q^{229}, respectively (Fig. 2.9). Ia3d is a system of two interwoven mirror-image networks of tubes connected three-by-three, Pn3m one network of tubes connected four-by-four and Im3m one network of tubes connected six-by-six. The cor-

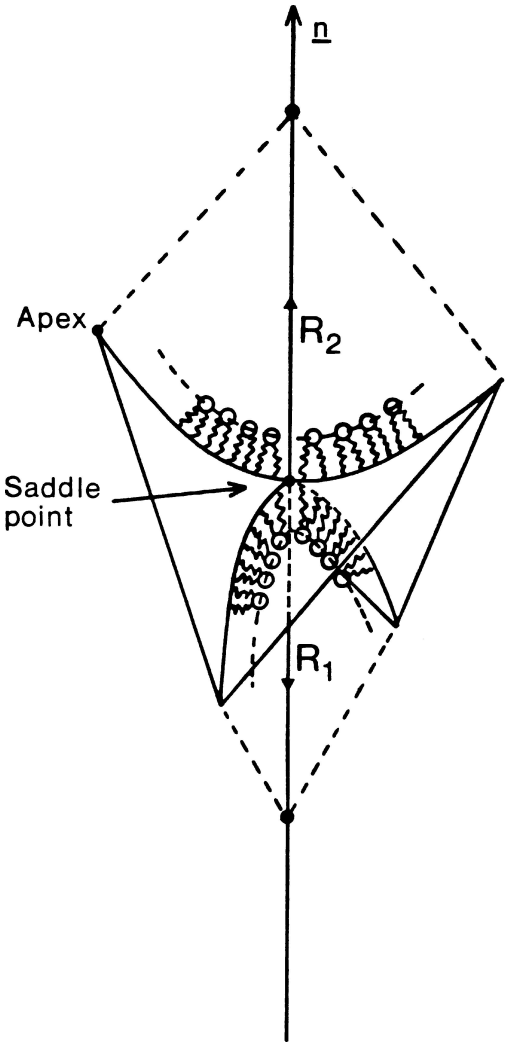

Figure 2.8: Saddle surface with a membrane draped over as in an inverse bicontinuous cubic phase [6]. Both monolayers are curved towards water.

responding minimal surfaces are Schoen's gyroid (G) for Ia3d, Schwarz's D surface for Pn3m and Schwarz's P surface for Im3m. The underlying minimal surfaces are related by the Bonnet transformation. They can be tranformed into each other by bending only, so the Gaussian curvatures are preserved in the process. The energy cost of such a transformation is very low. Several cubic-cubic phase transitions involving little enthalpy were observed. Nevertheless, it does not seem probable that the Bonnet transformation occurs in real lipid membranes, as it involves unphysical layer self-intersection. Sadoc and Charvolin [8] proposed that these transitions could occur by stretching apart the nodes of the structures, so creating, for instance, two four-fold nodes in Pn3m from one six-fold node in Im3m.

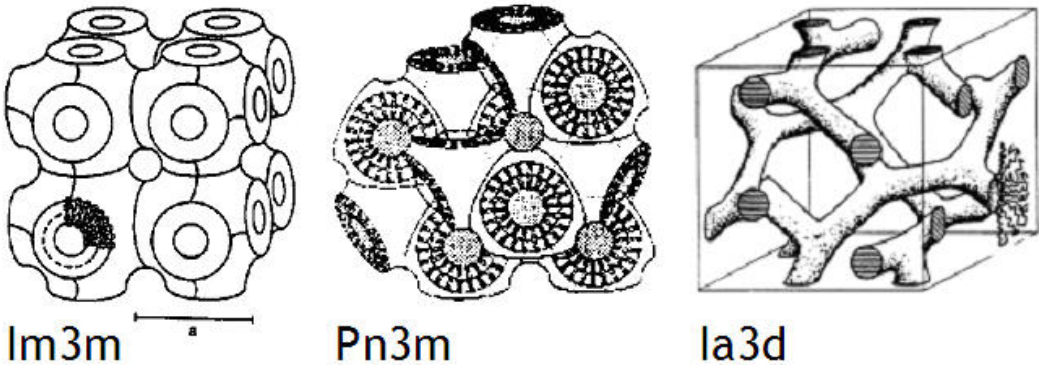

Figure 2.9: Structures of the bicontinuous cubic phases [6].

2.2 Antimicrobial peptides

Antimicrobial peptides are small, mostly amphipathic peptides with the ability to kill bacterial cells. They are part of the immune system of living creatures which use them as a powerful weapon against bacteria. Most of them are effective at μM concentrations [1]. They are a potential replacement for conventional antibiotics to which pathogenic bacteria quickly develop resistance. The advantage of antimicrobial peptides over conventional antibiotics is their nonspecific mode of action. They do not cause cell death by acting on a specific cell receptor, but through disruption or perforation of the cell membrane.

2.2.1 Melittin

One of the most studied antimicrobial peptides is melittin, a peptide isolated from bee venom. In addition to being antimicrobial, it is also highly hemolytic and so unsuitable for use as a drug, although several derivatives with suppressed lytic activity have been developed [9]. Moreover, it represents a model for antimicrobial peptides and also for α-helices of membrane penetrating peptides or curvature inducing peptides. The amino acid sequence is GIGAVLKVLTTGLPALISWIKRKRQQ-NH_2 [10]. The crystal structure solved by Terwilliger in 1982 is an α-helix with a bend around Pro14 (residues 11-15). The axes of 1-10 and 16-26 helices intersect at 120° [11, 12]. The crystal structure coloured according to hydrophobicity is shown in Fig. 2.10. Melittin assumes a random coil conformation in dilute aqueous solu-

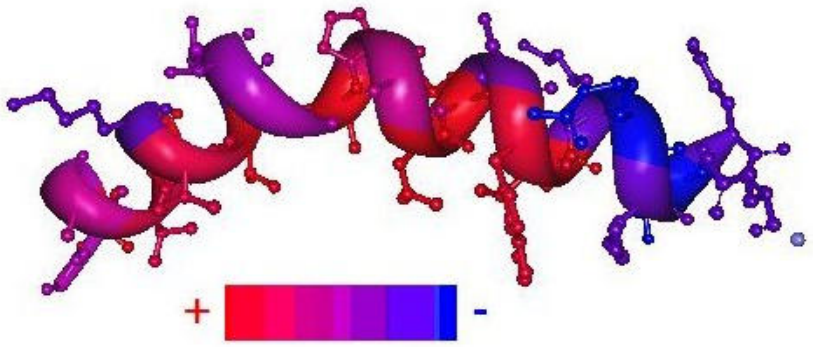

Figure 2.10: Crystal structure of melittin coloured according to hydrophobicity. Hydrophobicity increases from blue to red. [13]

tions and upon increasing the peptide or salt concentration aggregates into a tetramer formed by four α-helices. Melittin also folds into a helix on interaction with lipid membranes, the helix being somewhat more open than in the crystal, with an angle of $\sim$160° [14]. The arrangement of amino acids in the helix makes the structure amphipathic with the hydrophobic face inside the bend and the hydrophilic face on the outside (Fig. 2.11). This facilitates the localization of melittin on polar-apolar interfaces. Melittin bears six positive charges at physiological pH which in the helix add up to an effective charge +2.2 (number based on Gouy-Chapman analysis of binding isotherms). Melittin's hydrophobicity is H_c = -0.086 and the hydrophobic

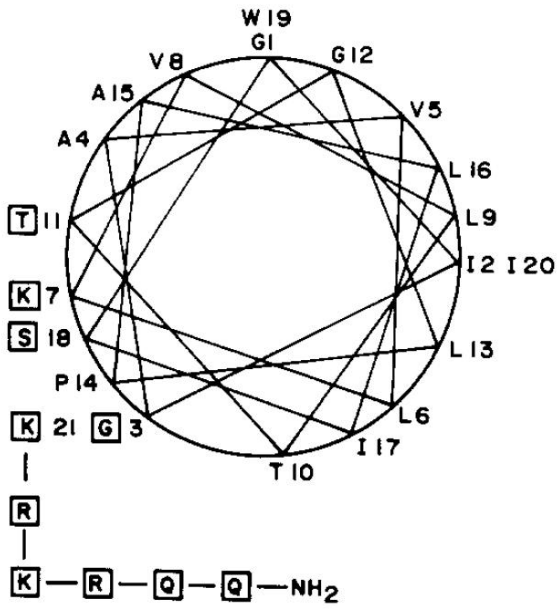

Figure 2.11: Helical wheel projection of the melittin helix - projection along the helix axis. Polar residues are boxed [1].

moment $\mu = 0.224$ [15]. The high hydrophobic moment seems to be responsible for the membrane activity, as active melittin analogs with lysine at position 7 replaced by another amino acid had a higher μ than inactive ones. Getting rid of the helix bend by replacing Pro14 by alanine reduces the hemolytic activity 2.5-fold [9]. Asthana *et al.* identified a leucine zipper motif on the hydrophilic face of the helix which may be responsible for the lytic activity of melittin [16].

2.2.2 Interaction of melittin with phospholipid membranes

Melittin associates with lipid membranes within milliseconds and the release of the vesicle content occurs within minutes [17]. The strongest binding and deepest penetration into the membrane was observed with anionic lipids and surfactants, weaker binding with neutral and zwitterionic and virtually no binding for positive ones. In all cases, melittin was found at the polar-apolar interface of the micelles [18]. It has been shown that melittin binds in lesser

extent to lipid membranes containing cholesterol as compared to cholesterol-free membranes [17]. Reported partition coefficients are on the order of a few mM (3.7 mM^{-1} for DPPC[1], 2.1 mM^{-1} for POPC [19], 4.6×10^{-5} for EYPC [15]). The association of melittin with phospholipid membranes was studied with phosphatidylcholines (PC), phosphatidylethanolamines (PE) and phosphatidylglycerols (PG). Most data is available on PCs. Below is a short overview of the lipid-melittin studies with a variety of techniques. Most studies used lipids from the zwitterionic and the charged category, without further distinguishing between the type of the headgroups and the chains, sometimes not even paying attention to the state of the lipid (gel or fluid). Many studies were done with small unilamellar vesicles, oriented membranes or at partial hydration, and melittin was often mixed with the lipid in an organic solvent. All these conditions are far from that of a real cell. Small unilamellar vesicles have a very high curvature which can affect the interaction with ligands [21]. Oriented membranes allow for the reconstruction of the electron density of the membranes, but in this state the phase transitions into non-lamellar phases are not possible. A hydration lower than full hydration affects the orientation of the melittin helix in the membrane [20]. Relatively high lipid to peptide ratios (L/P) were used in many studies.
In a spin-label ESR study, maximum perturbation was reached at L/P = 60 for DMPC membranes and the chain mobility was increased. The bilayer structure was preserved at all lipid to peptide ratios from 3 to 100 [22]. Chain ordering and a decrease in motional rates accompanied by a surface pressure increase was seen in DPPC monolayers [23]. In the same study, chain ordering was seen in bulk DPPC at room temperature. Incorporated into oriented DOPC bilayers, 5 mol% of melittin did not affect the mosaic spread of the membranes, which is a measure of the macroscopic order [24]. A Förster resonance (FRET) spectroscopy study shows that melittin is monomeric up to L/P = 200. An increasing concentration of melittin causes progressive membrane thinning in DOPC oriented membranes at 98% humidity, as seen by X-ray diffraction [25]. Melittin caused fusion of sonicated DPPC vesicles. During progressive addition of melittin to a solution of sonicated DPPC vesicles, the turbidity of the solution started to increase at L/P = 333 and reached maximum at L/P = 24. After that, it decreased again [19]. Melittin and its hydrophobic fragment (amino acids

[1]For full names of the lipids, please refer to the List of abbreviations in Appendix A, for the structures to Appendix B.

1 to 19) maintained an α-helical conformation in both gel and fluid DMPC multilayer dispersions, as seen by IR spectroscopy. The hydrophilic fragment, on the other hand, was a β-sheet with some random coils [26]. An infrared reflection-absorption spectroscopy (IRRAS) study of melittin in a DPPC monolayer on water showed that melittin conformation in monolayers and bilayers may differ [23]. The amide I frequency of melittin in the monolayer was substantially smaller (by 21 cm^{-1}) than the typical frequency for an α-helix. Melittin insertion caused lipid chain ordering, monitored by an increase in the CH_2 antisymmetric stretching. Penetration of melittin into a DPPC monolayer increased the surface pressure by 20 mN/m. Above L/P = 25 phase separation occurred in a mixed DMPC-melittin monolayer [27]. Orientation of melittin in fluid PC bilayers followed by oriented circular dichroism and neutron diffraction showed a correlation between the orientation perpendicular to the membrane and the presence of a pore. The pore inside/outside diameter was $\sim$4.4 nm/$\sim$7.6 nm. Only perpendicular orientation was detected in DLPC, DTPC and DMPC below L/P = 120, and only parallel orientation was seen in DPhPC. In POPC, both cases occurred: a perpendicular orientation at L/P = 15 and a parallel one at L/P = 40 [28]. A vesicle release study showed a higher capacity for binding melittin by POPG compared to POPC before a complete release of vesicle contents occurs [29]. In oriented layers at L/P = 50, the peptide orientation was transmembrane in POPC and parallel to the membrane in POPG. Melittin's tryptophan was positioned in a motion-restricted environment, which is consistent with the interfacial location. With increasing chain unsaturation in unsaturated PC, more water penetrated into the peptide-lipid interface (close to tryptophan), reflecting in a decrease of the fluorescence lifetime [30]. It is important to differentiate between dry and wet bilayers, as the orientation of melittin depends on the water content. It was shown in an attenuated total reflection Fourier transform infrared (ATR-FTIR) spectroscopy study that melittin orients parallel to membranes in hydrated single supported planar bilayers (asymmetric membrane - POPC/POPC+POPG 4:1), but perpendicular to membranes in dry bilayers (POPC, DPPC, POPC+POPG 4:1) [20]. In a DMPC monolayer at the air-water interface, the orientation was parallel to the membrane [31]. Partition coefficient for DPPC found in a red edge excitation shift spectroscopy (REES) study was 3.7 mM^{-1}. This is consistent with 2.1 mM^{-1} previously reported for POPC [19]. The free binding energy of melittin to EYPC large unilamellar vesicles (LUV) decreased with increasing compresion modulus, as was confirmed by Allende *et al.* [15]. In-

corporation of cholesterol or 6-ketocholestan into EYPC LUV increased the bilayer compressibility modulus K_T, which is the measure of the work needed to expand the surface area of the bilayer, and so makes it more difficult for the peptide to partition into the bilayer. Release of the vesicle content from POPC vesicles was inhibited by POPG and cholesterol. Interestingly, POPG promotes and cholesterol inhibits melittin binding [17].
In PE at L/P = 20, the hexagonal phase was suppressed at the expense of the fluid lamellar phase in DEPE and DOPE [32]. In oriented egg PE multilayers at 55% humidity, melittin decreased the lipid chain mobility and caused headgroup reorganization. This was seen by IR dichroism [33].
In a spin-label electron spin resonance (ESR) study, maximum perturbation was reached at L/P = 10 for DTPG. The lipid chain mobility increased in the gel and decreased in the fluid phase, and at the same time, the cooperativity of the main phase transition was destroyed. The maximum of the chain order parameter profile shifted deeper to the interior of the bilayer [22].
Less melittin molecules were able to penetrate into DPPC than into DPPG monolayers, because melittin molecules already adsorbed on the surface of the monolayer repulsed the melittin molecules in the solution and prevented further adsorption. Maximal adsorption occurred at the isoelectric point. At the same time, the increase in the area per molecule was greater in DMPC than in DMPG [27].

2.3 Alamethicin

Alamethicin is a peptide isolated from the fungus *Trichoderma viride*, 20 amino acids long. Its crystal structure is similar to melittin, an α-helix bent at Pro14. The distribution of amino acids in the sequence
Ac-AibPAibAAibAQAibVAibQLAibPVAibAibEQ-Phol makes the helix amphipathic (Fig. 2.12). Aib is the α-aminoisobutyric acid. The hydrophilicity of the convex face is due to nonbonded U10, G11, bound water, Q7, E/Q18, Q19 and NH_3^+; the concave face is hydrophobic (Fig. 2.13). The dipole moment is 60-79 D, which corresponds to net charge at both ends of $\pm 1/2$. The partition coefficient between the membranes and water is 10^{-3} M and the cooperativity parameter is 5.5. [34].

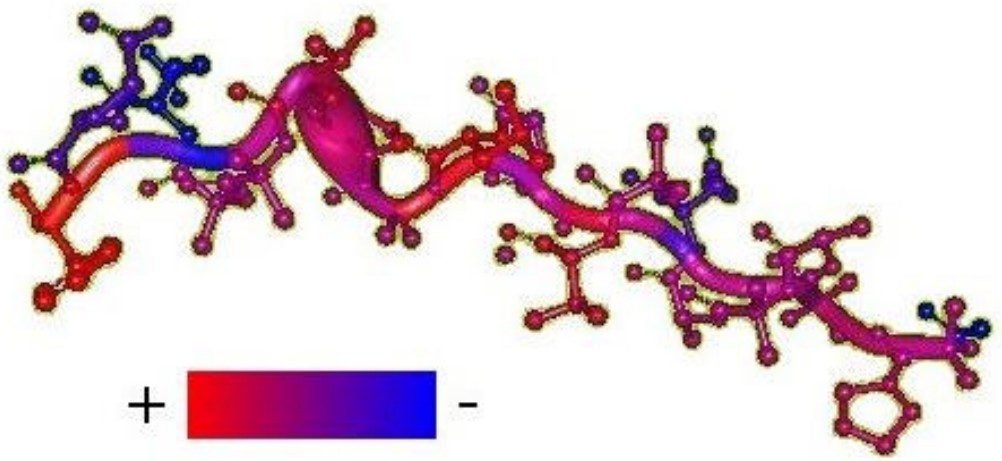

Figure 2.12: Crystal structure of alamethicin coloured according to the hydrophobicity. Hydrophobicity increases from blue to red. [13]

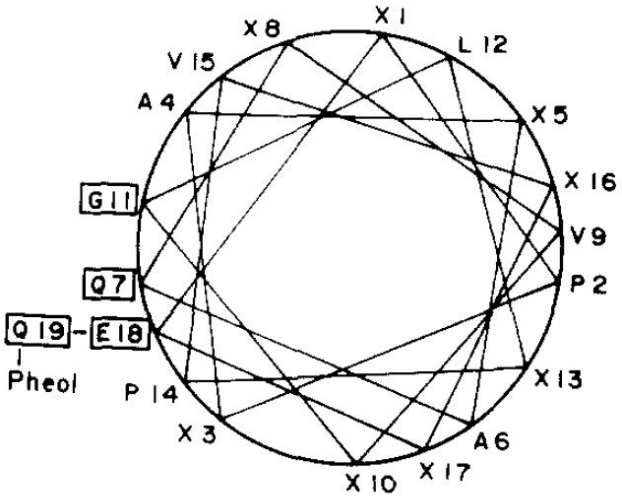

Figure 2.13: Helical wheel projection of alamethicin - projection along the helix axis. Polar residues are boxed [1].

2.3.1 Interaction of alamethicin with lipid membranes

Unlike melittin, alamethicin forms voltage-dependent pores in lipid membranes. The pores have highly asymmetric current-voltage characteristics. A positive voltage has to be applied to the side of the membrane to which the peptide was added to create a flow of current. It is supposed that barrel-stave pores are responsible for the multilevel conductance. The number of peptides forming the pore at a given moment (2 to 11 peptides) determines the conductance level [35]. Antimicrobial peptides usually show a sigmoidal concentration dependence of their activity. A study by oriented circular dichroism (OCD) and neutron scattering on alamethicin attempted to explain this with an elasticity-based theory. Alamethicin incorporated into fully hydrated DPhPC or DPhPC+DPhPE 5:1 oriented bilayers shows a concentration-dependent orientation and pore formation. At high L/P (120 for DPhPC), peptides lie on the membrane surface and cause membrane thinning, whereas at low L/P ($\leq$120 for DPhPC), they assume a transmembrane orientation and form pores. The membrane thinning in the transition region below the critical concentration for insertion (some peptides inserted, others parallel) depends linearly on the peptide to lipid ratio [36]. An OCD and X-ray diffraction study determined the critical concentration for insertion of alamethicin into oriented hydrated DPhPC bilayers, although full hydration was probably not achieved, as samples started to flow on the substrate before. Above the critical concentration, alamethicin caused a decrease in the bilayer thickness and an increase in the chain disorder, which points to the insertion of the peptide between the lipid heads. Such an insertion of the peptide causes a long-range deformation of the bilayer. At L/P = 150, when the distance between the molecules on the bilayer surface should be about 120 Å, the bilayer thinning is already homogeneous [37]. Orientation and conformation of alamethicin in wet and dry oriented DPPC bilayers was investigated by polarized ATR IR spectroscopy [38]. In dry membranes, alamethicin is an α-helix inserted into the membrane, with the long axis parallel to the lipid chains. The presence of the peptide causes ordering of the chains and reduces their tilt from 27° to 19°. In wet membranes, the peptide lies on the membrane surface as a β-sheet. The structure of the alamethicin pore in DPhPC and DLPC was found by in-plane neutron scattering [39]. In DLPC at L/P from 100 to 200, all the peptides are transmembrane. The pores are formed by 8$\pm$1 peptides and their outer/inner diameter is 20 Å/9 Å. 50% of the pore volume is occupied by lipids. In

DPhPC, full transmembrane insertion occurs below L/P = 17. Pores formed by 11 peptides have an outer/inner diameter of 50 Å/20 Å. Bilayer affinity measurements by vesicle titration found a partition coefficient of $\sim 10^{-3}$ M^{-1} for the alamethicin binding to DOPC. Alamethicin shows a higher affinity for PC than for PE, which also reflects the necessity of higher concentrations to observe pore activity in PE. Incorporation of PG into the vesicles increased the affinity [40]. The probability of conductance states of alamethicin pores in PE and PC membranes differs, reflecting the variation in free energy of embedded peptides. The conductance probability in PC/PE mixtures changes monotonically with relative lipid concentrations and correlate with the curvature of the lipid mixture. Probability variation is not due to changes in the membrane thickness [41]. In bulk, 1 mol% of peptide in a DOPC/DOPE 1:3 mixture induces a complex nonlamellar behaviour [42]. The simplest explanation for the different conductance levels of the channels are pores formed by aggregates of different sizes. Binding of alamethicin saturates at ∼10 lipids per peptide, at a solution concentration of 2 μmol and the free energy of binding is -6.2 kcal/mol. The free energy of binding becomes more negative with increasing peptide ratio in the membrane. The binding of alamethicin to DOPC proceeds in a cooperative manner under 1 μmol, while above this concentration the molecules aggregate [43]. During the adsorption of alamethicin to planar bilayers, the molecules interact even at negligible coverage, so the Langmuir isotherm does not apply. The voltage-dependent increase in membrane capacitance is smaller than for pure bilayers, but the difference cannot be explained by a change in the bilayer thickness [44]. It is supposed that alamethicin inserts into the headgroup region of the membrane, so the insertion should be facilitated by a smaller headgroup size. This idea was tested by the addition of small amounts of DPhPE into DPhPC membranes, but it was not confirmed, as the insertion decreased [45]. A new model for the alamethicin channel, the lipid covered ring, was presented by Ionov *et al.* [46]. The pore is composed of a ring of alamethicin molecules oriented parallel to the membrane and buried inside one monolayer of the bilayer. The hydrophilic C-termini point to the center of the ring. When voltage is applied, the incoming ions open a pore in the opposing monolayer and pass through. The asymmetric structure of the pore explains the experimentally determined asymmetric current-voltage characteristics of alamethicin pores. Alamethicin decreased DLPC and DPhPC bending elasticity, as detected by vesicle shape fluctuations [47]. The conformation of alamethicin in oriented bilayers found by ^{15}N solid-state NMR is

a transmembrane helix, tilted 10-19° from the bilayer normal [48]. A X-ray grazing incidence study found the structure of alamethicin pores in oriented DLPC and OPPC membranes. Alamethicin molecules were found to insert up to Pro14 and with a tilt. The tilt angle distribution was continuous. From the proposed pore models, the Ionov lipid covered ring and Huang elasticity model were consistent with the results of this study. The periodicity of the stacked membranes did not change with the addition of alamethicin at L/P = 25 to 100 and high mosaicity was also preserved, although positional correlations along the bilayer normal decreased [49].

2.4 X-ray diffraction on lipid bilayers.

The X-rays are scattered by the electron density distribution of matter. Only the elastically scattered part (Thomson scattering), about 3% of the incident intensity, is used in the diffraction measurements. Most of the intensity is lost through absorption (photoeffect - 59%) and inelastic scattering (Compton scattering - 1.5%) [50]. These values are for a layer of water 1 mm thick and radiation of wavelength $\lambda = 0.15$ nm, corresponding to a photon energy of 8 keV, and are a reasonable approximation for lipid dispersions in excess water. Both lipids and water are mainly composed of weakly scattering atoms like H, C, O, N, P and the aqueous solutions prepared for measurement usually contain a few percent of lipid by weight. Usually, the electron density of water taken as 333 electrons per nm^3 is considered the mean electron density of the lipid-water system. The electron density of the lipid heads is 440 e/nm^3, of the lipid chains 296 e/nm^3 and of the bilayer centre 165 e/nm^3 [51].
Lipids dispersed in water form structures with long range order, suitable for diffraction studies. Waves scattered on such a periodic structure constructively interfere in certain directions and destructively in others. These are described by Bragg's law, $m\lambda = 2dsin\theta$, where m is the diffraction order, λ is the wavelength of the diffracted radiation, d is the lattice spacing and 2θ is the scattering angle. Measurements of the intensity of the scattered radiation as a function of the scattering angle permit the determination of the lattice parameter and the electron density of the periodic structure. With membrane dimensions of several nm, the radiation is scattered at very small angles, up to 3° in SAXS (small angle X-ray scattering) and 20° in WAXS (wide angle X-ray scattering). Resolution is often defined as half the recipro-

cal distance of the highest-angle measured peak. The intensity $I(\vec{q})$ scattered from a finite stack of unoriented bilayers is given by

$$I(\vec{q}) \propto \frac{S(\vec{q})|F(\vec{q})|^2}{q^2},$$

where $q = 4\pi sin\theta/\lambda$ is the absolute value of the scattering vector [53]. $S(\vec{q})$, the structure factor, describes the ordering of the unit cells in the lattice, in this case the stacking of the bilayers. $F(\vec{q})$, the form factor, characterizes the electron density distribution inside one unit cell, i.e. the transverse electron density profile of the bilayer. For a layered structure, it is given by the Fourier transform of the electron density profile.
In experiments on lipid bilayers usually less than 6 orders of diffraction are observed. There are two reasons - disorder in the molecular packing of the bilayers and disorder in the bilayer stacking. Molecular disorder and fluctuations within one bilayer give rise to a broad electron density profile. Therefore, the higher order terms in the Fourier expansion of the form factor are small and so are the higher order peaks. Second, the bilayer stacks are not a one-dimensional crystal, but a smectic liquid crystal. The unit cells fluctuate with respect to each other [52]. The large scale (long-wave) fluctuations destroy the crystalline order and replace it with a quasi-long-range-order (QLRO) in which pair correlation functions diverge logarithmically instead of remaining bounded as in crystals. Because the long-range order is absent, the Debye-Waller theory of scattering from crystals with lattice fluctuations is not appropriate. Instead, QLRO changes the scattering peak shape from an intrinsic delta function by removing intensity from the central scattering peak and spreading it into tails of diffuse scattering centered on the original peaks. The magnitude of this shift in intensity increases with increasing diffraction order. For high enough order m, the scattering peaks are completely converted to diffuse scattering even if the form factors F_m for the local lipid bilayer are large. The number of observed diffraction peaks is not sufficient for a reconstruction of the electron density like in crystallographic measurements. To overcome this drawback, electron density reconstruction methods were developed that use additional information, for instance the intensity of the diffuse scattering [53], [54].

2.5 Sample preparation and measurement

Lipids (POPC, POPE, POPG) from Avanti Polar Lipids and LPS R595 and R60 and lipid A (isolated from *S. minnesota*, from Prof. K. Brandenburg, FZ Borstel) were dissolved in buffer solution (20mM Hepes, pH 7), vortexed thoroughly, sonicated and cycled over the main phase transition temperature at least three times. For POPE, the cycling was done in a water bath. The eppendorf tubes were thoroughly sealed by parafilm and inserted into a water bath. The bath temperature was programmed to ∼50°C and the samples were incubated for ∼1 hour. The heating was switched off and the water bath was left to cool to room temperature. For LPS, the temperature of the water bath was ∼60°C and the first heating was done in a bath sonicator, with simultaneous heating and sonication. POPC was frozen in a freezer at -20°C, then left to unfreeze at room temperature.
Synthetic melittin from Sigma, Germany was purchased (M4171, ≥97% by HPLC). Synthetic melittin was used, because the natural melittin isolated from bee venom contains a small amount of phospholipase A_2 which could damage the membranes. Melittin was dissolved in the Hepes buffer and mixed with the lipid dispersion in the fluid state to achieve lipid/peptide molar ratios[2] from 10 to 10 000. The peptide concentrations were between 0.01 and 3 mM. Lipid-peptide mixtures were again incubated above the main transition temperature in the water bath for about two hours, then left to cool to room temperature and stored at 4°C. Samples were filled into capillaries or sample holders and stored at 4°C for at least 24 hours prior to the measurement.
Alamethicin was purchased from Sigma, Germany (A4665, ≥90% by HPLC). It is a mixture of two homologs, alamethicin I (85%) and alamethicin II (12%) which differ by one amino acid [55]. For the calculation of concentration of the solutions, the molar weight of alamethicin I was used, M = 1960. Alamethicin does not dissolve in water above micromolar concentrations, and these were too low for our purposes. Alamethicin powder was therefore simply added to the buffer and mixed with a lipid dispersion at lipid/peptide molar ratio 10. This mixture was then homogenized in the way described for the lipid/melittin samples. After the homogenization, there were no visible traces of alamethicin powder in the buffer. Parts of this mixture were diluted with the lipid dispersion to obtain samples with higher lipid/peptide molar ratios.

[2] All lipid to peptide ratios (L/P) in this work are molar ratios.

These were homogenized as described previously. All the lipid/alamethicin samples prepared in this way were monophase, as evidenced by the diffraction patterns.
The samples were measured at the synchrotron soft condensed matter beamline A2 at HASYLAB at DESY in Hamburg, Germany (Fig. 2.14). Small- and wide-angle scattering (SAXS and WAXS) were measured simultaneously. Two linear position-sensitive gas-filled Gabriel detectors were used, one for small, the other for wide angles. Two different setups were used, for samples in copper sample holders with Kapton windows and for samples in capillaries. For copper sample holder measurements, the whole path of the beam before reaching the detectors was in vacuum. For capillary measurements, there was a short break in the vacuum for placing the capillary holder. The heating and cooling of the sample was regulated by a thermocouple connected to the temperature controller JUMO IMAGO 500 (JUMO GmbH & Co. KG, Fulda, Germany). Cooling was done by a flow of cold air. The beam was focused vertically by a mirror and horizontally by a bent single crystal germanium monochromator. A fixed wavelength of 0.15 nm was selected by the monochromator (photon energy of 8 keV). The beam size was determined by four sets of slits. The size of the beam at the sample position was about 2 mm by 0.5 mm (h×v). The detectors were calibrated with rat tail collagen (SAXS) and tripalmitin (WAXS).
The samples with POPE and LPS were usually heated and cooled from 5 to 85°C at 1°C/min. The samples with POPC were heated and cooled from 5 to 50°C at 1°C/min. Diffraction patterns were recorded at minute intervals with an exposure time of 10-15 s. The diffraction peaks were fitted with Lorentzians, and the lattice parameters were calculated from the position of the first peak. The widths of the peaks were used as a measure of the quality of ordering of the given phase and the integrated intensity to estimate the proportion of the phase in the sample.

2.6 Diffraction patterns of lipid membranes.

A typical data set is shown in Fig. 2.15. It is a set of 1D diffraction patterns, each taken at a different temperature during the heating and cooling from 5 to 85°C.
A typical diffraction pattern for the lipid gel phase shows equally spaced peaks in the SAXS region, reflecting the bilayer spacing and one sharp (10)

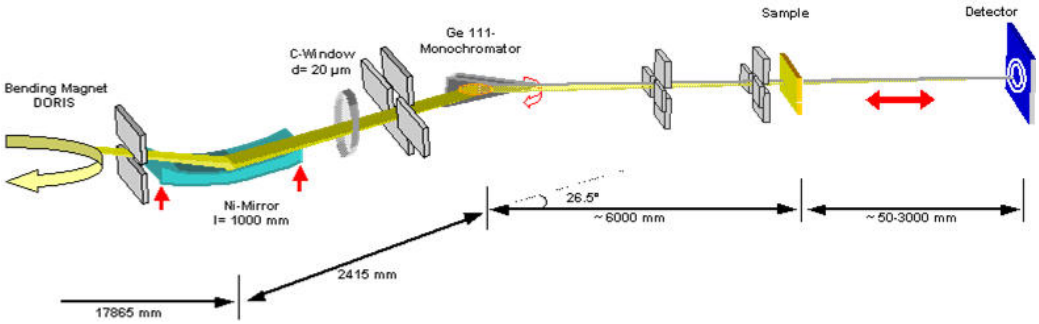

Figure 2.14: Beamline A2 in Hasylab.

peak in the WAXS region, showing the distances between the rows of lipid chains in the hexagonal lattice within the plane of the bilayer (Fig. 2.16). Occasionally, the (11) or (12) peaks show up in the WAXS region. For hexagonal chain packing in the gel phase, we can calculate the chain spacing using $d_c = 2/(\sqrt{3}s_{10})$ and the area per molecule as $A_{mol} = 4/(\sqrt{3}s_{10}^2)$, from the position of the (10) peak, s_{10}.

The SAXS diffraction pattern of the fluid lamellar phase shows a set of equally spaced peaks, $s_h = h/d$, where h is a positive integer and d is the bilayer lattice parameter, while only a very broad diffuse scattering appears in the WAXS region (Fig. 2.17).

The diffraction pattern of a hexagonal phase contains a series of peaks in the SAXS and a broad diffuse scattering in the WAXS region (Fig. 2.18). The SAXS peaks appear at positions $s_{hk} = 2(h^2 + k^2 - hk)^{1/2}/(\sqrt{3}a_h)$, where a_h is the distance between the centers of the neigbouring lipid cylinders.

The SAXS scattering pattern of a cubic phase shows a number of peaks at positions given by $s_{hkl} = (h^2 + k^2 + l^2)^{1/2}/a_c$, where a_c is the cubic lattice parameter (Fig. 2.19). A broad diffuse scattering is in the WAXS region. The cubic aspect can be determined from systematic peak absences, although absent peaks may also be due to the structure factor.

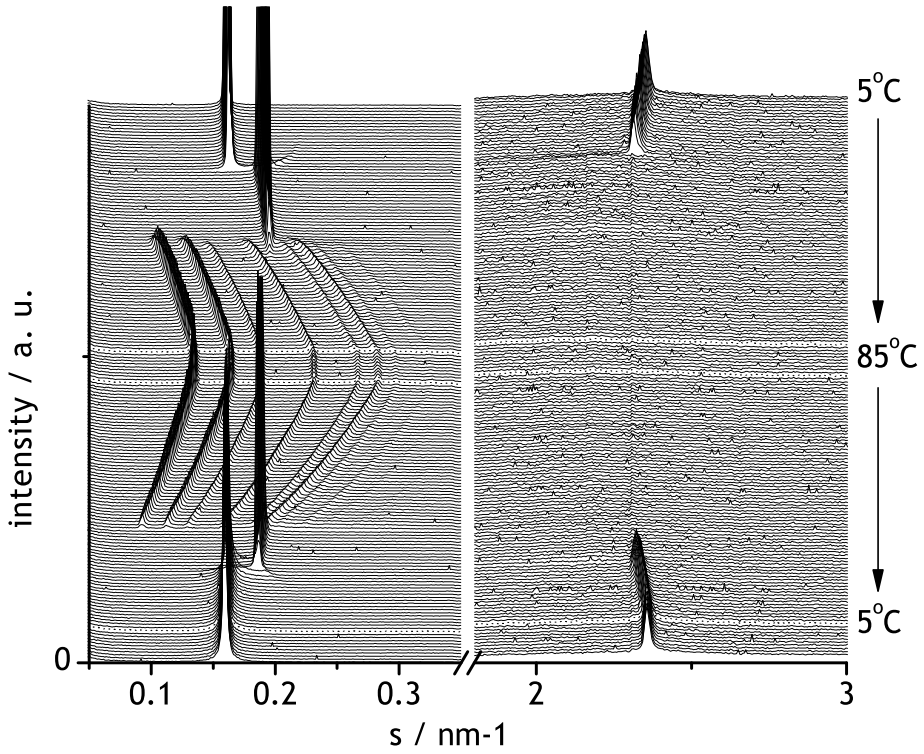

Figure 2.15: Example of a typical data set - a set of 1D diffraction patterns recorded during the heating and cooling from 5 to 85°C. The arrows show the direction of the temperature changes. Every line is a diffraction pattern taken at a different temperature. The break in the x-axis separates the angular regions covered by the two detectors, the small angle region (SAXS), from 0 to 0.35 nm^{-1} and the wide angle region (WAXS), from 1.8 to 3 nm^{-1}.

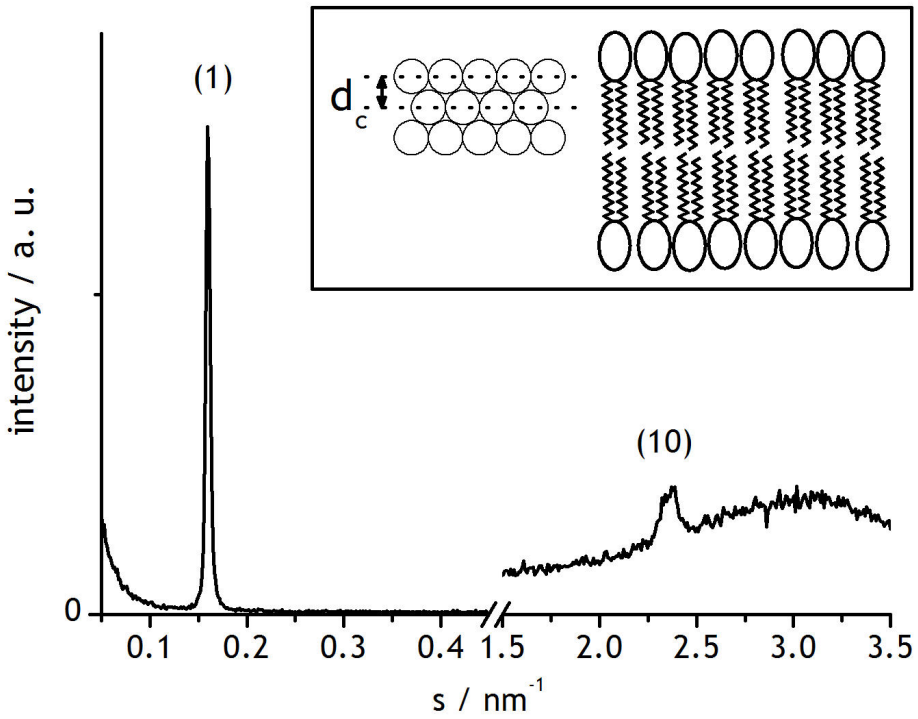

Figure 2.16: Diffraction pattern of the lamellar gel L_β phase. Only the first order peak is visible, as is usual in gel-state unsaturated PEs. The diffraction order is indicated. In the inset is shown a sketch of a membrane in the gel state and the view along the bilayer normal shows the ordering of the lipid chains in a hexagonal lattice.

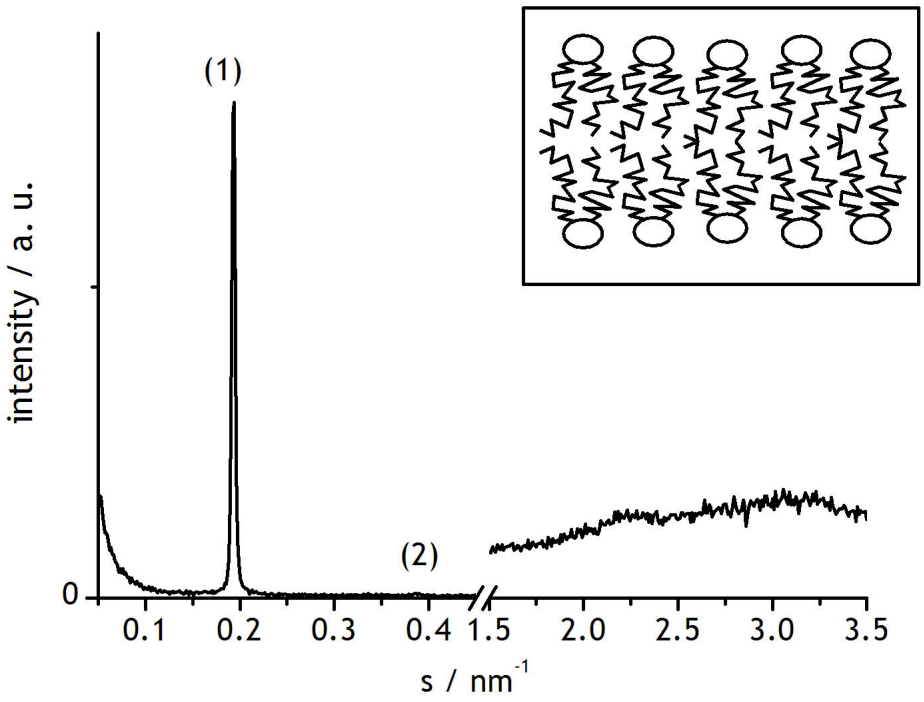

Figure 2.17: Diffraction pattern of membranes in the fluid lamellar phase L_α. The diffraction order is indicated. A sketch of the membrane is shown in the inset.

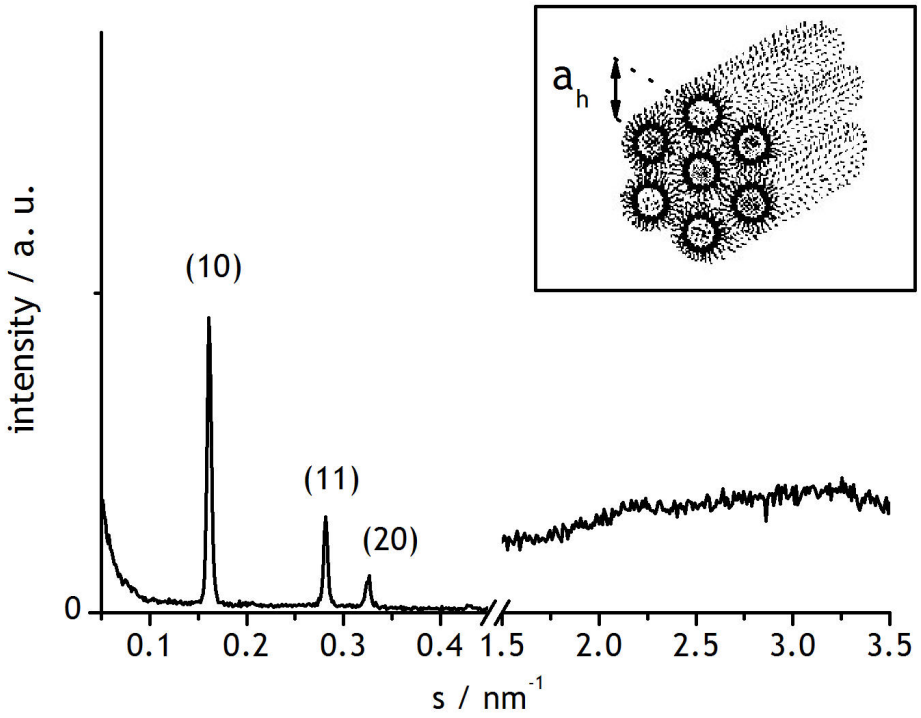

Figure 2.18: Diffraction pattern of the inverse hexagonal phase H_{II}. The diffraction order is indicated. The corresponding structure is shown in the inset.

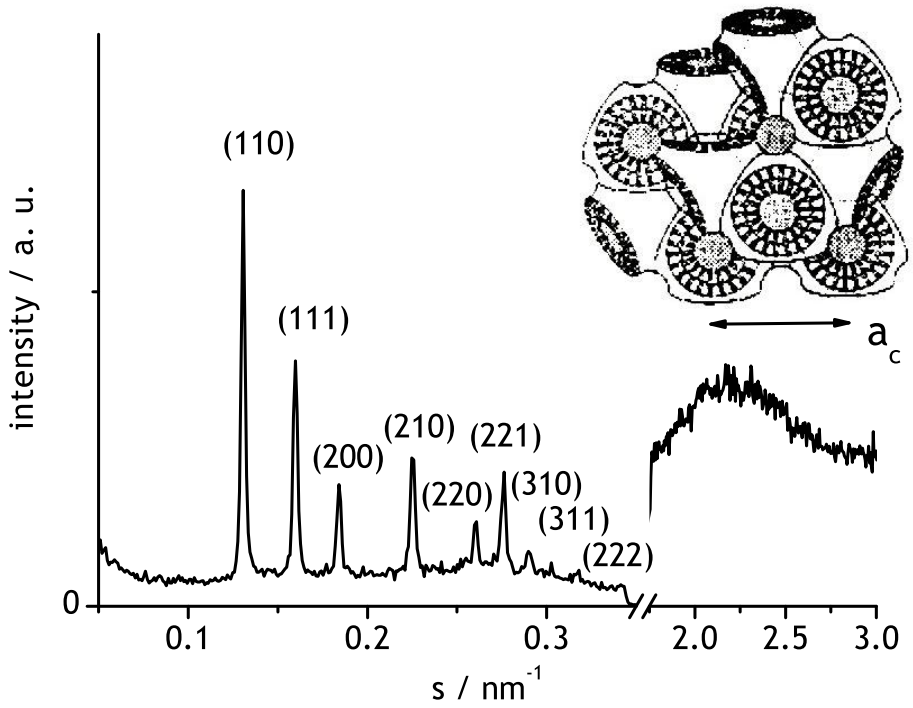

Figure 2.19: Diffraction pattern of the cubic phase Pn3m. The diffraction order is indicated. The corresponding structure is shown in the inset.

Chapter 3

Phase behaviour of lipid membranes with antimicrobial peptides.

Most antimicrobial peptides show higher activity towards certain kinds of cells. A perfect antimicrobial peptide for use as a drug should show a high activity towards bacterial (disease) cells and should not interfere with the human (host) cells. Indeed, many antimicrobial peptides show such a preference. To establish the affinity or mode of interaction with various cell types, experimenters use model membranes composed of different types of lipids. The most common approach is to model the bacterial membranes with negatively charged lipids, e.g. PG, and the human membranes with neutral lipids, e.g. PC. The experimenters highlight one aspect of the differences between the bacterial and human cell membranes, the membrane charge. This membrane property is certainly important and the approach is justified also from the point of view of the primary sequence of the antimicrobial peptides, most of which bear a positive charge, so the electrostatic interaction is expected to play a major role in the binding. The drawback of the method is that it overlooks other compositional differences between human and bacterial membranes and the structural and phase behaviour differences inside the class of neutral lipids which certainly play a role in peptide affinity and interaction with membranes. One very important property is the spontaneous membrane curvature which reflects the ability to form non-bilayer phases. Membrane curvature influences the function and conformation of membrane proteins [56, 57]. Keller [41] noticed the difference in

the conductance probabilities of alamethicin transmembrane channels in PC and PE membranes and explained them by the differences in the spontaneous curvature. She also observed the formation of cubic phases in mixed DEPE-alamethicin membranes [42]. Angelova [58] studied the phase behaviour of DOPE and DOPC membranes with alamethicin and found profound differencies. In DOPC, alamethicin induced an additional lamellar phase with dimensions only slightly different from the pure DOPC lamellae. In DOPE, cubic phases evolved in the temperature interval between the lamellar and the hexagonal phases. In this work, the phase behaviour and structures induced by two antimicrobial peptides in two different classes of neutral lipids, the phosphatidylcholines and the phosphatidylethanolamines, are investigated. POPE was chosen because it is possible to study its entire phase behaviour between 0 and 100°C. This was not done in the study of Angelova. The induced cubic phases, their structure, phase behaviour, coexistence with the lamellar and hexagonal phases and the mutual relationships have been studied in depth. The phosphatidylcholine complementary to POPE is POPC. With this lipid, only the fluid lamellar phase was characterized because cooling below 0°C was difficult with our experimental setup.

3.1 POPC phase behaviour

Fully hydrated POPC membranes were studied in the temperature range 5 to 50°C and 0 to 80°C. Three different samples were measured at different times and after different storage periods at 4°C. All samples were in the fluid lamellar phase L_α, as evidenced by two equidistant peaks in the SAXS region and no significant peak in the WAXS region. The lattice parameters and thermal behaviour differed. As a reference sample, the one behaving similarly to published data (e.g. d = 6.02nm at 5°C, see [59]) with a decreasing bilayer spacing during the heating was chosen.

3.2 Phase behaviour of POPC membranes with alamethicin

POPC-alamethicin mixtures were prepared at lipid/peptide ratios 10, 30, 50, 100, 200, 500 and 1000. The diffractograms were recorded during the heating and cooling from 5 to 50°C. All samples showed similar diffraction patterns

with two equidistant peaks in the SAXS region and no significant peaks in the WAXS region, corresponding to a fluid lamellar phase. An example is shown in figure 3.1. The lattice spacings of all samples and of the reference POPC sample are shown in figure 3.2.

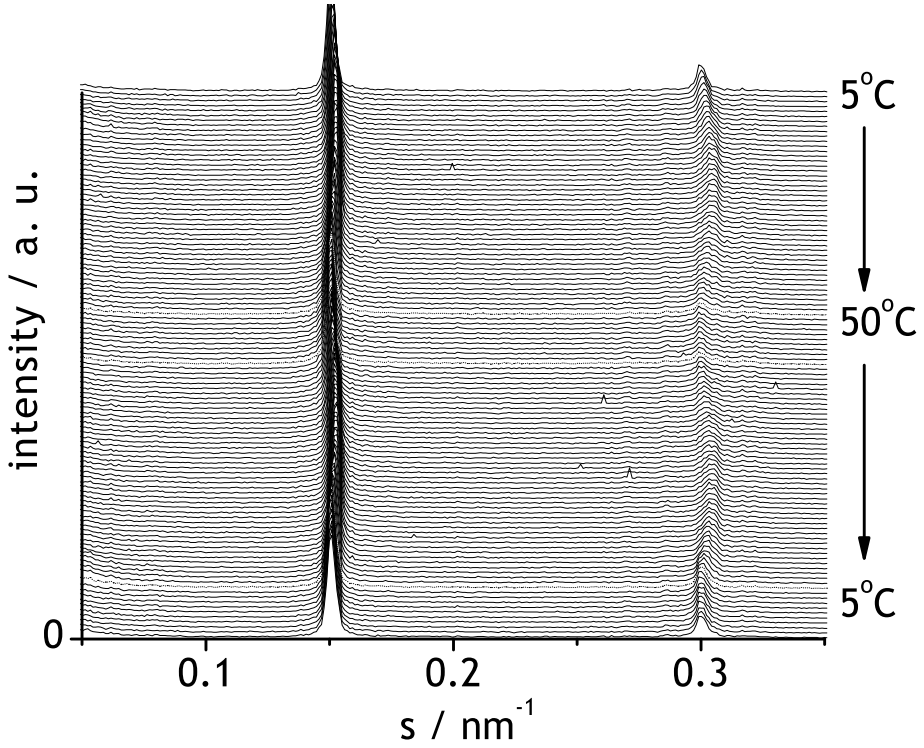

Figure 3.1: SAXS diffraction patterns of POPC membranes with alamethicin at L/P = 100 recorded during heating and cooling from 5 to 50°C. The arrows indicate the direction of the temperature changes.

Alamethicin increased the lattice parameter and changed the thermal evolution of the POPC membranes. While the lattice spacing of the pure POPC membranes decreases monotonically with increasing temperature, the spacing of the POPC membranes with alamethicin initially decreases slightly and then increases again. The increase is more pronounced in samples with a higher amount of alamethicin. At L/P = 10, the difference between the membrane spacing at 5 and 80°C is nearly 1 nm. The lattice parameter increases

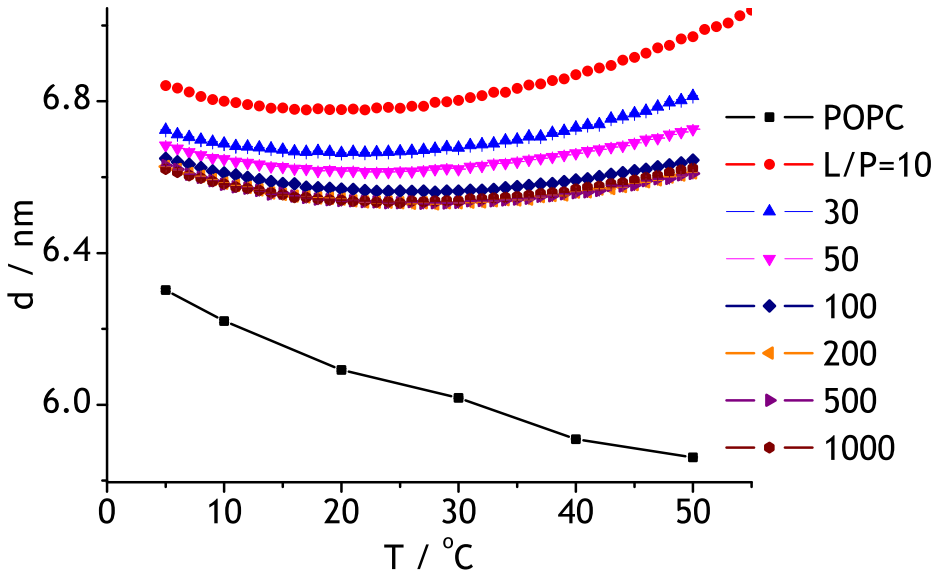

Figure 3.2: Lattice parameters of POPC membranes with alamethicin. The black curve is pure POPC. The POPC to alamethicin ratios L/P are indicated.

with alamethicin concentration. The increase can be explained in two ways. One possibility is that the intermembrane water layer becomes thicker because of the repulsion of the adjacent bilayers whose surface charge increased as a result of the adsorption of alamethicin. The cylindrical molecular shape of POPC does not allow a deeper penetration of the peptide into the bilayer for steric reasons, so the peptide's charged residues cannot be screened by the partial lipid charges. The study of Pabst [60] on alamethicin-membrane binding suggests that this possibility is unlikely, because the electrostatic interaction between the adjacent membranes is weak. Another reason for the lattice parameter increase could be the undulation of the bilayers which then cannot maintain the original spacing. The insertion of alamethicin between the POPC headgroups causes small depressions in the bilayer as observed by Chen [36], or bulging towards the water layer, in an effort to increase the average headgroup cross-sectional area. Either process perturbs the membrane packing and causes membrane undulation and a consequent increase in the lattice parameter. The larger membrane spacing weakens the intermembrane forces and causes membrane swelling at high temperatures.

The increased short and long range disorder in the structure should be reflected in the width of the diffraction peaks (FWHM). The full widths at half maximum of the first order diffraction peaks (FWHM1) are plotted in the figures 3.3, 3.4 and 3.5. According to the thermal behaviour of FWHM1, we can divide the samples into three groups. In the first group are the samples with L/P = 1000, 500 and 200, those with the smallest increase in the lattice parameter with respect to pure POPC. Their FWHM1 during heating is shown in figure 3.3. In these samples, FWHM1 does not increase significantly until above 30°C. The second group includes samples with L/P = 100 and 50 (Fig. 3.4). FWHM1 increases from the beginning of the heating, although the rate of increase diminishes progressively. The third group are POPC-alamethicin membranes with L/P = 30 and 10 (Fig. 3.5). Here, FWHM1 increases from the beginning and more steeply at higher temperatures. The level of disorder in the POPC multilamellar structure clearly increases with increasing amount of alamethicin. This supports the hypothesis stated earlier. As more and more alamethicin binds to the membranes, the more undulations and packing imperfections within one bilayer are produced and the membranes are forced to move farther apart, what weakens the intermembrane correlations.

The behaviour of PC membranes with alamethicin observed here seems contrary to the one observed by Chen *et al.* [36]. In their case, alamethicin caused

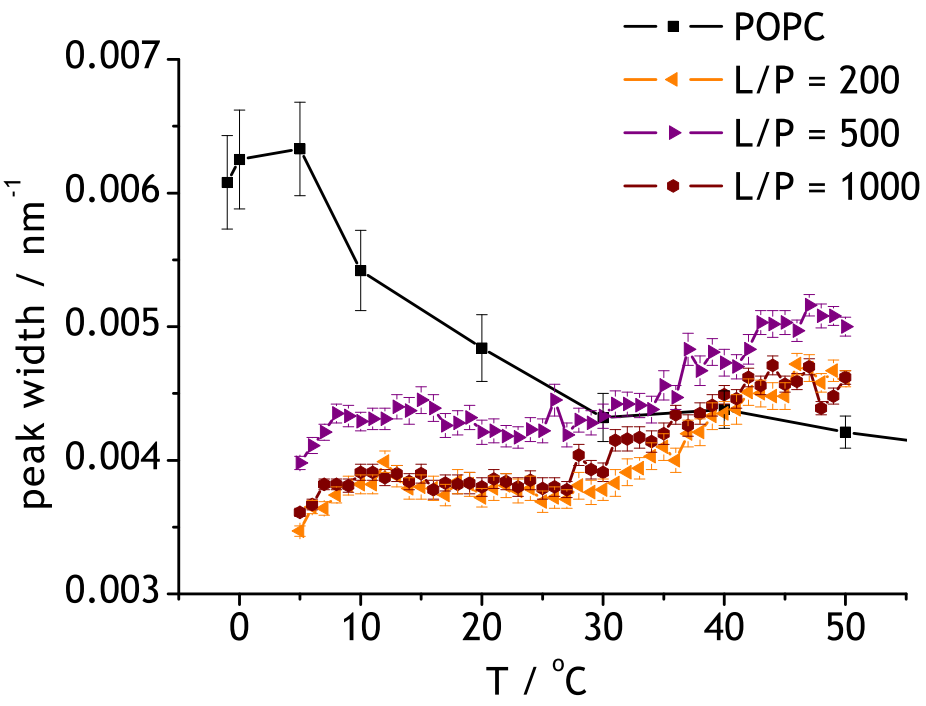

Figure 3.3: Width of the first-order diffraction peak for POPC membranes with alamethicin at L/P = 1000, 500 and 200.

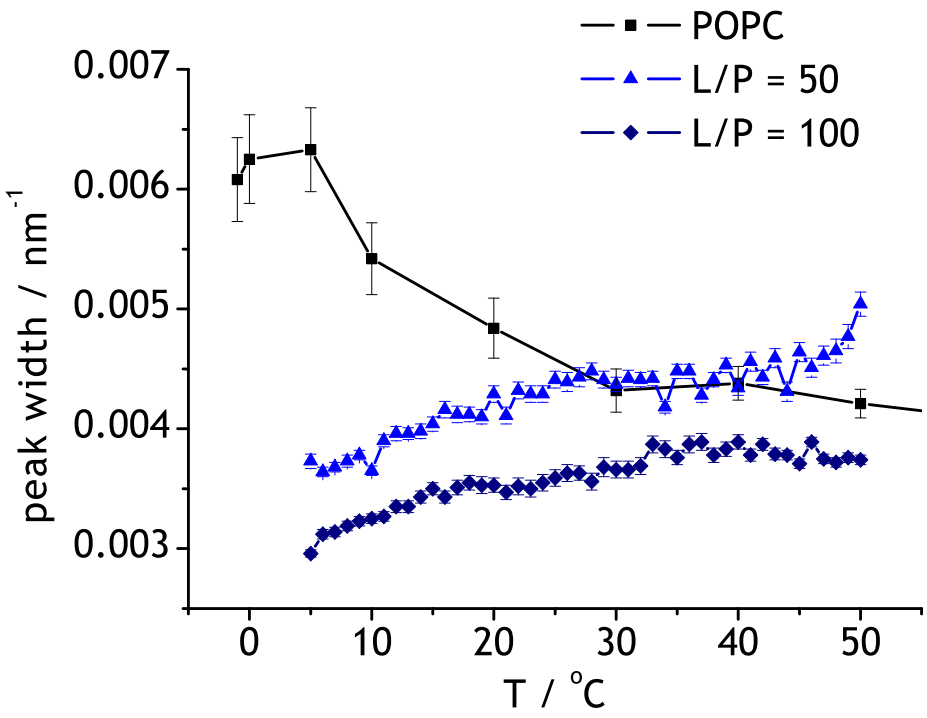

Figure 3.4: Width of the first-order diffraction peak for POPC membranes with alamethicin at L/P = 100 and 50.

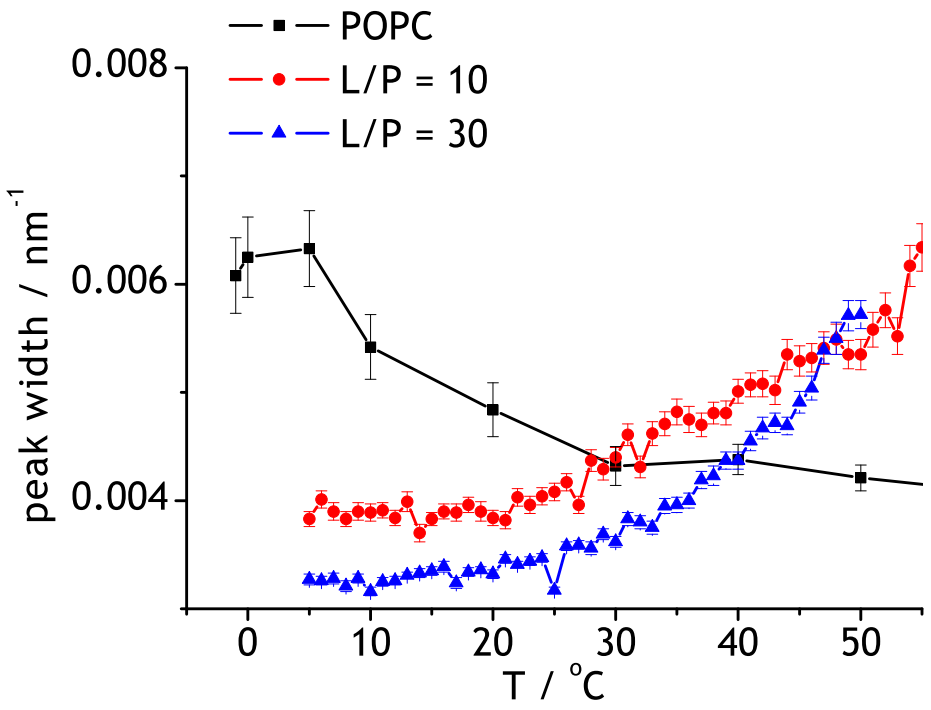

Figure 3.5: Width of the first-order diffraction peak for POPC membranes with alamethicin at L/P = 30 and 10.

a thinning of the membranes, while in our experiments the lattice spacing increased. Although we cannot draw any conclusions about the membrane thickness, these findings are not conflicting. The increase in the bilayer spacing is the consequence of the undulations and is perfectly compatible with a membrane thinning. Pabst [60] observed both phenomena in DOPC membranes with alamethicin.

Chen *et al.* [36] identified three stages in the binding of alamethicin to membranes. In the first stage, at low concentrations, peptides lie on the membrane surface. With increasing concentration, they start to insert perpendicularly into the membrane until finally all peptides are inserted. The FWHM1 plots also suggest a three-stage interaction, and indeed the stages might correspond to the three levels of peptide insertion into the membrane. The reason behind the peak broadening is the imperfect stacking of the membranes (disorder in the crystal lattice), not the disorder within one bilayer (disorder inside a unit cell) (see chapter 2, section 2.4). Alamethicin lying on the membrane surface changes the ratio of the mean headgroup to chain cross-sectional area, which must be close to 1 in flat bilayer systems, and forces the bilayers to bend. Bent bilayers cannot maintain a perfect stacking, so the crystalline order is perturbed. Alamethicin inserted in the membrane can induce local membrane thinning because of the necessity of hydrophobic matching between the lipid and the peptide. The hydrophobic length of the crystallographic bent helix is 2.2 nm and of a straight α-helix 1.8 nm [48]. The hydrophobic thickness of the fluid POPC bilayer at 30°C is 2.7 nm [61], so the membrane has to deform locally. This, in the end, makes the lateral membrane profile wavy, and considering the high lipid to peptide ratio, the perturbation should be significant. Moreover, the membrane thinning requires that the lipid chains become shorter, i.e. more *gauche* isomers. We can regard this as a virtual heating of the membrane. In general, lipid membranes are more elastic at higher temperatures and are more prone to undulations.

Two samples, at L/P = 10 and 30, were measured repeatedly. In both cases, the lattice spacing was larger in the second measurement (Fig. 3.6). The lattice spacing at L/P = 30 measured 4 months after the preparation nearly reached the one at L/P = 10 measured one month after the preparation. It seems that during long storage, water slowly penetrates through the defects in the membranes and these swell. The swelling seems to have a limit, as the increase in lattice parameters is about 1 Å in both cases, after one and four months storage time, so it is improbable that the membrane will ever completely unbind and dissolve into unilamellar vesicles.

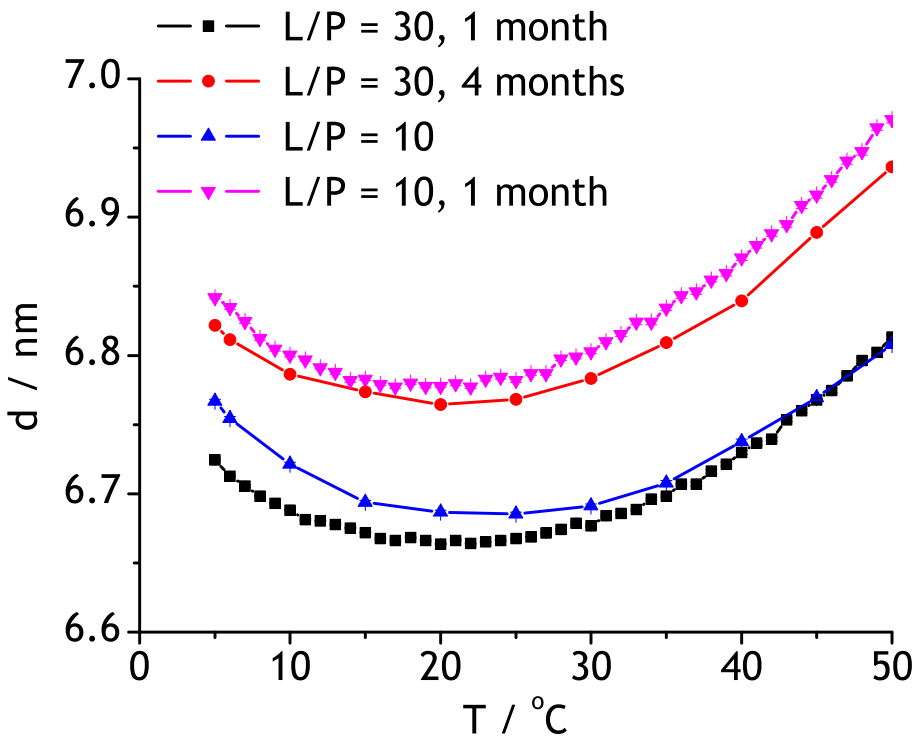

Figure 3.6: Lamellar spacing of POPC membranes with alamethicin at L/P = 50 and 10 measured repeatedly. The time interval between sample preparation and the measurement is indicated.

3.3 Phase behaviour of POPC membranes with melittin

Three sets of samples of POPC-melittin mixtures were prepared and measured, giving different results. The first set consists of samples *pc50*, *pc100*, *pc200*, *pc500*, and *pc1000*, with L/P ratios 50, 100, 200, 500, 1000, respectively. The diffraction patterns were recorded, shortly after preparation, during heating and cooling between 5 and 50°C. All samples are in the fluid lamellar phase. The lattice parameters are higher than in pure POPC and similar at all L/P ratios (Fig. 3.7). They decrease monotonically during heating, and during cooling the behaviour is reversible, like in pure POPC. The width of the diffraction peaks, on the other hand, behaves quite differently from POPC (Fig. 3.8). At low temperatures, the width decreases as in pure POPC, but later starts to increase, indicating the growing loss of correlations in the bilayer stacking. Curiously, the increase in width starts at the same temperature for all L/P ratios. The similarity of behaviour at such different POPC-to-melittin ratios suggests that melittin binding to POPC either saturates already at high L/P ratios, or the binding is only superficial, so the peptide does not completely disrupt the lipid packing even at high concentrations. The decreasing bilayer spacing and a simultaneous decrease in the quality of the stacking are difficult to reconcile, but both facts are consistent with a weak, superficial binding of the peptide to the membrane. The superficial binding has a weak effect on the lipid chains, so these behave as in a pure lipid and the membrane thickness (and lattice spacing) decreases with increasing temperature. On the other hand, even a weakly bound peptide causes a small depression in the membranes as observed by Chen [25], so the membrane thickness is not uniform and consequently the bilayers are not perfectly parallel and the mean bilayer distance increases. The same but stronger effect manifested in the POPC-alamethicin membranes might be explained by a deeper penetration of the peptide into the membrane due to its higher hydrophobicity (see the helical wheel projections in Fig. 2.11 and 2.13).

The second set of samples consists of samples *p200*, *p500* and *p10000* with lipid:melittin ratios 200, 500 and 10000, respectively. The diffraction patterns were taken during heating between 20 and 90°C. The lattice parameters are shown in figure 3.9. In the whole temperature interval, the samples are in the fluid lamellar phase and at some point undergo a phase separation into

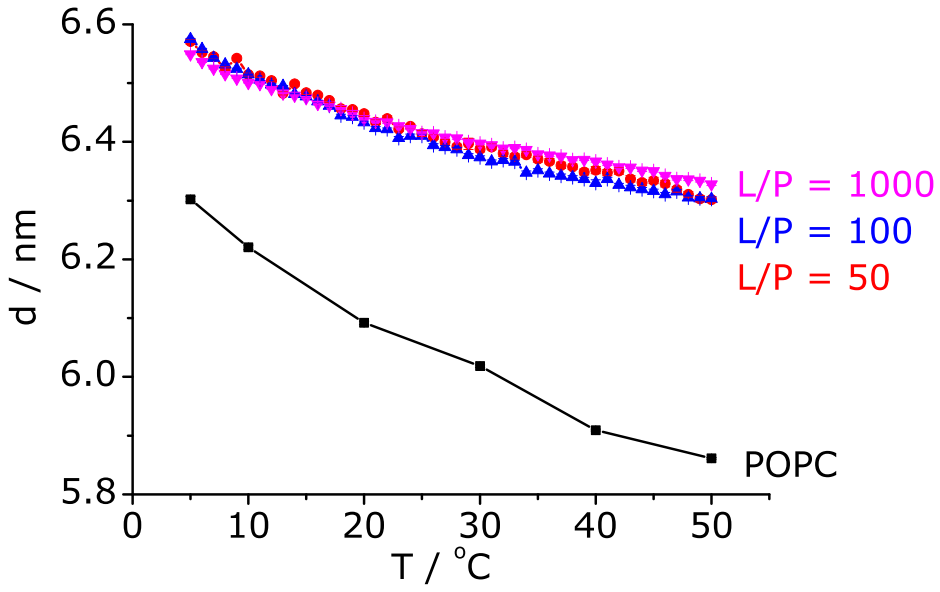

Figure 3.7: Lamellar spacing in POPC membranes with melittin in the first set of samples. The POPC to melittin ratios, L/P, are indicated in the picture.

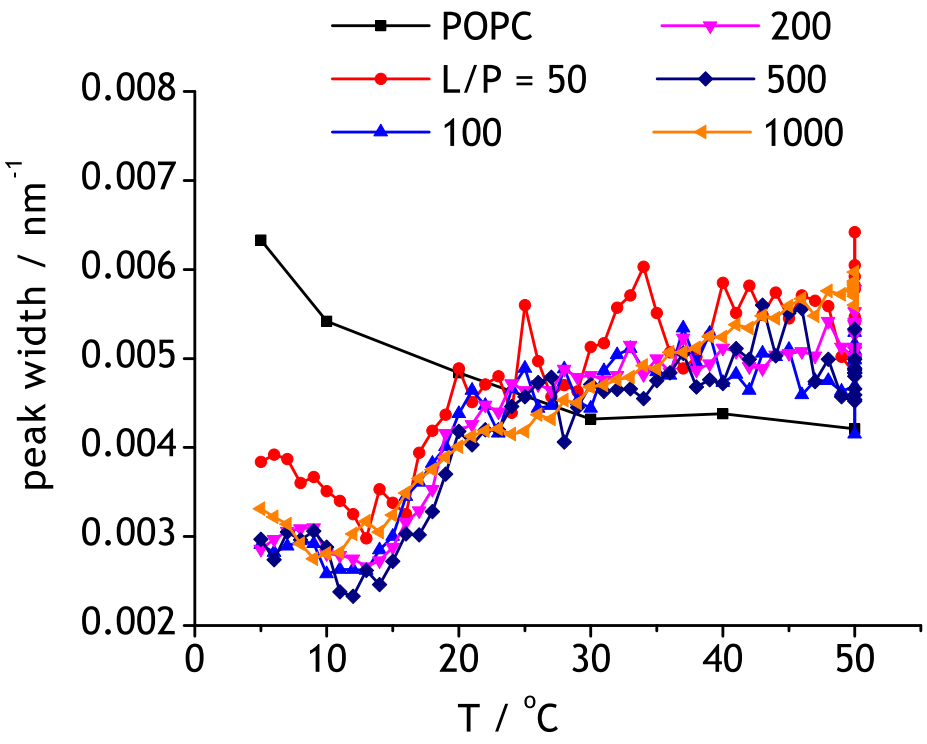

Figure 3.8: Width of the first-order lamellar peak in the POPC-melittin sample. The POPC to melittin ratio, L/P, is indicated.

two lamellar phases (Fig. 3.10). The splitting occurs at lower temperatures in samples with lower melittin concentrations. The lattice parameters of both phases are larger than those of pure POPC. The bilayer spacing of one phase decreases during heating, as in the first set of samples, while the spacing of the other phase increases, as observed for the POPC membrane with alamethicin. This set of samples was prepared several days before the measurement, so the membranes had more time for equilibration. The delayed appearance of the second phase suggests that melittin binding is a continuous process. In the first stages, the peptide adsorbs on the surface of the membrane and slightly increases the lattice parameter. Later, it penetrates deeper, disorders the lipid packing, causes membrane undulations and a larger increase in the mean lattice spacing.

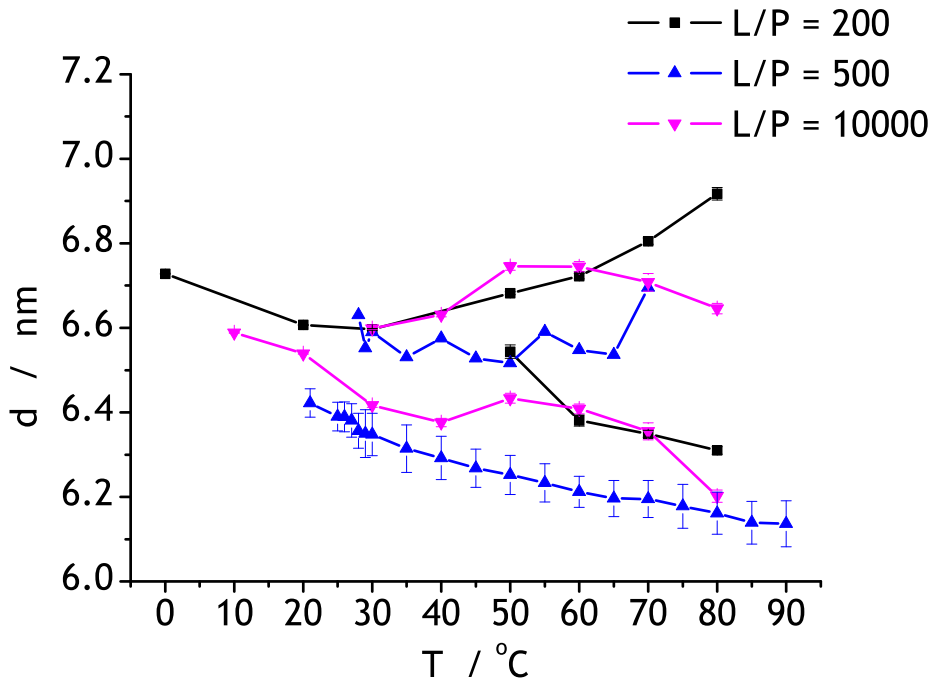

Figure 3.9: Lattice parameters in POPC membranes with melittin in the second set of samples. The POPC to melittin ratios, L/P, are indicated in the picture.

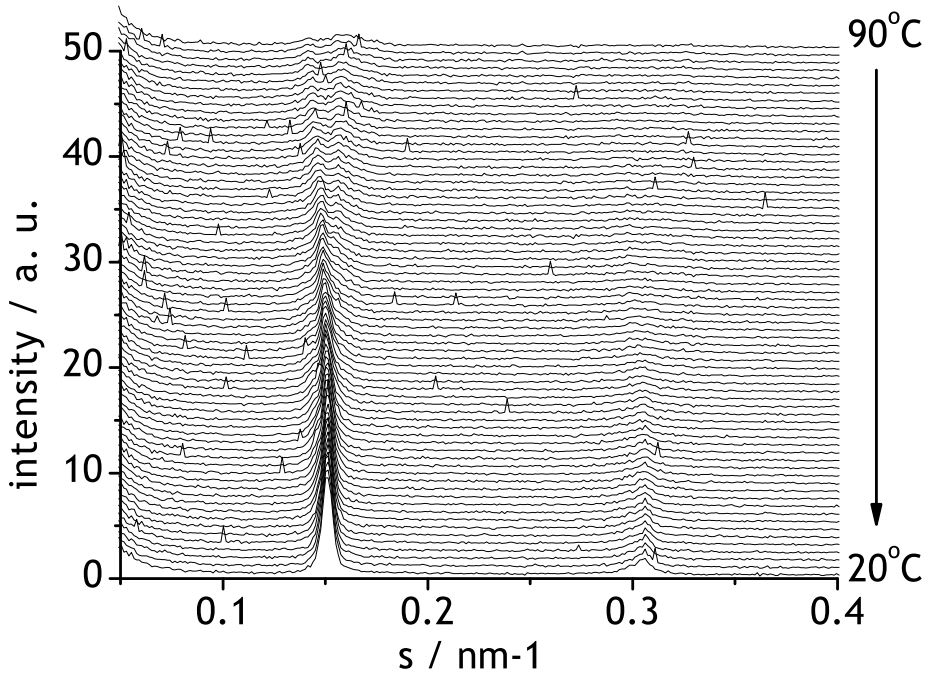

Figure 3.10: Diffraction patterns of the sample labeled p200 during the cooling from 90 to 20°C. Notice the phase separation at high temperatures.

The next set of samples, *c50*, *c150* and *c200* with lipid:melittin ratios 50, 150 and 200, respectively, supports this hypothesis (Fig. 3.11). Sample *c150* is in the first stage, a superficial peptide adsorption, low level of disorder in the lipid packing and a resulting small increase in the lattice parameter. Samples *c50* and *c200* had a longer equilibration time (few days instead of a few hours) and are in the second stage, where the peptide penetrated deeper into the membranes and caused more undulations and a larger increase in the mean bilayer spacing. With the large bilayer spacing, the intramembrane forces are weaker and allow a further widening of the gap between adjacent bilayers with increasing temperature.

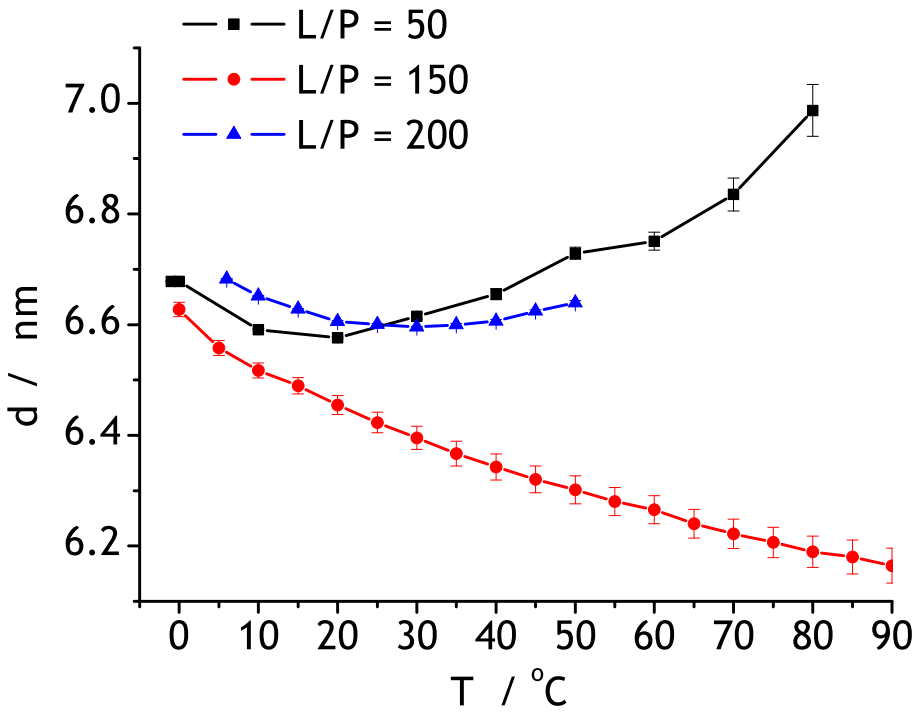

Figure 3.11: Lattice parameters of POPC membranes with melittin in the third set of samples. The POPC to melittin ratios, L/P, are indicated in the picture.

3.3.1 Model of the antimicrobial peptide interaction with PC membranes.

From the findings described in the previous sections, we can now construct a model for the peptide-membrane interaction. It applies to peptides similar to alamethicin and melittin and PC membranes (Fig. 3.12). The whole process of the peptide insertion into the membranes is continuous rather than stepwise and the important factor is time and possibly the number of the heating-cooling cycles to which the sample was subjected. In the early stages, the peptide adsorbs on the membrane surface and slightly perturbs it (Fig. 3.12b). Each molecule makes a small depression in the membrane, so the bilayers are no longer perfectly flat and parallel and they are forced to increase the spacing between them. Later, the peptide penetrates deeper into the membrane, probably to the polar-apolar interface (Fig. 3.12c). The lipid packing is now significantly perturbed and the membranes strongly undulated, so the bilayer spacing increases even more. The undulations get more pronounced at higher temperatures, so the lattice parameter increases with increasing temperature.

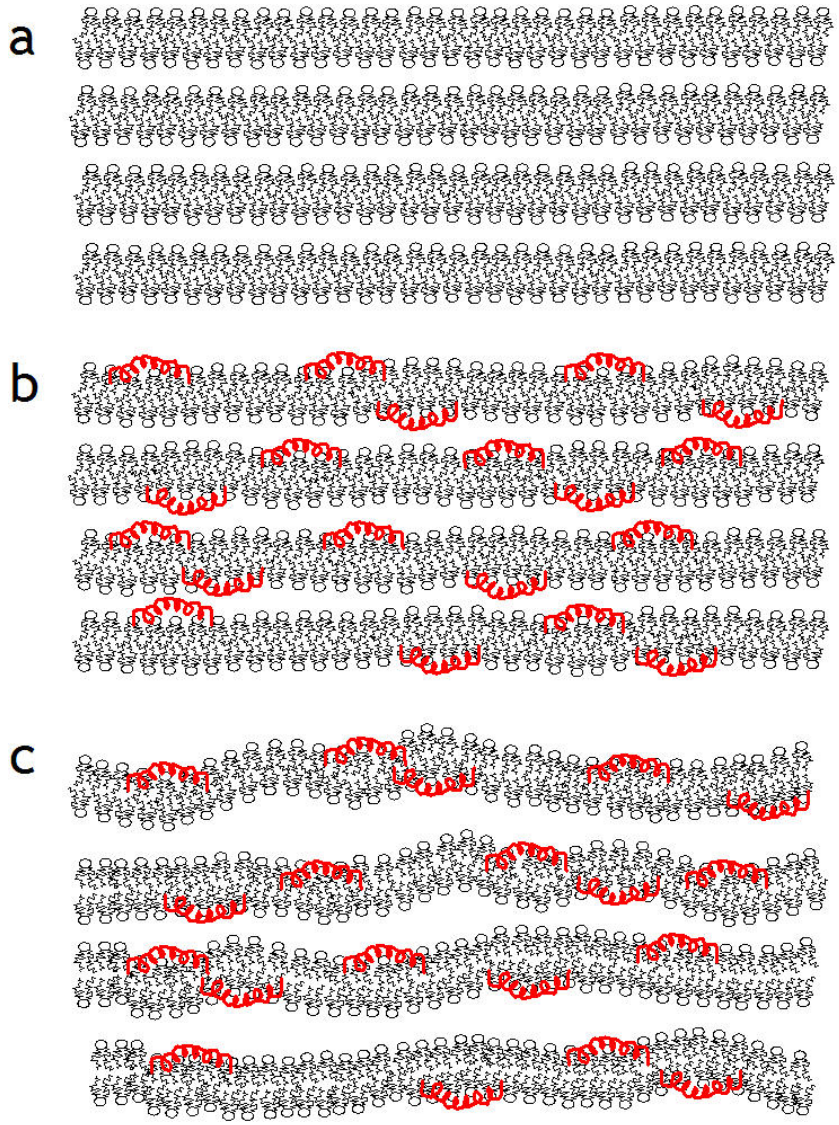

Figure 3.12: Stages of peptide-PC membrane interaction. a - A stack of peptide-free PC membranes - the membranes are flat and parallel. b - Peptide adsorbed on the membrane surface - the membrane flatness and the stacking are perturbed slightly. The lattice parameter is slightly larger. c - The peptide has penetrated to the polar-apolar interface and causes strong membrane undulations. The lattice parameter is larger and the quality of the stacking reduced.

3.4 Melittin and POPE thermal phase behaviour

Melittin added to POPE membranes influences the dimensions of its original lattice parameters and induces the formation of new phases; the cubic phases Im3m and Pn3m. The characteristics and the thermal behaviour of the phases in the POPE-melittin mixtures yields information about the interaction of the peptide with the membranes, about its position in the membrane and about the insertion process. In this section the influence of melittin on the dimensions of the original POPE phases, the newly formed cubic phases and their topology, and finally the mutual influences between all the present phases are presented.

3.4.1 Influence of melittin on the original POPE phases

In a typical experiment, the POPE-melittin mixtures were heated from 5 to 85°C, incubated at 85°C for 10 minutes, cooled back to 5°C and again incubated for 10 minutes. The typical heating rate was 1°C/min. The start and end temperatures varied by plus-minus 10°C and the incubation times by plus-minus 10 minutes in some measurements. The response of most samples to changes in temperature was not immediate, the lattice parameters continued to change during the first few minutes of the incubation time (Fig. 3.13). As a result, there is always a slight hysteresis in the plots of the lattice parameters vs. temperature. The temperature response of the lamellar and the hexagonal phases was quite fast, so the hysteresis was not very large. The temperature response for the cubic phases was much slower and in one case, the lattice parameter changed by 0.50 nm during a 20 minute incubation time. The reason for the temperature lag will be described later.
For pure POPE, the usual heating rate of 1°C/min was slow enough and we did not observe any change in lattice parameter once the sample reached the temperature of the incubation time (Fig. 3.13). Here, the hysteresis in the plot of the lattice parameters vs. temperature is due to the difference in the actual temperatures during data taking. The diffraction pattern was always recorded during the last 10 or 15 seconds of each minute. The "official" temperature assigned to that diffraction pattern was the one reached at the end of the given frame. Consequently, the real temperature for the patterns recorded during heating is always slightly lower than the "official"

temperature, while during the cooling the real temperature is always slightly higher than the "official" temperature.

During heating from 5 to 85°C, fully hydrated POPE membranes go from

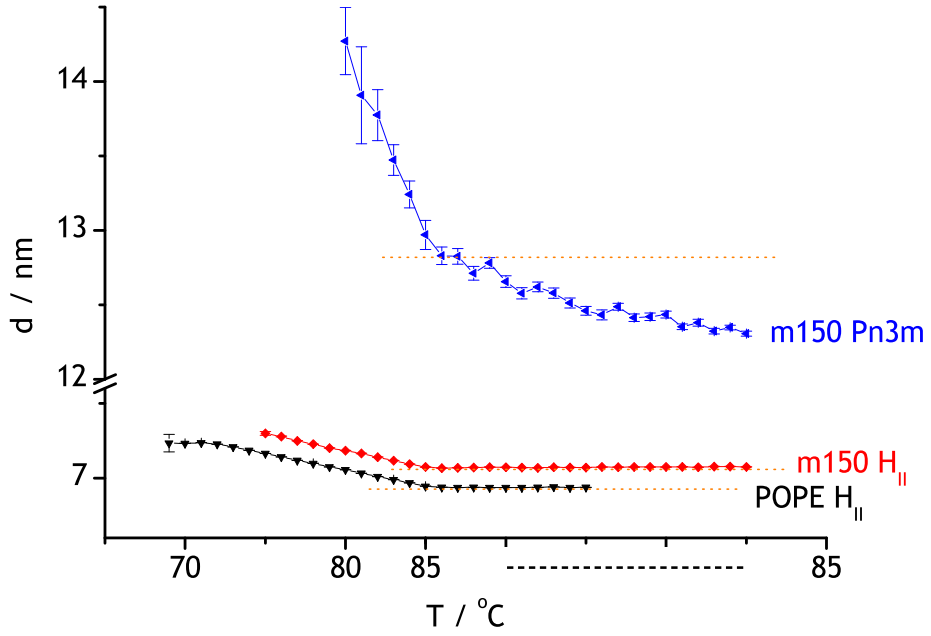

Figure 3.13: Kinetics of the change in the lattice parameter of different phases during heating. The temperature on the x-axis is the temperature reached at the end of each frame. The dotted line marks the value of the lattice parameter reached at the beginning of the incubation time. The time between two experimental values is always one minute.

the gel lamellar to the fluid lamellar phase at 22°C and from the lamellar to the hexagonal phase at 75°C. POPE membranes with melittin go through all the original POPE phases - L_β, L_α, H_{II} and the phase transitions are at the same temperatures, although the phase dimensions change. Eventually, all lattice parameters became smaller than their pure POPE counterparts and the values during cooling were smaller than those during heating (the reasons for this were discussed in the previous paragraph). This kind of thermal behaviour means that the sample has reached equilibrium, so the phases

observed during heating are the same as those during cooling. They have the same composition (concentration of melittin incorporated in the membrane) and the same packing of lipid and melittin molecules. This equilibrated state was mostly not observed during the first measurement of the sample and until it was reached, the lattice parameter values during cooling were larger than those before, or were even larger than the values in pure POPE.
The decrease of the lattice parameters with respect to POPE was accompanied by an increase of the area per molecule in the gel phase. These two findings suggest that the decrease in the lattice parameter is due to the decrease of the bilayer thickness, induced by the insertion of melittin molecules between the lipid headgroups, pushing the lipid molecules farther apart. The resulting free space in the chain region is compensated by a higher number of *trans-gauche* isomers, so the chain length, and at the same time the bilayer thickness, decreases.
The evolution to equilibrium can be followed on several examples of samples measured repeatedly. The sample labeled *mm* containing 0.031 mM melittin at L/P = 1000 was measured first during two heating-cooling cycles and again during one cycle after 12-month storage at 4°C. The lattice parameters are shown in figure 3.14. In the gel phase, the lattice parameter increases during the first two cycles. The area per molecule is more or less constant (Fig. 3.15). In the third cycle, the lattice parameter is significantly smaller, although it increased again during cooling, and the molecular area is larger than previously. The lattice parameter of the fluid lamellar phase behaves similarly to that of the gel phase. In the hexagonal phase, the decrease with respect to the POPE values is visible already during the second cooling. The transient increase in lattice parameters before they reach the final values, smaller than POPE, indicates that the insertion of melittin into the POPE bilayer is not immediate. As in the case of the interaction of melittin with POPC, the peptide might initially adsorb on the surface of the bilayer and only later penetrate deeper inside to the polar-apolar interface and cause membrane thinning. The position of melittin in the membrane might change at phase transitions, so not all the phases reach equilibrium at the same time.

Another example of the equilibration process is the sample labeled *pe30*, with a much higher melittin concentration of 0.458 mM at L/P = 30 (Fig. 3.16). The higher concentration of melittin does not result in a faster equilibration process. The initial values of the lattice parameters are considerably larger than those of POPE, because the high number of adsorbed peptide molecules must have caused considerable perturbation of the membrane flat-

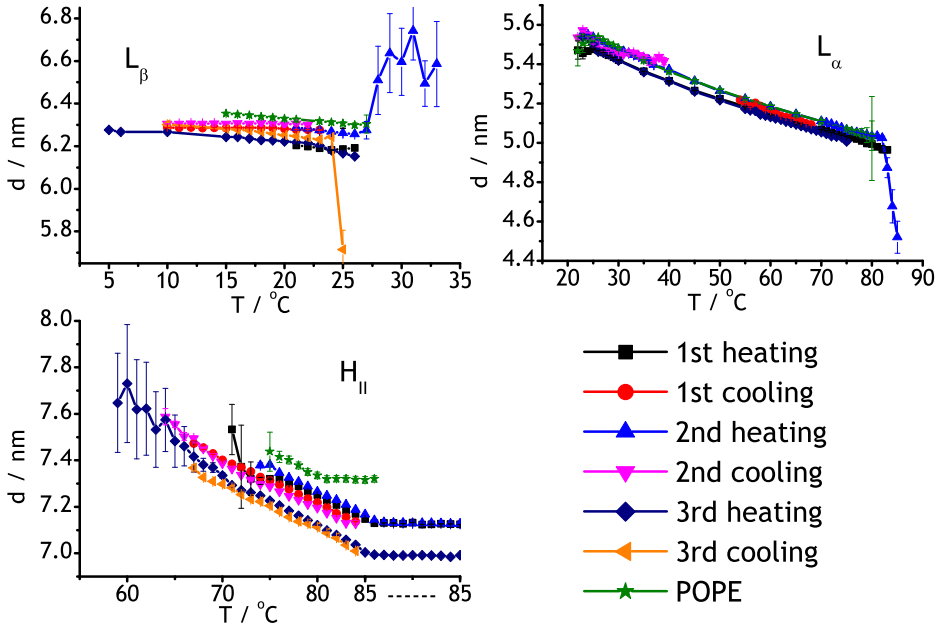

Figure 3.14: Sample *mm* - evolution until equilibrium. Lattice parameters of L_β, L_α and H_{II} during three heating-cooling cycles.

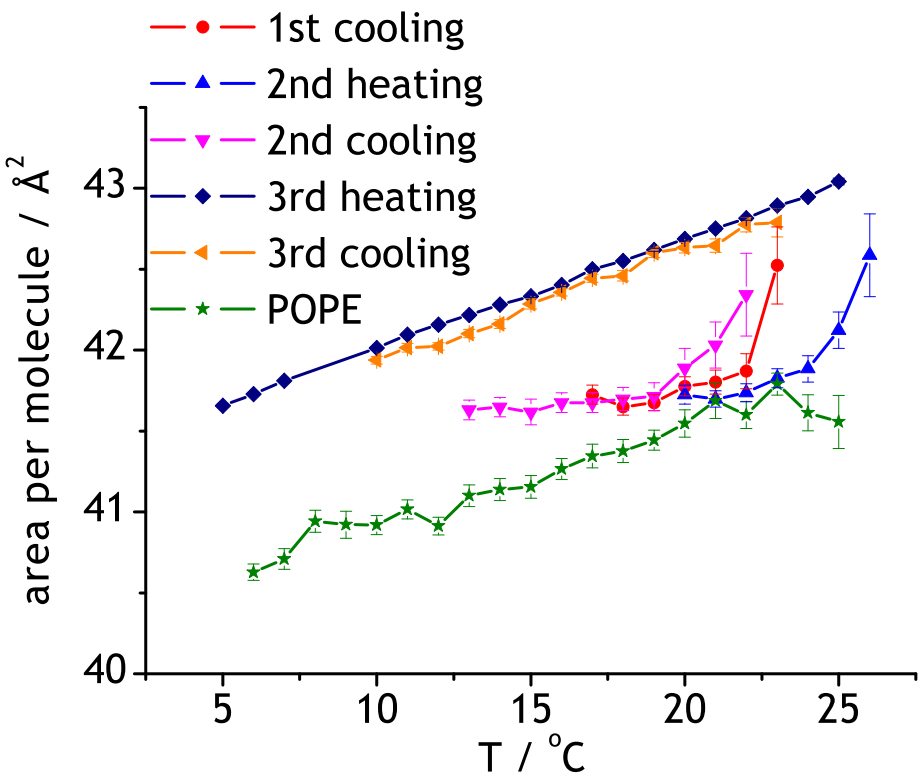

Figure 3.15: Sample *mm* - evolution to equilibrium. Area per molecule in the gel phase during three heating-cooling cycles.

ness and stacking. In the second heating five months later, the lattice parameters already fell to the level of the POPE values or slightly below.

Yet another example is the sample labeled *m150* at 0.127 mM melittin and

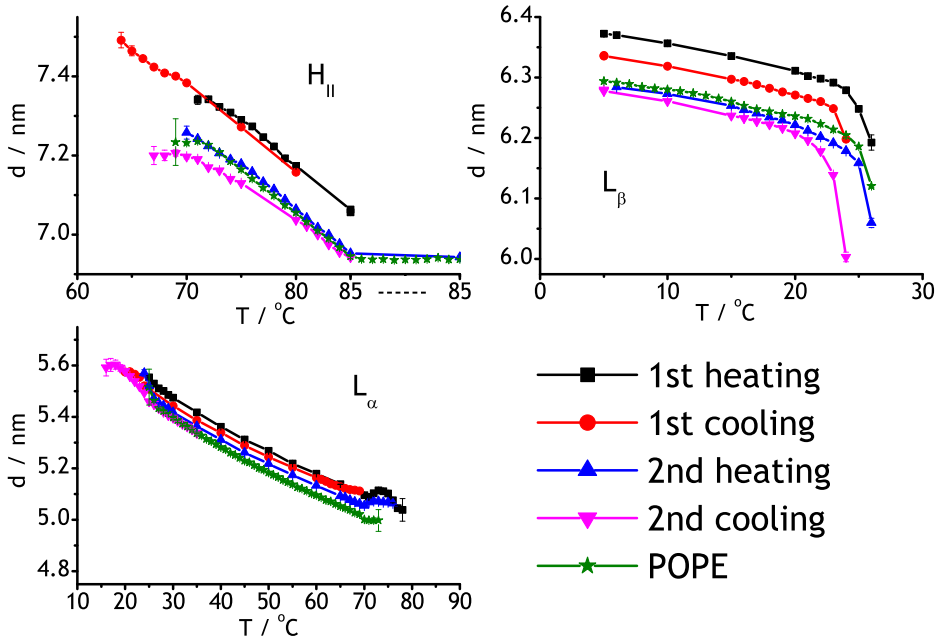

Figure 3.16: Sample *pe30* - evolution to equilibrium state. Lattice parameters of L_β, L_α and H_{II} during two heating-cooling cycles.

L/P = 150 (Fig. 3.17), measured twice. While the hexagonal phase seems equilibrated already during the first heating, the lamellar phases move in that direction only during the second cooling.

In two cases, in the samples labeled *m200* with L/P = 200 and *m50* with L/P = 50, we observed phase separation in the lamellar phase during heating. The second phase had a larger spacing and its appearance was accompanied by a drop in the intensity of the original lamellar peak. The combined intensity of both peaks did not reach the original value. The new phase was probably induced by penetration of more melittin molecules from the bulk solution into the outer layers of the liposome.

The usual procedure for sample preparation was to mix the melittin solution

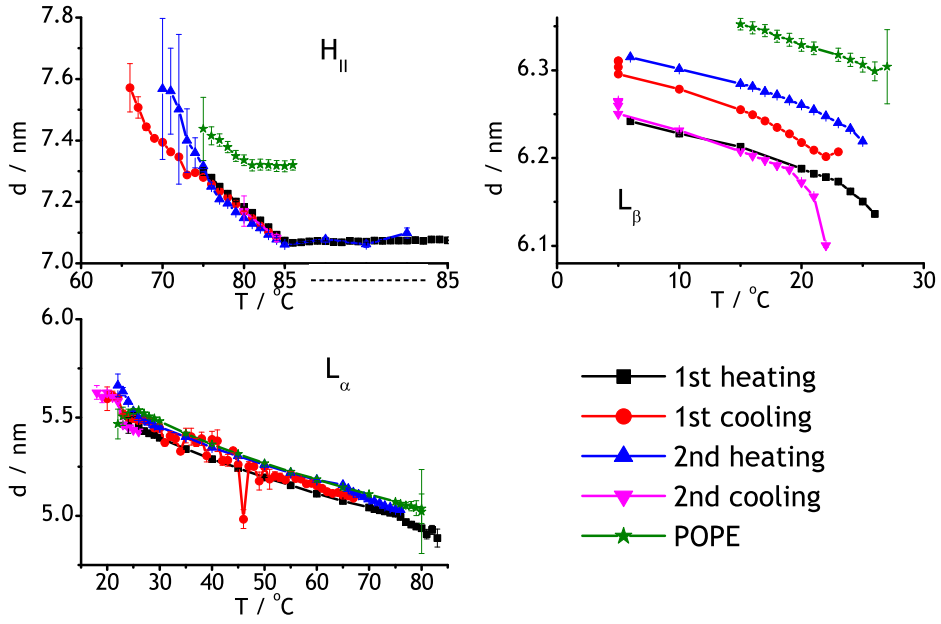

Figure 3.17: Sample *m150* - evolution to equilibrium state. Lattice parameters of L_β, L_α and H_{II} during two heating-cooling cycles.

with the lipid in the fluid phase and let the mixture go through at least three heating-cooling cycles. The sample tube was also shaken and vortexed in order to mix the sample properly. The sample labeled *m100* with L/P = 100, though, was mixed with the lipid in the gel phase, directly put into the sample holder and measured. The resulting SAXS scattering patterns are shown in Fig. 3.18. During the heating, we can see a strong gel lamellar first-order

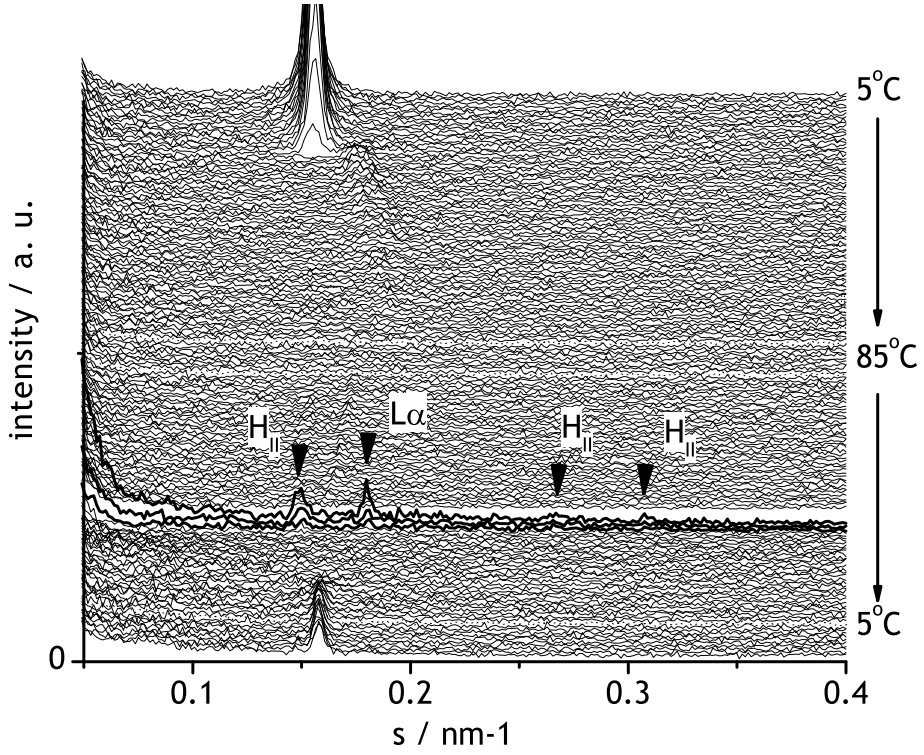

Figure 3.18: Sample *m100*. SAXS scattering patterns on heating and cooling from 5 to 85°C. The arrows mark the peaks arising from the lamellar and hexagonal phases.

peak that is replaced by a very weak first-order fluid lamellar peak. During the cooling, we can discern only four peaks around 35°C (marked by arrows in Fig. 3.18) and later the gel lamellar peak. The four peaks can be indexed as the first-order fluid lamellar and the first three hexagonal peaks, (10), (11) and (20). Another batch of the sample was measured during heating from

5 to 35°C and one month later during heating and cooling from 5 to 85°C. All patterns are of low quality because of a poorly ordered structure in the sample, but we can still identify the phases and their evolution immediately after the mixing with melittin. The lattice parameters are shown in Fig. 3.19. During the first heating, the lattice parameters of the gel and the fluid

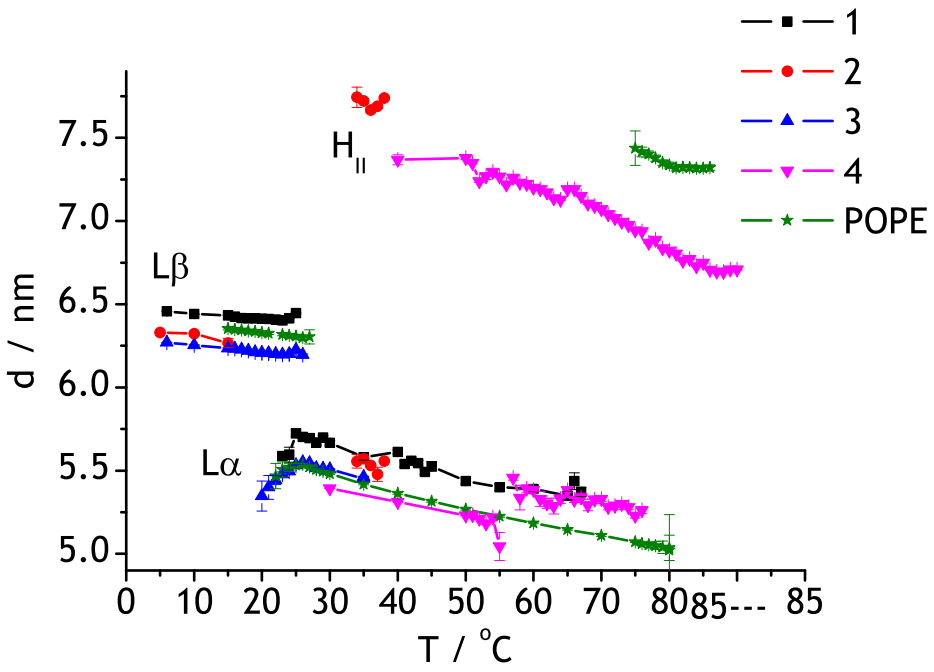

Figure 3.19: Lattice parameters in the sample *m100* during 3 measurements. 1, 2 - 1st heating and cooling, 3 - measurement with another batch of the sample, 4 - the same batch as in 3, measured one month later.

lamellar phases were larger than those of POPE. The sudden decrease in the intensity of the peaks and finally their complete disappearance suggest that melittin broke up the membranes into micelles. Still, a small part of the membranes preserved a periodically ordered structure and we can catch a glimpse of it for a short moment during the cooling (the peaks marked by arrows in Fig. 3.18). They are visible only for a short time, because the thermal convection moves the pieces of membranes inside the sample holder,

so the beam does not always hit them. The presence of the hexagonal phase at such a low temperature is surprising. Most studies reported an increase in the lamellar to hexagonal phase transition temperature [71]. In the gel phase, the membranes reconstituted, this time with a smaller lattice parameter. For the second heating, the sample holder was refilled from the stock sample that was stored at 4°C for one day. Again, we observed strong and sharp peaks in the gel phase and weak peaks in the lamellar phase. Both lattice parameters were smaller than previously. The third measurement of *m100* was made one month later and we see a further decrease of the lamellar lattice parameters. The measurement was started at 30°C with the hexagonal phase already present. Its lattice parameter was considerably lower than in other samples throughout the entire temperature range. The lamellar phase disappeared at 55°C, at an unusually low temperature, but another low intensity peak continued until 76°C (labelled Lαx in Fig. 3.20). The peak probably belongs to a lamellar phase with a larger spacing, similar to the one observed in the very first heating of *m100*. The scattering pattern is of very low quality, but we could still identify three other peaks that seem to arise from a cubic phase, judging by their thermal behaviour and position, although we cannot index them (Fig. 3.20).

All samples prepared in the usual manner are monophase at the beginning of the measurement and the lattice parameters have changed with respect to POPE. This is the evidence that melittin has crossed the bilayers and distributed equally in all layers of the liposomes. The usual manner of sample preparation involves incubation of the sample at temperatures above the main phase transition. The thermal behaviour of the only sample where this was not done, *m100*, suggests that melittin can only cross a lipid membrane easily in the fluid state. In the gel state, the process is slow and the results are visible only after longer storage. Moreover, it seems that rather than translocating through the intact bilayer, melittin breaks up most part of the bilayers into micelles and these later reconstitute into multilamellar structures, as has been observed for the sample labeled *m100* (see above). This hypothesis is supported by the thermal behaviour of the sample labeled *m200*. This sample was prepared in the gel state, but after mixing the POPE and melittin solutions, it was incubated for 1 hour at 35°C. The scattering patterns had a normal intensity and show the usual phase sequence of POPE-melittin mixtures.

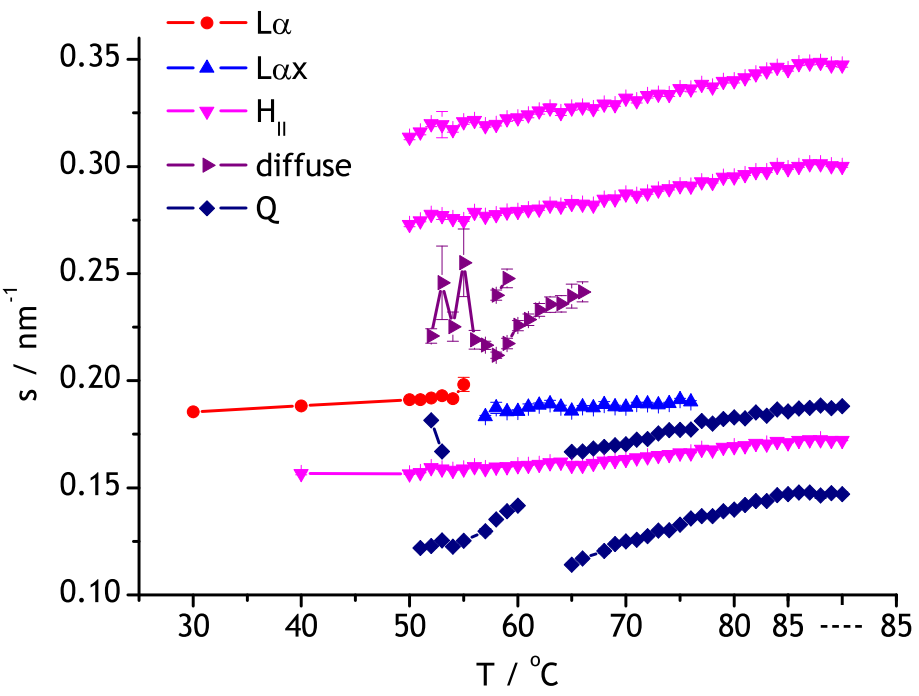

Figure 3.20: Sample *m100*, peak positions during the third heating. Peak labelled Lαx is a low intensity peak observed after the disappearance of the first-order fluid lamellar peak. Peaks labeled as Q probably arise from a cubic phase.

Mixed POPE-POPG membranes

To simulate a bacterial membrane mixed POPE-POPG membranes were prepared with a POPE:POPG molar ratio of 4. These membranes bear a negative charge and because of their mutual repulsion form unilamellar liposomes. However, mixed with melittin at L/P = 100, they reconstitute into multilamellar structures due to the charge screening provided by the peptide bound to the headgroup region. The resulting phase diagram is similar to that of POPE membranes with melittin (lattice parameters shown in Fig. 3.21). The hexagonal phase does not form, because the mean headgroup cross section in the mixed membrane is too large. Only one cubic phase was observed, Im3m. Its dimensions and thermal behaviour are nearly identical to the Im3m phase observed in POPE-melittin mixtures (see below). Interestingly, the lattice spacing in the gel phase is smaller than usually seen in POPE-melittin mixtures, while the fluid phase spacing is even larger than in pure POPE. This suggests that melittin binds in a different way to the mixed POPG-POPE membranes than to POPE membranes, at least in the fluid phase. The bilayer spacing in the gel phase is close to the short-lived peak occasionally seen during the gel to fluid transition (e.g. in the sample with L/P = 100, whose lattice parameters are plotted in Fig. 3.22). The reason for the large lattice spacing in the fluid phase might be an increase in the membrane thickness, because melittin screened the lateral electrostatic repulsion between the lipids and allowed them to move closer together. This mechanism was proposed by Li and Salditt [62] who observed membrane thickening in DMPG-alamethicin mixtures. The interaction is probably driven more by electrostatic attraction than by the need to bury the hydrophobic parts of melittin inside the membrane. Also, a second peak is present in the gel phase, roughly at half the s value as the first-order gel peak. The two peaks do not seem to belong to the same structure, because with increasing temperature, they move in opposite directions. This might be a highly swollen lamellar phase with a small amount of melittin, so not enough charge screening is produced and the neighbouring membranes cannot approach closer to each other.

In the sample prepared at L/P = 1000, the charge screening between the membranes produced by the adsorbed melittin was insufficient, and the unilamellar liposomes did not transform into a multilamellar structure.

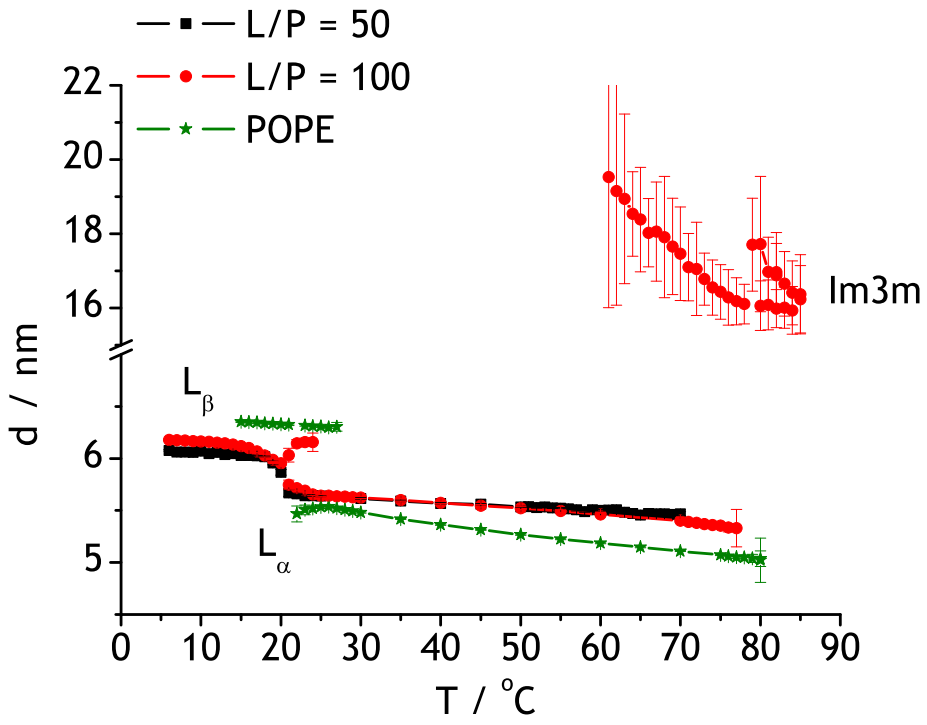

Figure 3.21: Lattice parameters of the phases induced by melittin in mixed POPE/POPG = 4:1 membranes. The lipid to peptide ratios are indicated and the lattice parameters of pure POPE are plotted for comparison.

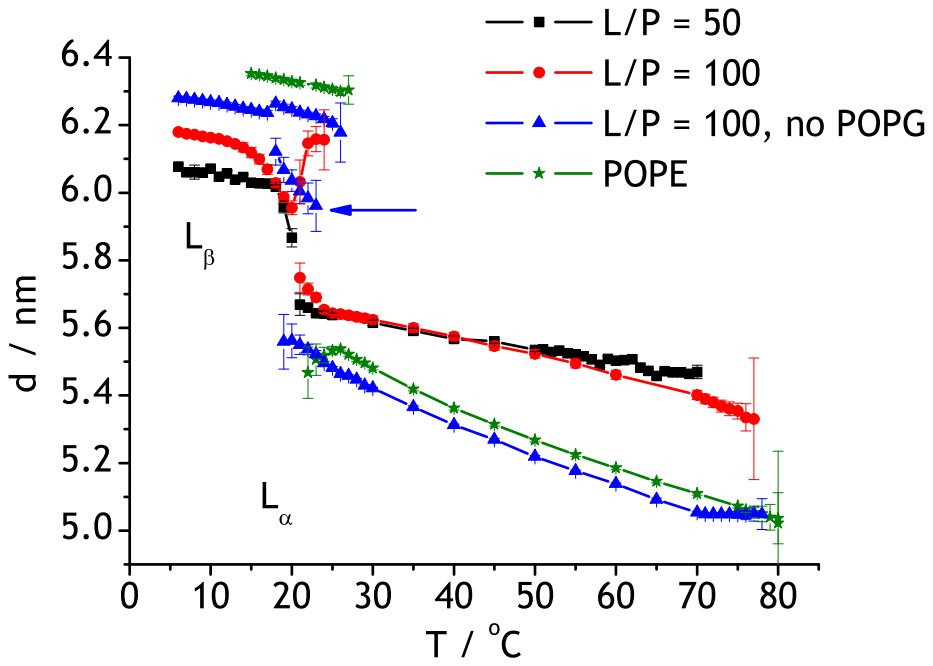

Figure 3.22: The lattice parameters of the lamellar phases in the mixed POPE/POPG and POPE membranes with melittin. The lipid to peptide ratios L/P are indicated. The gel lamellar lattice spacing in POPE/POPG-melittin mixtures is close to the transient gel phase seen in some POPE-melittin mixtures (the blue triangle sequence marked by an arrow).

Cubic phases

In addition to changing the dimensions of the original POPE phases, melittin induced the formation of cubic phases in the POPE membranes. They usually formed together with the hexagonal phase or later during its existence and lasted until the sample returned back to the gel phase during cooling. Usually, two coexisting phases formed, Im3m and Pn3m, with different relative intensities in different samples. Their dimensions and thermal behaviour were influenced by the coexistence with other phases. Despite a wide variety of melittin concentrations (0.458 mM - 0.031 mM) and lipid-peptide ratios (30 - 1000), the resulting cubic phases had very similar dimensions and thermal behaviour (Fig. 3.23). Also the cubic phase formed in the mixed POPE/POPG = 4:1 membranes had practically the same lattice parameters (Fig. 3.24). A different thermal behaviour was found when the sample was heated and cooled with a lower heating rate, at 0.5°C/min (Fig. 3.25), but the dimensions were still very similar. Such a similarity and the mutual influences of all the observed phases can be explained by the onion vesicle model [64].

A bicontinuous cubic phase is constructed from saddle surfaces, such as those shown in Fig. 2.8 in Chapter 2. The triply periodic minimal surface at the midplane of the bilayer has a negative Gaussian curvature. All the planes parallel to the minimal surface have a smaller area than the minimal surface, so both monolayers constituting the cubic phase are curved towards water. If mixed POPE-melittin membranes adopt a cubic phase, it suggests that their mean lipid headgroup area is smaller than their mean lipid chain area. However, the principal curvatures of the cubic membranes are lower than those of the POPE hexagonal phase which means that the difference in the mean headgroup area compared to the mean chain area is smaller in the cubic than in the hexagonal phase. These two findings indicate that melittin is located in the headgroup region of the POPE bilayer. The insertion of melittin has increased the mean POPE headgroup area, but still the mean headgroup and chain areas are not equal, so the membranes have to adopt a non-lamellar phase.

The lattice parameters of the cubic phases Im3m and Pn3m maintain a ratio close to the theoretical prediction 1.279 through their whole existence. The ratio is predicted for the lattice parameters of two cubic phases at the moment of their phase transition and is related to the transformation of the triply periodic minimal surfaces that run through the bilayer centre of the

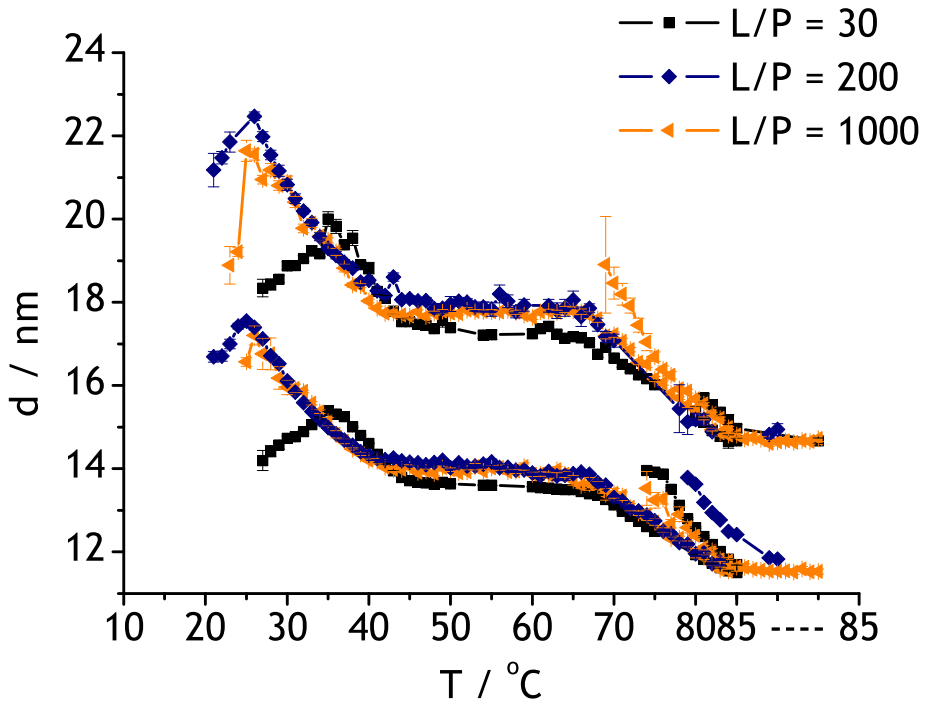

Figure 3.23: Dimensions of cubic phases are very similar over a wide melittin concentration range. Lattice parameters of cubic phases during heating and cooling are shown, the lipid to peptide ratios are indicated.

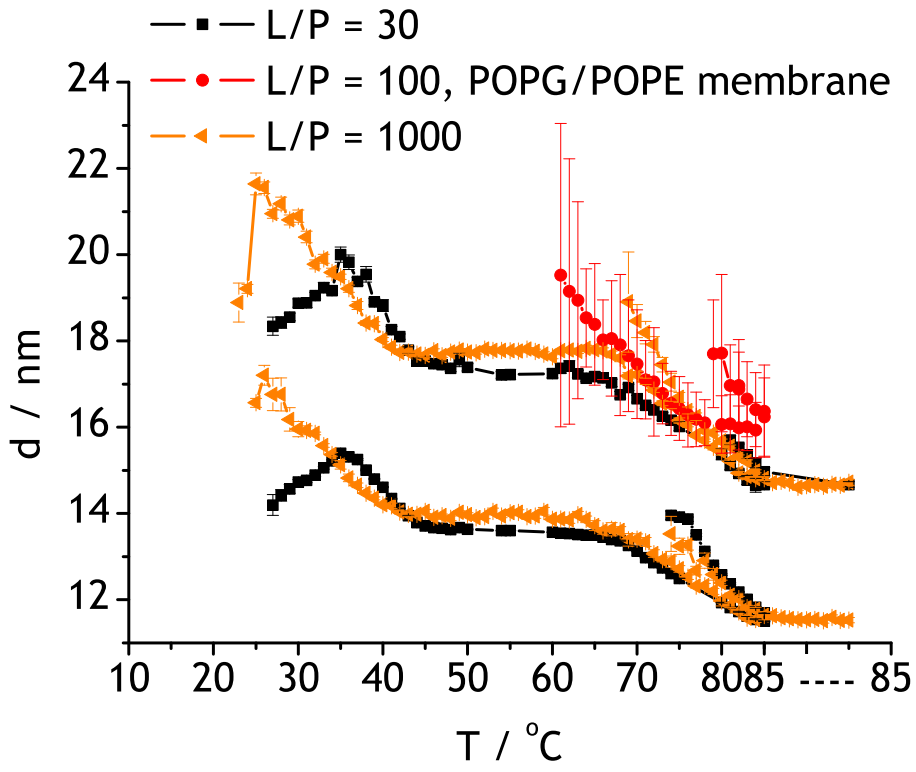

Figure 3.24: Melittin induced nearly identical cubic phases in POPE and mixed POPE/POPG = 4:1 membranes. Lattice parameters of cubic phases during heating and cooling are shown, the lipid to peptide ratios are indicated.

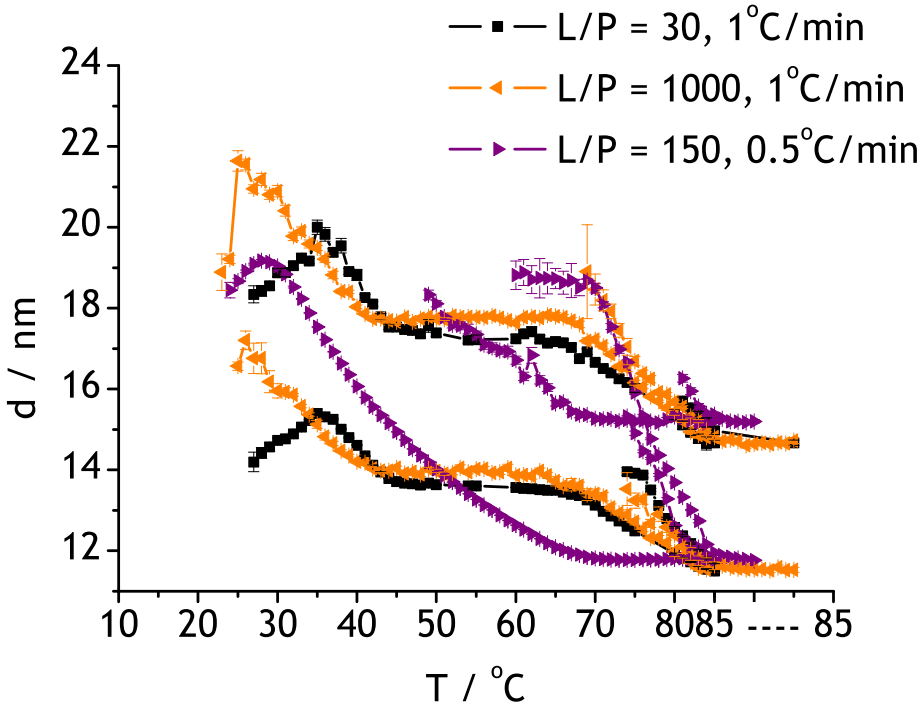

Figure 3.25: Thermal behaviour of the cubic phases depends on the heating rate. Lattice parameters of cubic phases during heating and cooling are shown, the lipid to peptide ratios and the heating rates are indicated.

cubic structures. The transformation of the minimal surfaces proceeds without topological changes, i.e. the angles, areas and distances on the triply periodic minimal surfaces are preserved. Real cubic-cubic phase transitions do not proceed in this way, because it would involve breaking and crossing of the membranes. Rather, they occur by pulling away or merging of the junctions of the water channels and at the same time a change in the shape and rescaling of the unit cell. Throughout the whole transformation, the bilayer midplane is a minimal surface. For very thin bilayers with respect to the radius of curvature, such a transformation proceeds with no measurable enthalpy change, because the bilayer is not torn and the initial and final structures have the same bending energy [5], [63].

In most cases, the cubic phases develop together from the lamellar and/or hexagonal phase, and do not transform into each other. The development of the cubic phases from the lamellar phase begins by the formation of stalks between adjacent bilayers which later, at sufficient bilayer tension, break to form channels and later a disordered bicontinuous structure - a maze of bilayer channels without global symmetry [64]. This results in broad diffuse scattering in the diffraction pattern, as was often observed in our samples before the appearance of the cubic peaks. The disordered maze of lipid channels finally develops into a bicontinuous cubic phase. A multilamellar vesicle with the cubic phase inside is called an onion vesicle. The disordered bicontinuous structure develops first in the inside of the multilamellar vesicles where the curvature is the highest and later the whole liposome turns into a cubosome - the equivalent of a multilamellar vesicle formed by cubic phases [64]. The constant ratio of the lattice parameters of the cubic phases in the POPE-melittin mixtures indicates that they both develop inside each vesicle by a series of topology conserving transformations from the same disordered bicontinuous structure. Later, they are bound together in the same cubosome which constrains their thermal evolution and makes them change in a cooperative way. The growth of a new phase or changes in the dimensions of an already existing phase influences all the other phases in the cubosome or the onion vesicle. Changes in the course of growth of the cubic phases were observed each time the hexagonal phase disappeared during cooling or the lamellar phase appeared (Fig. 3.26).

The differences in the course of the cubic lattice parameters during cooling depend on the presence or absence of the fluid lamellar phase and the existence of an epitaxial relationship between the hexagonal and cubic phases. After the disappearance of the hexagonal phase, the released lipid has to be

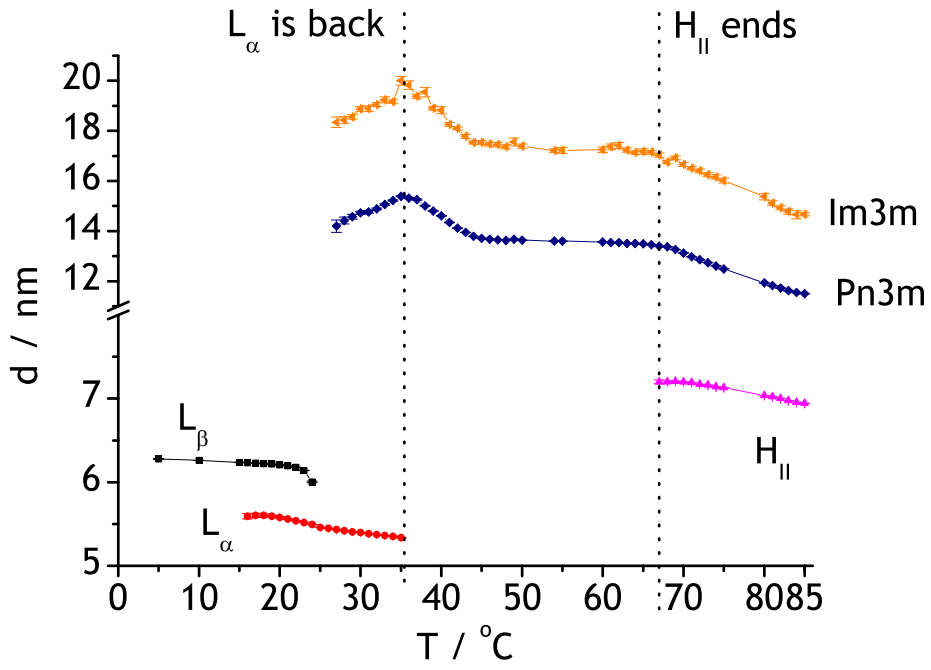

Figure 3.26: Lattice parameters during the cooling in the sample *pe30*, L/P = 30. Note the changes induced in the lattice parameters when a new phase appears or a phase disappears.

incorporated somewhere. If it is taken up by the lamellar phase, the cubic phase does not have the capacity to grow, so the expansion of the lattice parameter stops. If the released lipid is taken up by the cubic phase, the incorporation of the lipid sometimes perturbs the structure of the phase, so the cubic peaks broaden or disappear into the diffuse scattering for a certain time. If the dimensions of the cubic and hexagonal phases are not epitaxial, the transport of lipid from one phase into the other is complicated and a rebuilding of the cubic phases might be necessary. The released lipid organizes into different cubic phases that have an epitaxial relationship to the hexagonal phase. These new cubic phases later absorb the lipid from the initial cubic phases. Similarly, when the lamellar phase forms again during cooling, it draws the lipid from the cubic phases and they start to decrease their dimensions. Different ways of reorganization of the cubic phases will be discussed in more detail in the following subsection.

The thermal behaviour described above is valid for samples heated at 1°C/min. A few of the samples were heated at 0.5°C/min and their thermal behaviour was different. First, Im3m tended to prevail over Pn3m. This is related to different water contents of the two cubic phases as discussed below. Second, in sample labeled *m150* the course of the cubic lattice parameters was reversed. They were constant during the coexistence with the hexagonal phase and expanded afterwards. The only feature that was conserved was that the appearance of the lamellar phase caused shrinkage of the cubic phases.

In sample labeled *mm* with a very small amount of melittin, the cubic phases in the first measurement formed with lattice parameters about 2 to 3 nm larger than in other samples (Fig. 3.27). They went through the usual expansion during coexistence with the hexagonal phase and entered the constant lattice parameter stage, but did not recover the expansion later. However, the lattice parameters just before the cubic-lamellar transition were similar to those seen in other samples. Such dimensions of the cubic phases might be necessary for an epitaxial relationship between the cubic and the lamellar phase, a requirement for the cubic-lamellar transition. Interestingly, two peaks from the cubic phase were still visible in the gel state and at the beginning of the following second heating.

The slow temperature response of the cubic phases has already been mentioned. This is due to the large amount of water and lipid that need to be displaced during the growth of the phases. The cubic phases consist of lipid channels filled with water. When the phases change their dimensions, not only the lipid has to rearrange, but also large volumes of water have to flow

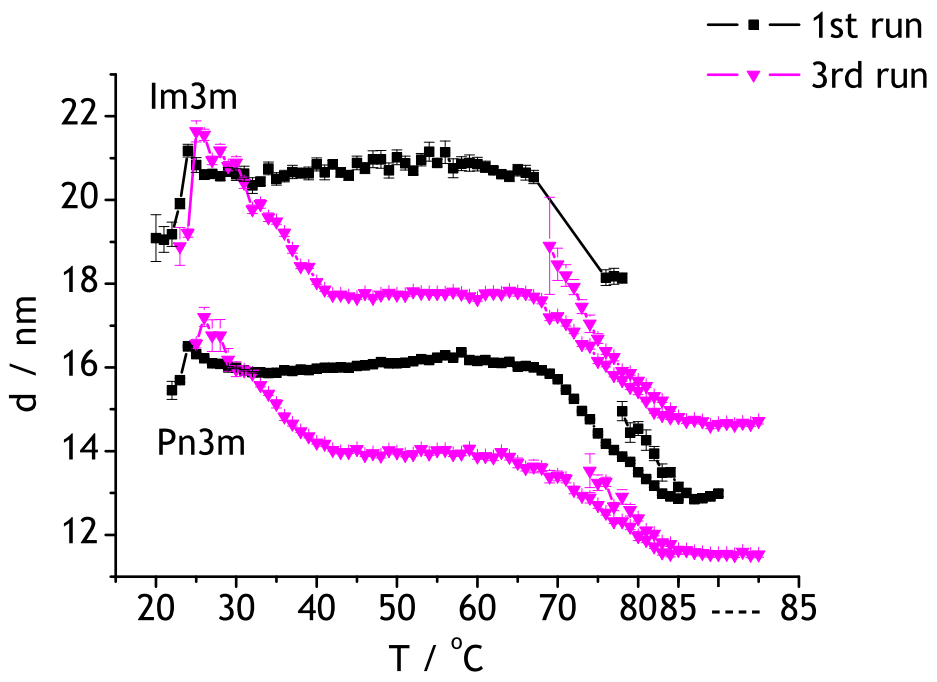

Figure 3.27: Lattice parameters of the cubic phases in the sample *mm* during the first and the third measurement.

in or out because the diameter of the water channels changes. The lipid channel walls are very thin, so water forms a substantial fraction of the cubic phase. The speed of water flow is probably the step-limiting process.
The water content of the bicontinuous cubic phases differs. The phase with the most water is Im3m, then Pn3m and the phase with the least water content is Ia3d [63]. The difference in the water content might be responsible for the proportion of a given phase in a sample. The proportion of each cubic phase differed in each sample and even changed within one sample in different heating-cooling cycles. When the arrangement of the phases in the sample is such that water can flow rapidly in and out of the vesicle or when the heating rate is slower, the amount of Im3m prevails over Pn3m. During the formation of the cubic phases, water flows into the lipid mass and after the cubic phases transform into the lamellar phase, a large amount of water is released from the membranes. The water flux is limited by the phase on the surface of the onion vesicle. A pure cubic vesicle absorbs water in a different way, probably faster, than a vesicle with a lamellar phase on the outside.
We can estimate the proportion of a given phase in the sample from the integral areas of the peaks. The peak area depends primarily on the electron density and so on the structure factor, but the dimensions of the cubic phases change synchronously and so do their structure factors. In the samples heated at 1°C/min, Pn3m tends to prevail over Im3m. In the samples heated at 0.5°C/min, Im3m tends to prevail or both phases are equally intense. When the heating is slower, more water can penetrate into the sample in the same temperature interval, so more of the water-rich Im3m phase forms. However, in repeated measurements of the sample *m150* heated at 0.5°C/min, proportions of both cubic phases were equal in the first heating-cooling cycle while Pn3m dominated in the second and the third cycle (Fig. 3.28). Different phases coexisted in the sample in the three heating-cooling cycles. In the first cycle, the lamellar phase transformed directly into the cubic phases during heating, while in the second and third cycles the hexagonal phase coexisted with the cubic phases during a certain temperature interval. This has probably affected the speed of the water penetration into the vesicle. Also in the other samples where Im3m dominates over Pn3m, both phases form with equal intensity and Im3m becomes more intense only when the hexagonal phase disappears during cooling (Fig. 3.29).

Because of the special ratio of lattice parameters of Im3m and Pn3m, some of their peaks nearly coincide. During the early stages of the existence of a sample, the peaks are broader and these nearly coinciding peaks cannot

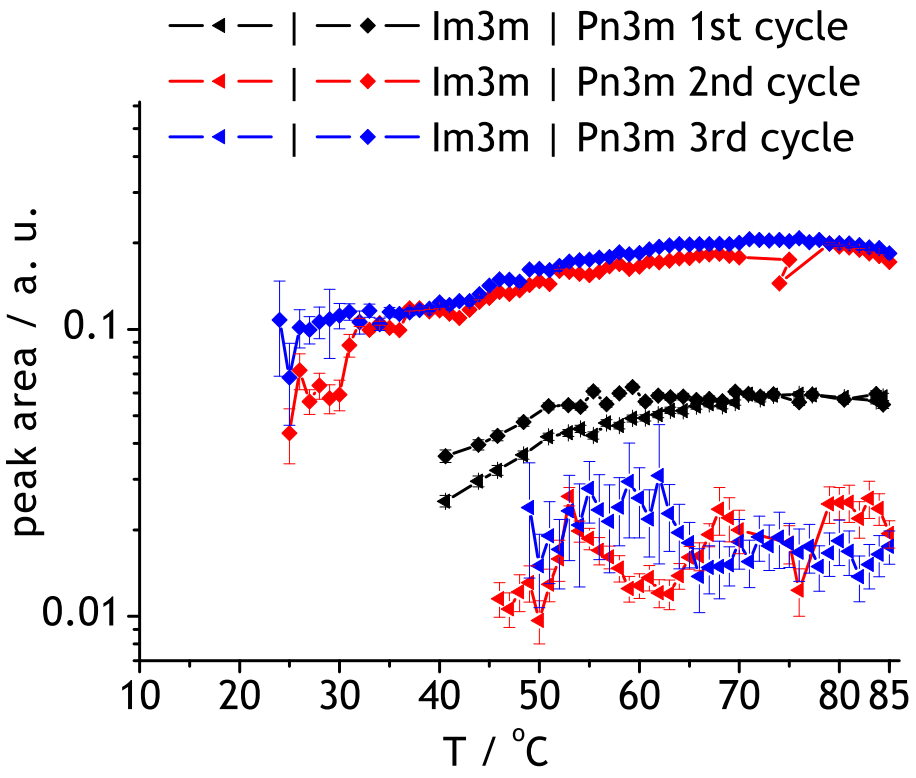

Figure 3.28: (110) peak areas of the cubic phases in sample labeled *m150* with L/P = 150 during cooling in three measuring cycles. The y-axis is a logarithmic scale.

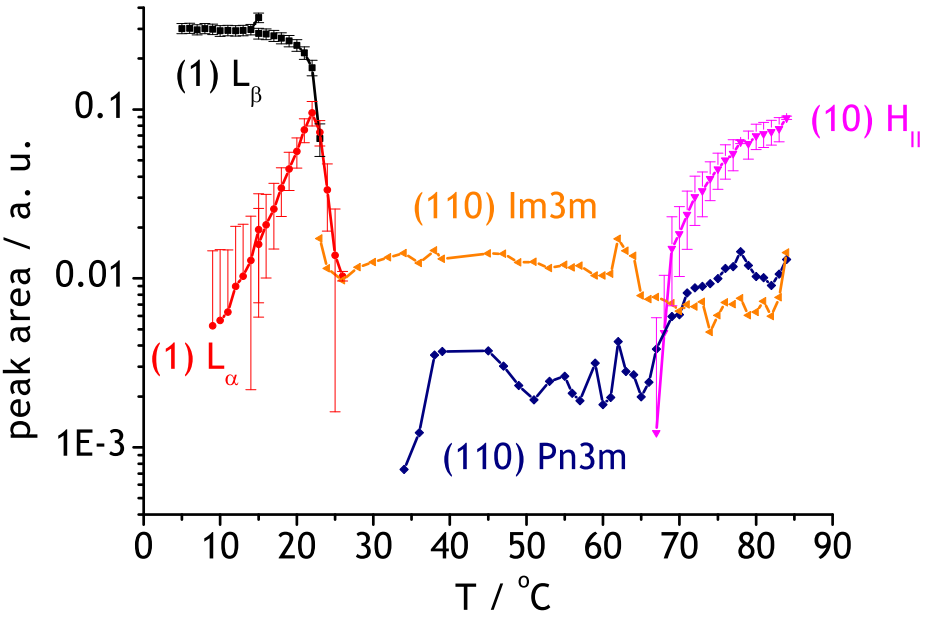

Figure 3.29: Peak area of the selected peaks in the sample labeled *bope150* with L/P = 150 during the cooling. Notice the growth of the Im3m (110) peak while the hexagonal peak disappears. The y-axis is a logarithmic scale.

be distinguished. Later, when the packing of the cubic structure improves, the peaks become narrower and fully resolved. This can be observed in the scattering patterns of the sample labeled *m150* which was measured in three consecutive cycles. In the first and the second cycles, there are a number of peaks which can be indexed as belonging to both phases (Fig. 3.30). In the third cycle during the cooling, all these peaks split into two and can be clearly assigned to one or the other phase (Fig. 3.31). The lattice parameters in the first and the third cycle are nearly identical. Table 3.1 shows peaks that overlapped during the first cooling, but were resolved later.

Im3m	Pn3m
(310)	(211)
(321)	(220)
(321)	(221)
(411)/(330)	(311)
(420)	(222)
(332)	(321)

Table 3.1: Overlapping Im3m and Pn3m peaks.

Interconversion of phases in the onion vesicle

The dimensions of the cubic phases do not vary much in samples of different composition. Partly, this is the result of the confinement of all phases into an onion vesicle and the resulting constraints that they impose on each other. When two phases transform into each other at a phase transition, the dimensions of the newly forming phase depend on the preceding phase. Certain scattering planes from the original structure also exist in the new structure. These epitaxial relationships are visible in the scattering pattern as peaks of one phase that continue as peaks of the following phase. The usual epitaxy between the hexagonal and the cubic phases was the (10) hexagonal peak continuing as the (211) Im3m peak. Two times, there was epitaxy between the peaks (10) of H_{II} and (220) of Im3m, and once between the (10) peak of H_{II} and the Pn3m (211) or (200) peaks. In the lamellar-cubic or cubic-lamellar transition we observed epitaxies between the first-order fluid lamellar peak and one of the cubic peaks (211), (220), (221) and (310) of Pn3m and (321) of Im3m. Especially, in some samples the (211) Im3m reflection gradually increased just before or together with the appearance of the lamellar phase.

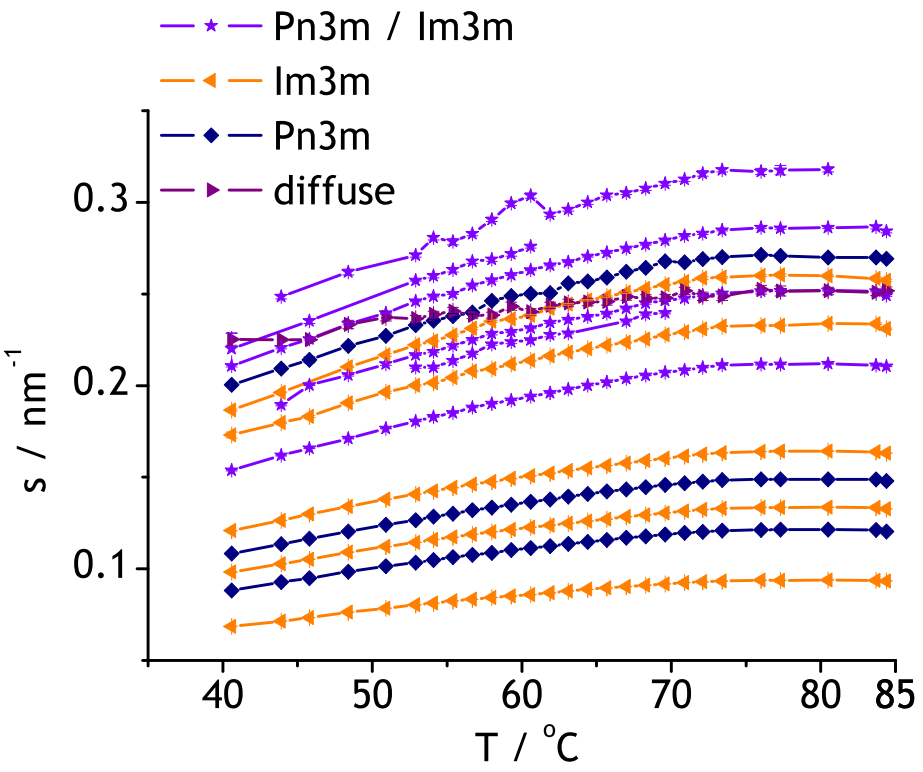

Figure 3.30: Peak positions recorded during the first cooling of sample *m150*. Notice the number of peaks assigned to both cubic phases.

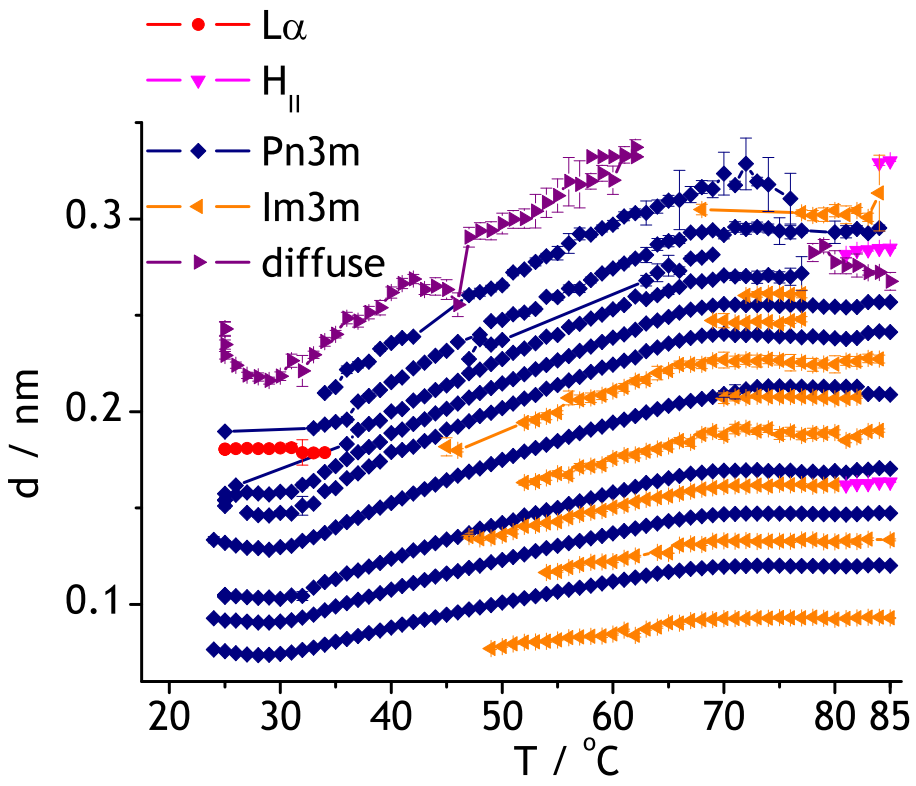

Figure 3.31: Peak positions recorded during the third cooling of sample *m150*. All the peaks are resolved and none overlap.

These scattering planes must be important in the structure on the interconversion path from the cubic to the lamellar phase.
From the epitaxies, one can try to guess the interconversion path of the phases and calculate the relative dimensions of the phases at the moment of the transition. The common scattering planes of the hexagonal and cubic phases can be visualized in a projection of the cubic lattice in the [111] direction, a direction parallel to the (211), (220) and (221) scattering planes (Fig. 3.32, 3.33). The projection is a triangular lattice. The cylinders constituting the hexagonal phase run perpendicularly to the plane of the projection, centered on the cross sections. The other common planes, Im3m (220) and hexagonal (11), are perpendicular to the (10) planes. The epitaxial relationship reveals the mutual orientation of the phases at a given moment. The cubic phases exist before H_{II} disappears, so the hexagonal phase is absorbed by the cubic phases (the lipid from the hexagonal phase is incorporated into the cubic phase). The temperatures at which this happens vary, so the important parameter seems to be the ratio of the dimensions of the phases. The most common and convenient epitaxy is between the planes H(10) - I(211). Once, H(10) - P(211) was observed, when the Im3m phase was not present. The direction [111] is parallel to both (220) and (211) scattering planes, so in principle, both epitaxies require the same mutual orientation of the phases. The same epitaxy was seen by Clerc, Levelut and Sadoc for surfactant-water systems [65]. The scattering planes involved in the epitaxy are those with the highest density of matter, and the preferred growth direction [66].

From the epitaxy between the hexagonal and Im3m phases, the ratio between their lattice parameters at the transition can be calculated. The result is visualized in Fig. 3.34.
$s(211)_{Im3m} = s(10)_{Hex}$
$\sqrt{6}/d_{Im3m} = 2/(\sqrt{3}(d_{Hex})$
$d_{Im3m}/d_{Hex} = 3\sqrt{2}$.

It is interesting that the cubic phases respond to the appearance of other phases by expansion or contraction, not by decreasing the amount of the phase. It suggests that the diffusion of lipid within the cubic membrane and water inside the lipid channels is very fast. Also, it is easier for the lamellar and hexagonal phases to grow from or disappear into the cubic phases while their lattice parameters preserve a certain ratio. This facilitates the transition because the lipid within certain scattering planes does not have to rearrange, but continues to exist within the new structure. The preservation of the scattering planes gives rise to epitaxial relationships.

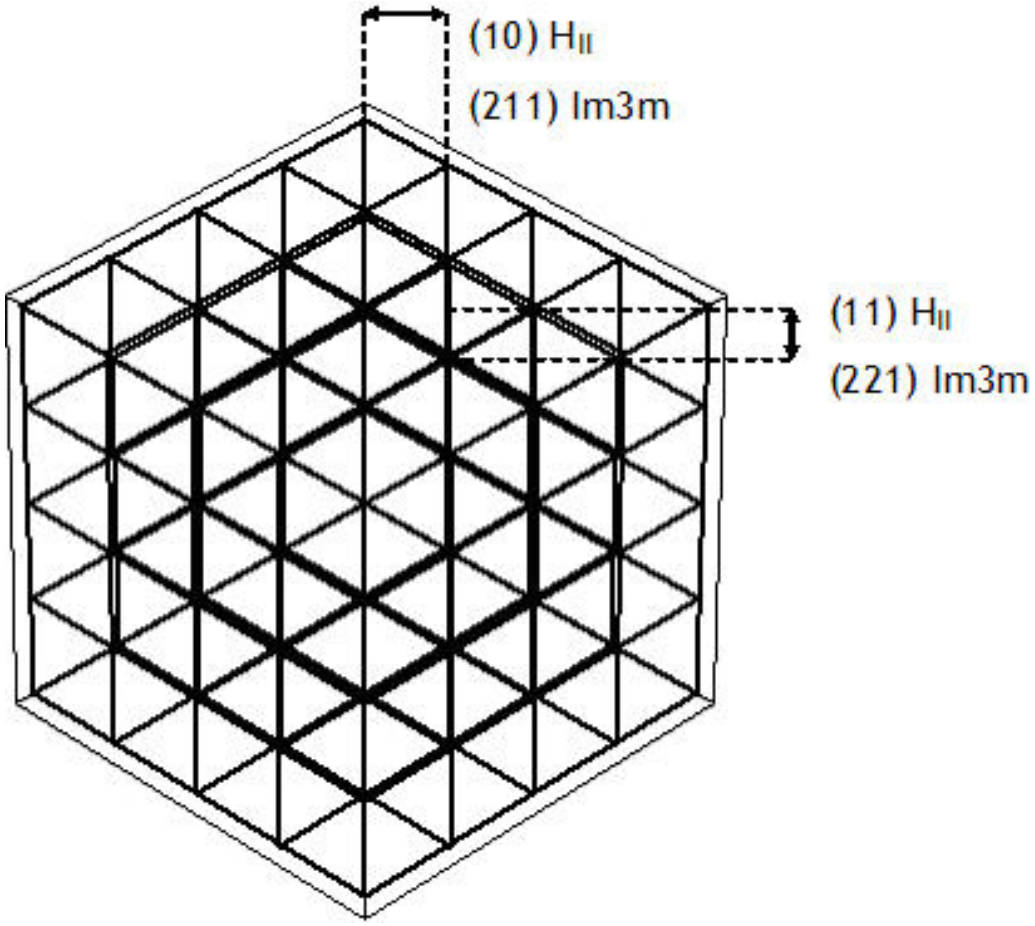

Figure 3.32: Projection of the Im3m rod structure in the [111] direction. Common scattering planes of Im3m and the hexagonal phase can be seen.

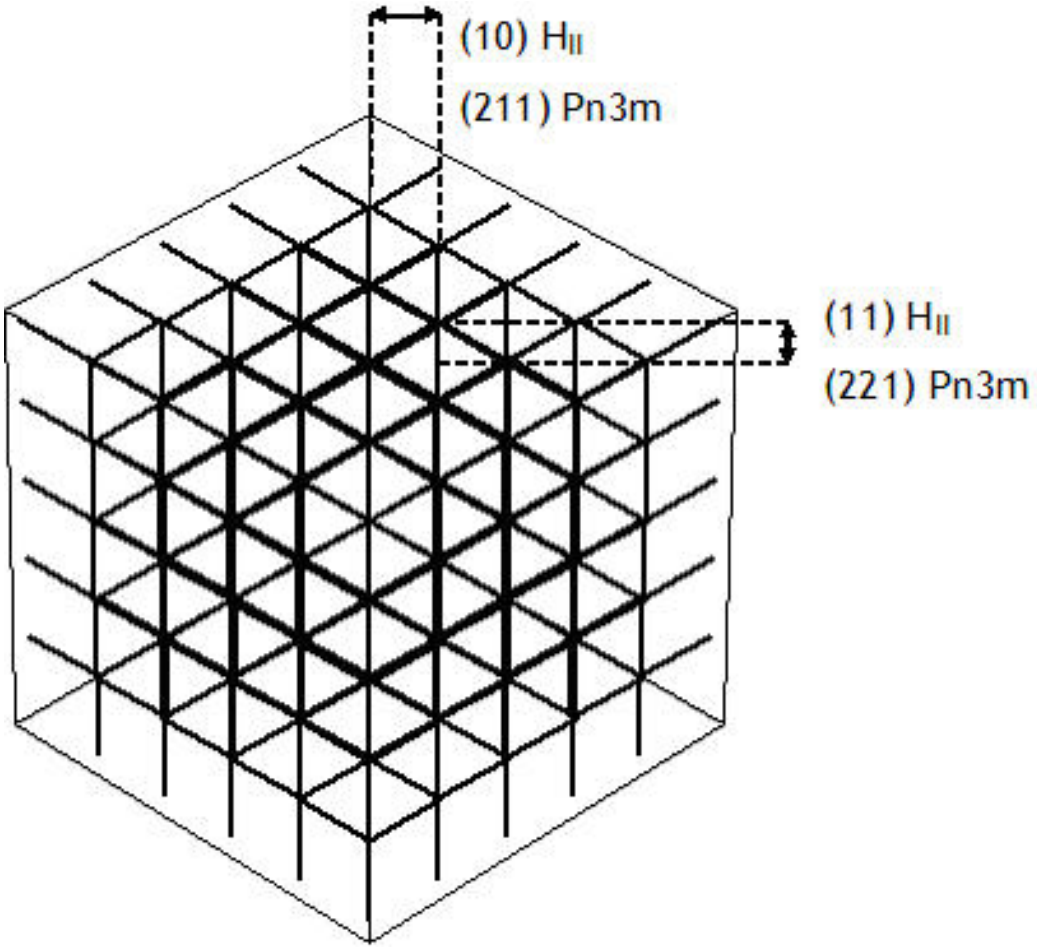

Figure 3.33: Projection of the Pn3m rod structure in the [111] direction. Common scattering planes of Pm3m and the hexagonal phase can be seen.

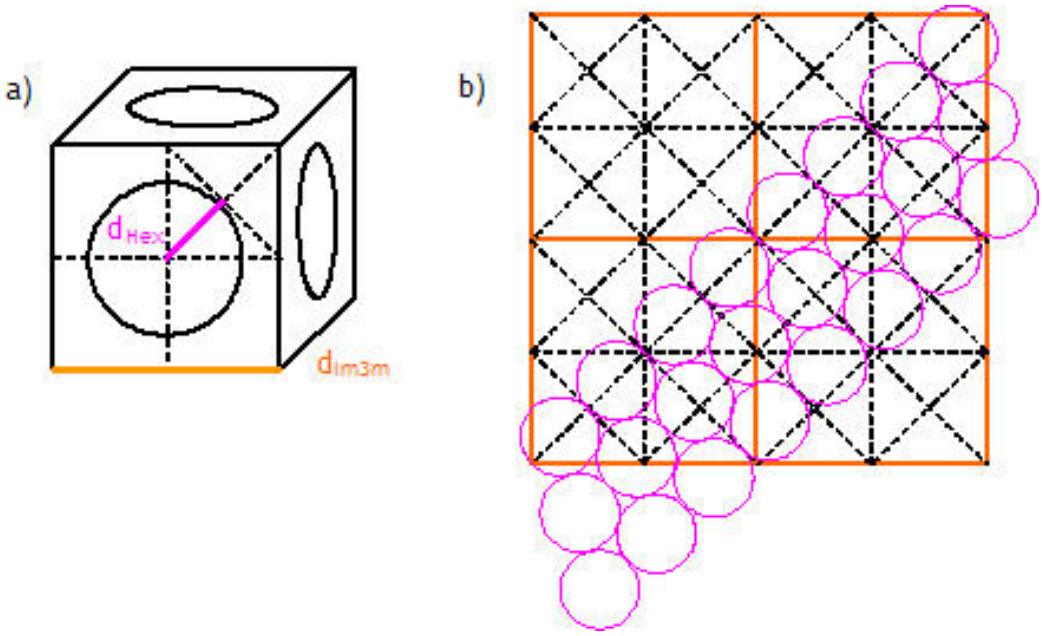

Figure 3.34: Comparison of the dimensions of Im3m and the hexagonal phase at the moment of their transition. An epitaxial relation exists between the two phases.

Interconversion of cubic phases

Often, the cubic phases formed initially during the heating of the sample were later replaced by another pair of Im3m and Pn3m. This happened either during the formation or after the disappearance of the hexagonal phase. Each new phase grows preferentially in a certain orientation with respect to the preceeding phase and consequentially with a certain lattice parameter. At the point of the hexagonal phase disappearance, the lipid is displaced into the cubic phase. The existing cubic phases might be unsuitable for the incorporation of lipid from the hexagonal phase because of incompatible dimensions and no possibility for an epitaxial relationship (preserving certain scattering planes). In this case, another cubic phase grows and replaces the initial one. Such a reorganization of cubic phases was observed on several occasions.

The sample labeled *pe100* with L/P = 100 was heated at 0.5°C/min, but cooled at 0.8°C/min. The initial set of cubic phases appeared after the lamellar to hexagonal transition. During cooling, they expanded together with the hexagonal phase and after the latter disappeared, most of the cubic peaks disappeared into the diffuse scattering and only three very broad peaks remained, the original (110) and (211) Im3m peaks and something between the original (200) Im3m and (110) and (111) Pn3m peaks (Fig. 3.35). During this short chaotic period, the lamellar peak reappeared. Around 55°C, the sample became better ordered and two new cubic phases appeared (Fig. 3.36). The (211) Im3m peak continued as the (111) peak of the new Pn3m phase. The new phases preserve the special ratio of lattice parameters. In both Im3m phases the (211) peak is large and grows with cooling, although the intensity of the other peaks does not change very much (Fig. 3.37). It seems that the cooling rate is too fast and does not allow an orderly incorporation of the lipid released from the hexagonal phase. Also, the dimensions of the cubic phases do not seem to be suitable for epitaxy. Indeed, the new Pn3m phase has a smaller lattice parameter than the initial one. The lamellar phase probably forms only to store some part of the released lipid that cannot be used to build up a cubic phase because of low local water content [63].

The sample labeled *m200* with L/P = 200 was heated and cooled at 1°C/min in three consecutive cycles and the cubic phases went through a similar reorganization. The newly formed Pn3m had a smaller lattice parameter than the old one. After the hexagonal phase disappeared, the cubic peaks became

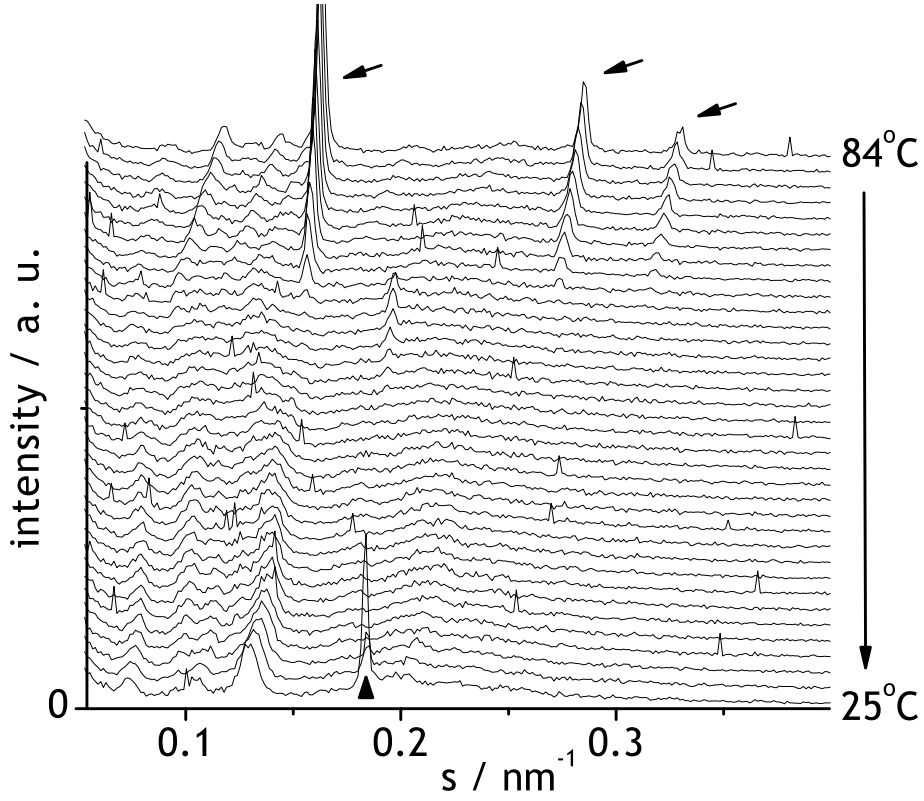

Figure 3.35: Scattering patterns of the sample *pe100* during cooling from 84 to 25°C. Notice the loss of order in the cubic phases after the end of the hexagonal phase and the following reorganization. The hexagonal peaks are marked by arrows. The very sharp peak in the last few frames marked by an arrowhead is the first-order fluid lamellar peak.

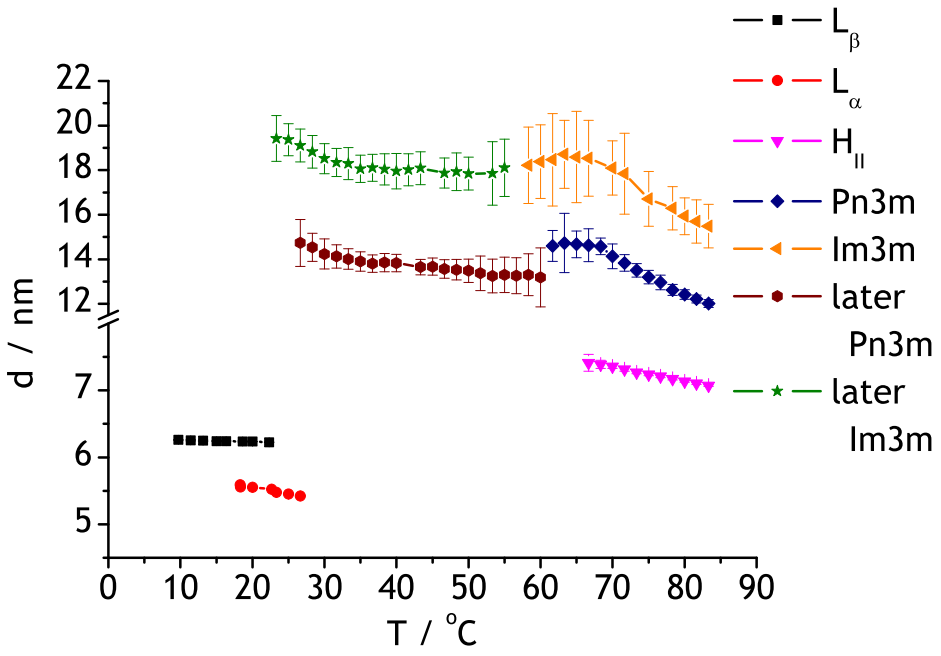

Figure 3.36: Lattice parameters of the phases in sample *pe100* during cooling.

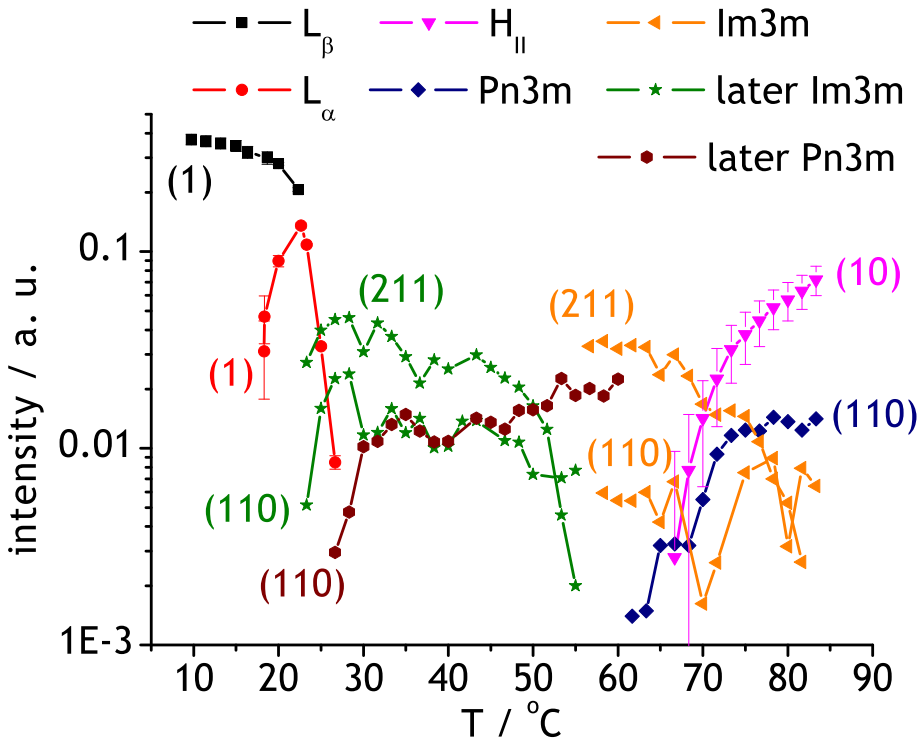

Figure 3.37: Integral areas of scattering peaks in sample *pe100* during the cooling. Notice the high intensity of the Im3m (211) peaks. The y-axis is a logarithmic scale.

very diffuse for a temperature interval of about 20-25°C and at the same time, the expansion of the cubic phases stopped. At the end of this temperature interval, the expansion began again and the peaks gained intensity and became better defined. This "diffused peak" interval is when the cubic phases accommodate the lipid released from the hexagonal phase. The reorganization proceeds differently in the first and the third cycles. In the first cycle, the Im3m (110) peak can be followed all the way through the cooling (Fig. 3.38). The reorganization starts just below 70°C. The initial Pn3m (110) peak continues for a while, still close to the theoretically predicted ratio 1.279 with respect to the Im3m (110) peak. At the same time, a new Pn3m (110) and (111) peaks emerge and both (110) peaks continue close to each other for some time. The hexagonal (10) peak continues as a new Im3m (211) peak, and below appears a new Im3m (200) peak. This new Im3m phase expands during the reorganization, in contrast to the initial Im3m which does not change its dimensions. In the third cycle, the reorganization causes only broadening of the peaks. The structure of both cubic phases becomes less correlated and their dimensions do not change during a few minutes (Fig. 3.39).

An interesting interconversion of cubic phases occurs in the sample with L/P = 155 labeled *mmm* (Fig. 3.40). The Im3m and Pn3m phases develop at 80°C during heating and are replaced by a second Im3m phase at the beginning of the cooling. Above 50°C, the (200) and (211) Im3m peaks continue as (110) and (111) peaks of a second Pn3m phase, while a new Im3m (211) peak develops to fit with the (110) peak of the second Im3m phase (Fig. 3.40, 3.41). An epitaxial relationship exists between the Im3m (321) peak (very broad) and the gel lamellar peak.

The cubic interconversion happens mainly during the early stages of the life of a sample when the melittin molecules are not yet perfectly distributed. This does not necessarily mean that they need to be distributed equally in all parts of the liposome. The inner layers are more curved and therefore may be able to accept more melittin molecules before the lamellar structure disrupts. The higher curvature is also the reason why the cubic phases start to form from within the vesicle. An extreme case would be the formation of micelles from the inner layers of the liposome which would then reside in the water reservoir in the core of the vesicle. These micelles could indeed work as a storage system for lipid that might be later incorporated into the cubic phases and ensure their growth even if in the diffraction pattern, no other phases disappear at the same time. This could explain the usual increase in

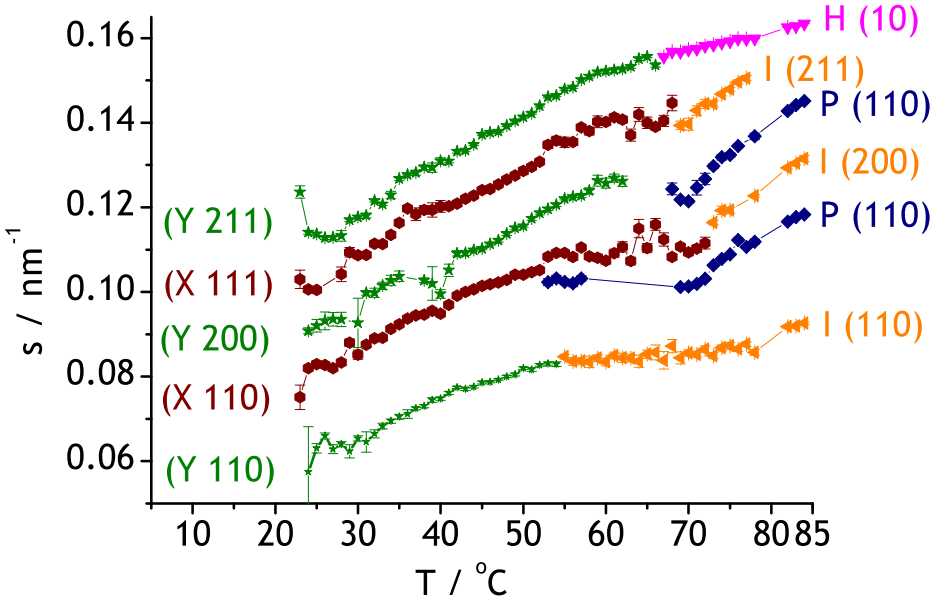

Figure 3.38: Reorganization of the cubic phases after the disappearance of the hexagonal phase in sample labeled *m200* during the first cooling. The peaks are indexed and the phases are indicated as follows: H - hexagonal, P - Pn3m, I - Im3m, X - late Pn3m, Y - late Im3m.

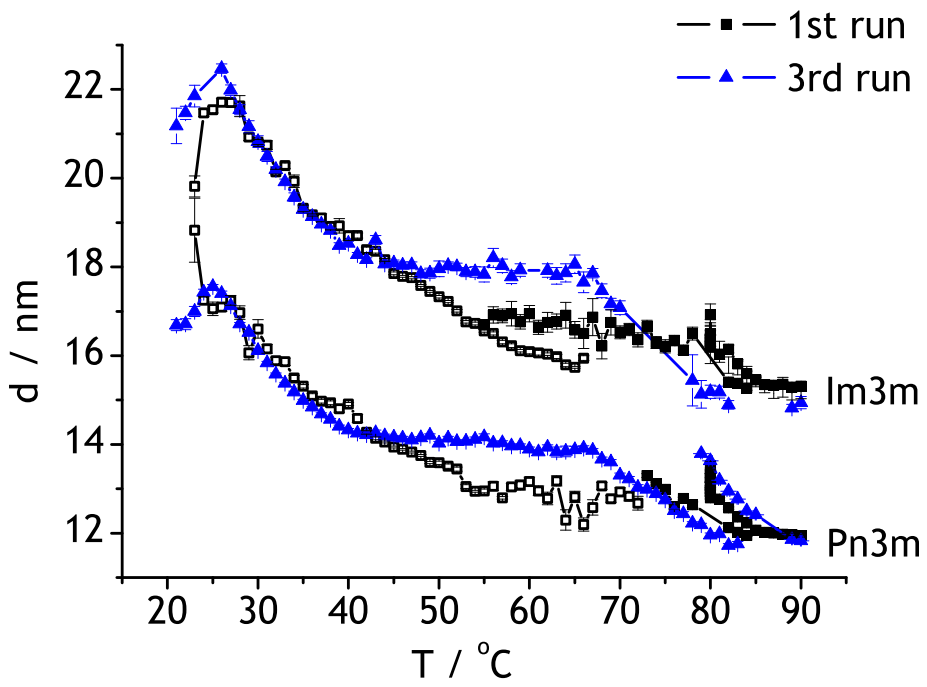

Figure 3.39: Lattice parameters of the cubic phases in sample *m200* in the first and the third heating-cooling cycles. The empty symbols represent the cubic phases after the interconversion.

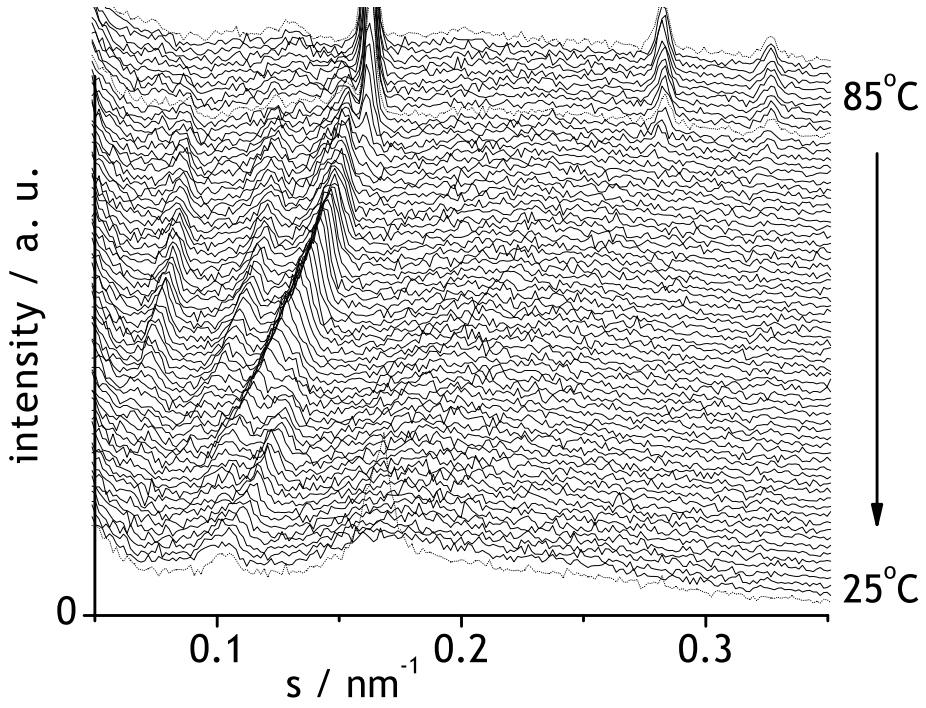

Figure 3.40: Scattering patterns of sample *mmm* during the waiting period at 85°C and the following cooling to 25°C, showing the reorganization of the cubic phases. The arrow indicates the direction of the temperature changes. The lattice parameters of the phases are plotted in the following figure.

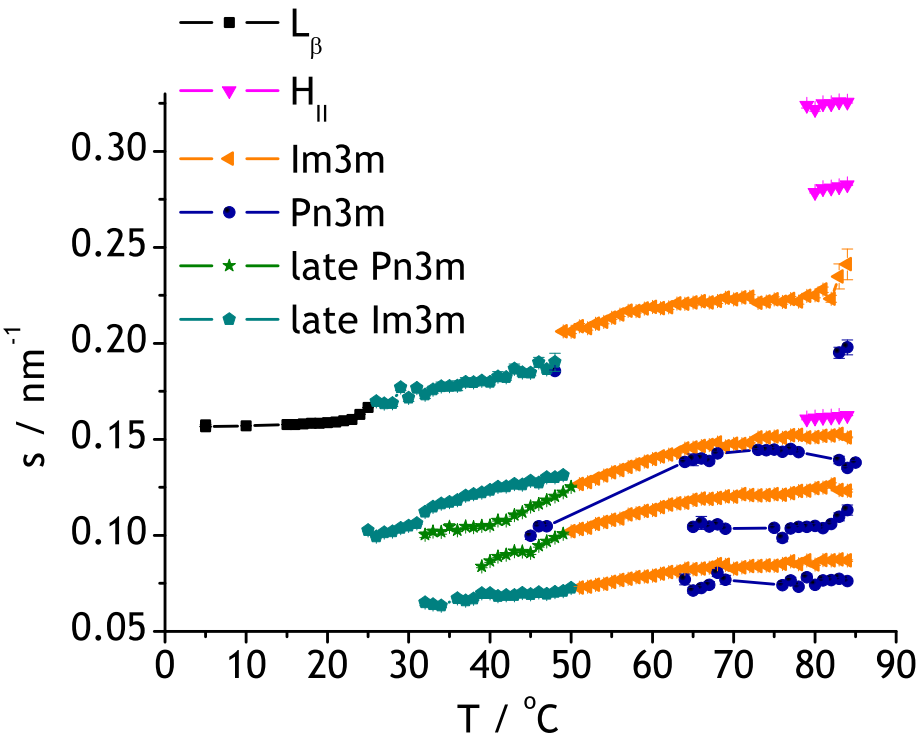

Figure 3.41: The peak positions of the phases in sample *mmm* during cooling. Notice the interconversion of the cubic phases. The scattering patterns are shown in the previous figure.

the cubic lattice parameter around 45°C (Fig. 3.26).

3.5 POPE membranes with alamethicin

POPE membranes with alamethicin were prepared in the same way as described for POPC membranes. The lipid-to-peptide ratios were 10, 30, 50, 100, 200, 500 and 1000 (samples labeled ape10 to ape1000). Diffraction patterns were taken in the temperature range 5 to 85°C during heating and cooling. Some samples were measured again after several months, to see the effect of long term storage. Samples filled in capillaries were stored at 4°C. Many features observed in POPE-melittin mixtures, such as the special ratio of the cubic lattice parameters and the mutual dependence of the coexisting phases, are also seen in POPE-alamethicin membranes. These will not be discussed again, but we will concentrate on the particular characteristics of POPE-alamethicin membranes.

POPE membranes with small amounts of alamethicin (1 molecule of peptide per 500 or 1000 molecules of lipid) preserve the original phase sequence and phase onset temperatures of POPE. Additionally, they form two coexisting cubic phases, Pn3m and Im3m. These form at about 60°C during heating and disappear during cooling at about 35°C. Unlike the original POPE phases, the cubic phases show a slight hysteresis, so the lattice parameters are slightly smaller during cooling than at the corresponding temperatures during heating. This suggests that the cubic phases have lower thermal flexibility. In both cases, Pn3m is the dominant phase, with a higher number and intensity of diffraction peaks. Judging from the integral areas of the diffraction peaks, the original hexagonal phase is still dominant over the new Pn3m phase at L/P = 1000, but in coexistence with the lamellar phase, Pn3m is more intense (Fig. 3.42). At L/P = 500, Pn3m becomes equally intense as H_{II} and L_α is completely inhibited. The coexisting phases are not two separate non-interacting domains, but influence each other. When the hexagonal phase disappears during cooling, we observe a substantial disordering of the Pn3m phase, evidenced by the increase in the width of the peaks (Fig. 3.43). The expansion of the Pn3m lattice is slowed down until the hexagonal phase disappears completely (Fig. 3.44). The amount of the Pn3m phase gradually increases during the cubic-hexagonal coexistence during cooling and after the hexagonal phase disappears, it decreases again. The mutual influence of the phases suggests that they are embedded in the same structure, an onion vesicle, as already described for POPE-melittin mixtures. The two cubic phases change their dimensions synchronously, with the lattice parameter ratio always close to the same number, $a_{Im3m}/a_{Pn3m} = 1.279$. Clearly, there is an

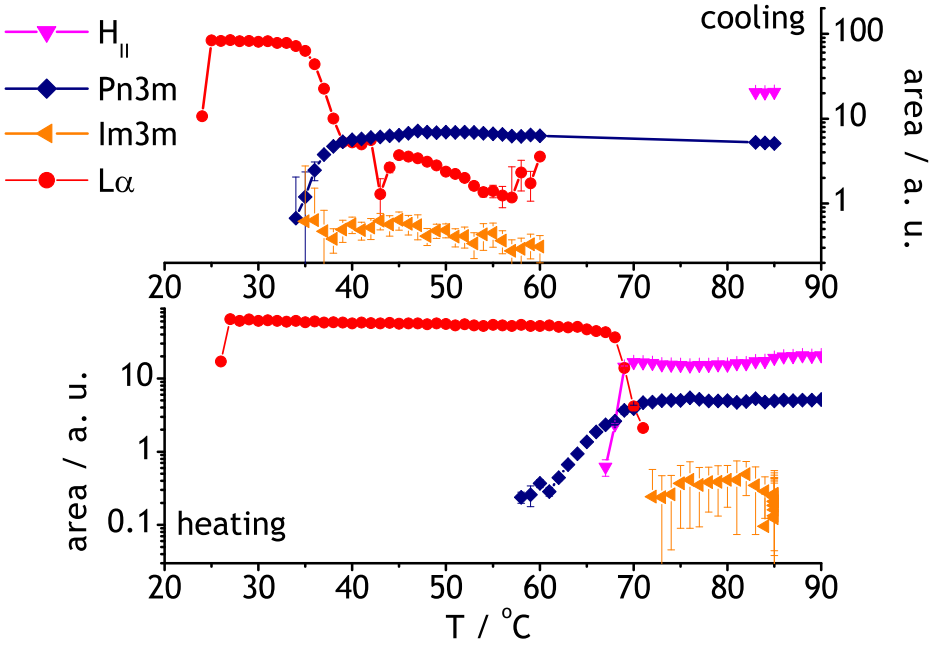

Figure 3.42: Area of the most intensive peak of each phase, L/P = 1000. The y-axes are logarithmic scale.

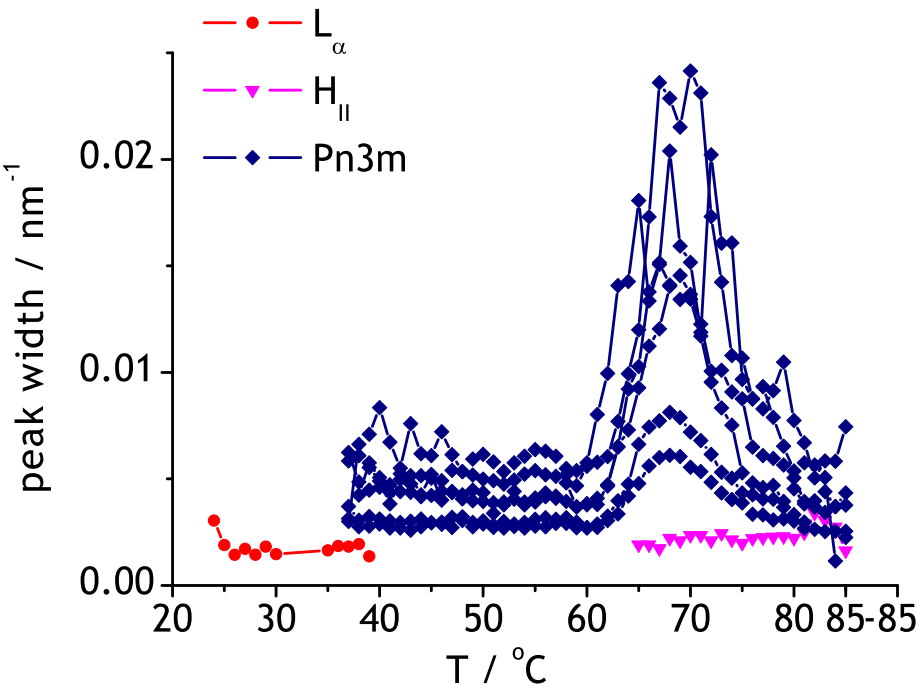

Figure 3.43: The peak width during cooling of the sample with L/P = 500. The cubic peaks widen substantially when the hexagonal phase disappears.

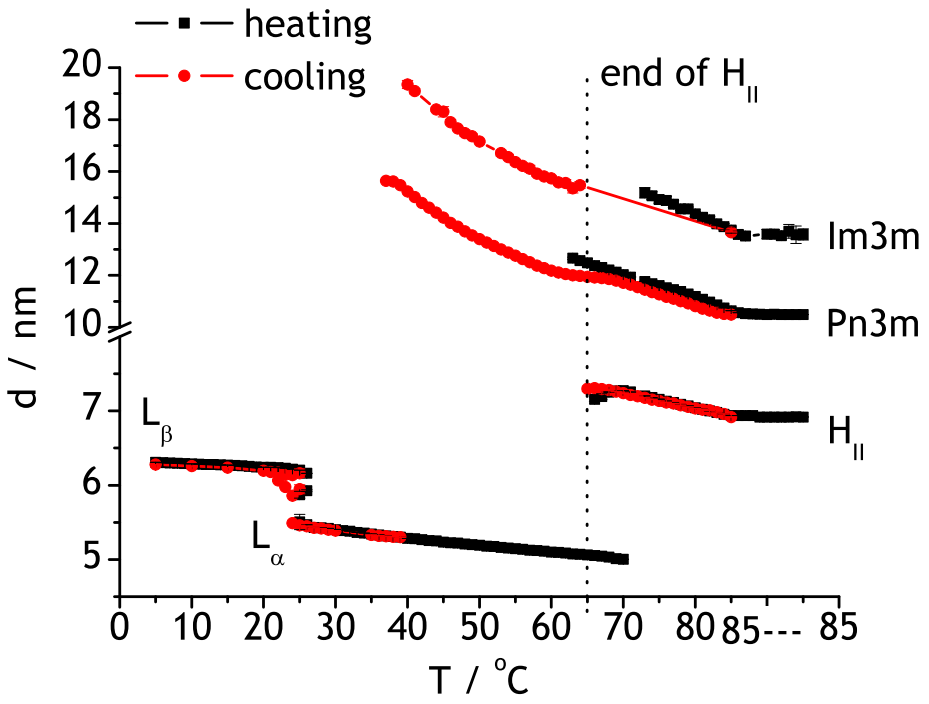

Figure 3.44: POPE membranes with alamethicin, L/P = 500. Lattice parameters of all phases during heating and cooling.

epitaxial relation between them, indicating that they evolved from the same primary structure.
Increasing the amount of alamethicin to L/P = 200 completely eliminates the original POPE hexagonal phase and shifts the onset of the cubic phases to lower temperatures. The dimensions of the cubic phases are not significantly altered in comparison to samples with lower alamethicin content (Fig. 3.45). However, the relative amounts of the non-lamellar phases changed (figures 3.46 and 3.47). Whereas at L/P = 1000 the amount of hexagonal phase pre-

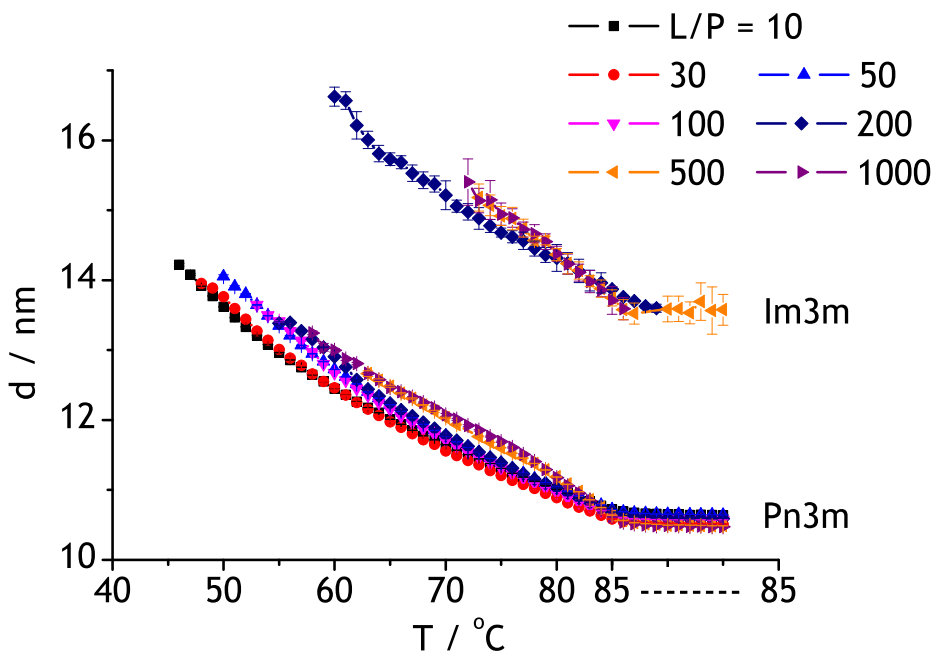

Figure 3.45: Lattice parameters of cubic phases in POPE-alamethicin mixtures during heating. The POPE to alamethicin ratios L/P are indicated.

vails about four times over the amount of Pn3m, as suggested by the integral areas of the respective lowest angle peaks (10 and 110, resp.), both phases are equally important at L/P = 500. The amount of Pn3m increases slightly from L/P = 1000 to L/P = 500 and at L/P = 200 it is about twice as large as at L/P = 1000. The amount of Im3m is the same in all three samples. Con-

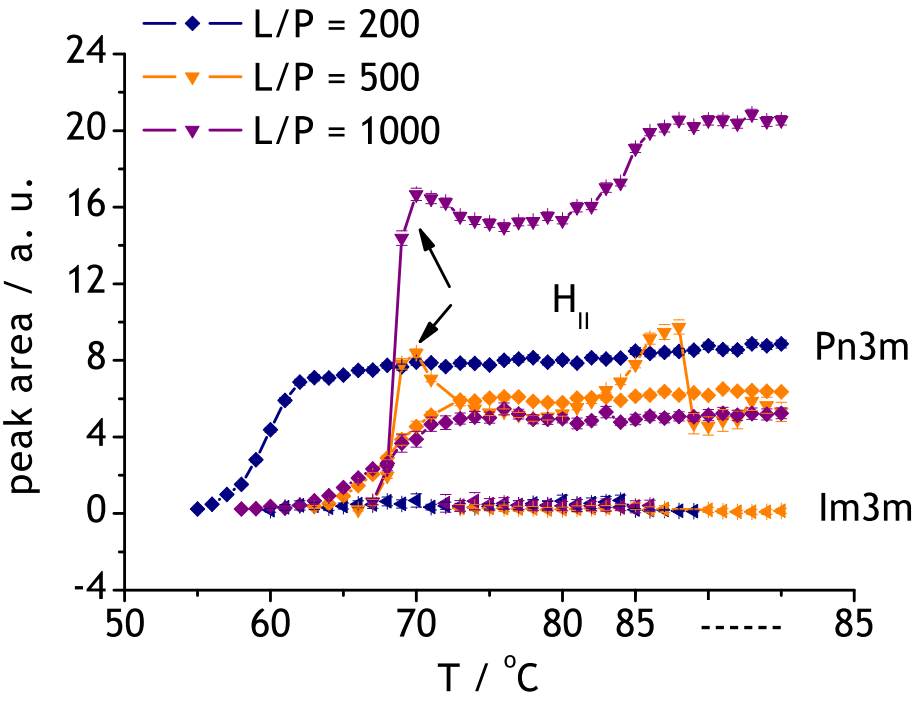

Figure 3.46: The areas of selected peaks of the non-lamellar phases for L/P $\geq$ 200 during heating. The POPE to alamethicin ratios L/P are coded by color as indicated in the figure and the peaks by the symbols as follows: down triangle - hexagonal (10) peak; diamond - Pn3m (110) peak; left triangle - Im3m (110) peak.

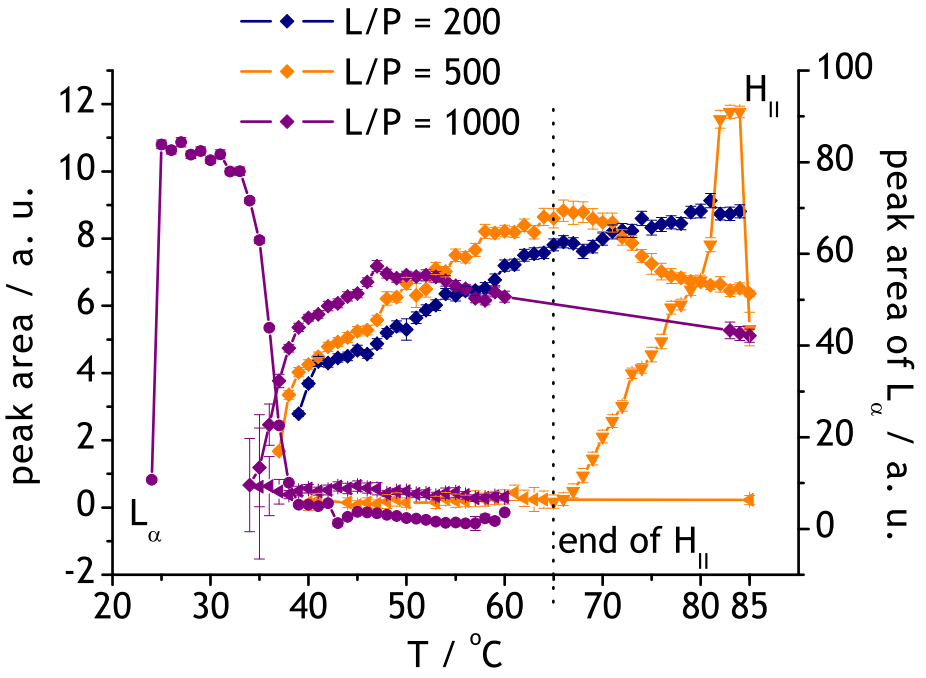

Figure 3.47: The areas of selected peaks for L/P $\geq$ 200 during cooling. The POPE to alamethicin ratios L/P are coded by color as indicated in the figure and the peaks by the symbols as follows: circle, - lamellar (1) peak; down triangle - hexagonal (10) peak; diamond - Pn3m (110) peak; left triangle - Im3m (110) peak.

sidering the changes in the integral peak areas at different L/P ratios, it is possible to estimate the actual number of lipids per one peptide in the Pn3m phase at a given overall L/P ratio. In the calculation, it is assumed that the hexagonal phase does not contain any peptide at all and the presence of the Im3m phase which is very small compared to the other phases is neglected. The assumption of a peptide-free hexagonal phase is not completely correct, because its repeat distance changed slightly with the addition of alamethicin (Fig. 3.48). Also, it is assumed that all peptide in the samples is bound to the lipid. Comparison of the integral peak areas of the hexagonal and the Pn3m phase gives us a proportion of the lipid molecules contained in each phase, N (see Table 3.2). The number of lipid molecules per peptide bound

L/P	N ((10) H_{II} : (110) Pn3m)
1000	3.92
500	1.57

Table 3.2: Ratio of the integral peak areas of the (10) hexagonal to (110) Pn3m peak at different L/P ratios at 85°C. This ratio gives the proportion of lipid molecules contained in each phase.

in the cubic phase is then (L/P)×1/(1+N). For L/P = 1000, we get ∼203 lipids per peptide and for L/P = 500 we get ∼194 lipids per peptide. In both cases, the proportion of lipids to peptides is about 200. This number seems realistic, because it is at this L/P ratio when the hexagonal phase is fully replaced by the cubic phases. However, the binding of alamethicin does not saturate at L/P = 200, because the Im3m phase is still present and the dimensions of Pn3m change with further increase of the alamethicin content.

At the POPE to alamethicin ratio L/P = 200, the hexagonal phase is no longer present and both cubic lattice parameters get smaller. At L/P = 100, there are still traces of the Im3m phase and the Pn3m lattice parameter is just a little smaller. The (110) Pn3m peak area reaches a maximum at L/P = 100 and 200. Towards higher L/P ratios, it progressively increases at the expense of the other non-lamellar phases and towards lower L/P ratios, it progressively decreases (Fig. 3.49). The reason for the decrease towards the low L/P ratios might be in the structure factor. The change in the structure factor can be caused by a change in the lattice parameter or in the electron density profile of the bilayer. The lattice parameter does not change in accordance with the peak area (Fig. 3.45), so the electron density profile must have changed. This means that the relative thicknesses of the lipid bilayer

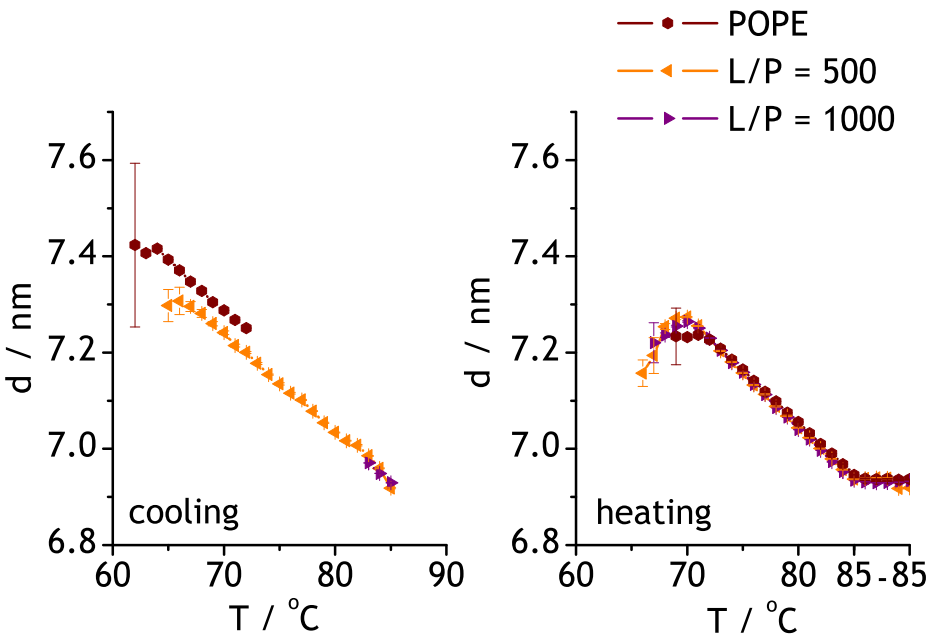

Figure 3.48: Lattice parameters of hexagonal phases of POPE with and without alamethicin. The POPE to alamethicin ratios L/P are indicated.

and the water channel have changed. According to the model described for the insertion of melittin into POPE, more peptide inserted between the lipid heads causes more membrane thinning. The thinning was observed in the lamellar phases [36], but it should also be possible in the cubic phases.

The next qualitative change occurs at L/P = 50. Only one cubic phase is

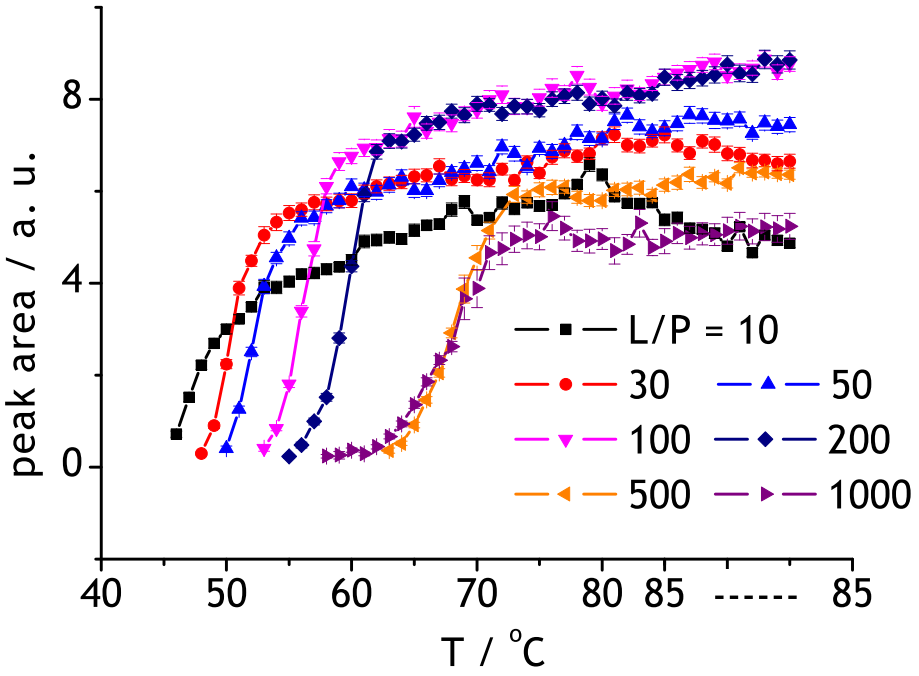

Figure 3.49: Area of the (110) Pn3m peak for POPE-alamethicin mixtures. The POPE to alamethicin ratios L/P are indicated.

observed, Pn3m, and with a smaller lattice parameter than at higher L/P ratios. At L/P = 10, the size and the thermal behaviour of the lattice parameter and the Pn3m (110) peak area changed.

The width of the Pn3m (110) peak decreases with increasing temperatures below L/P = 100 (Fig. 3.50 and 3.51). This is in contrast to the behaviour of the lamellar phases where the thermally disordered lipid chains negatively influence the long-range organization of the phase. In the cubic phase, the higher flexibility of the lipid chains probably facilitates the incorporation of

the peptide in the bilayer and so promotes the overall ordering of the phase.

The partial phase diagrams during heating and cooling are shown in Fig.

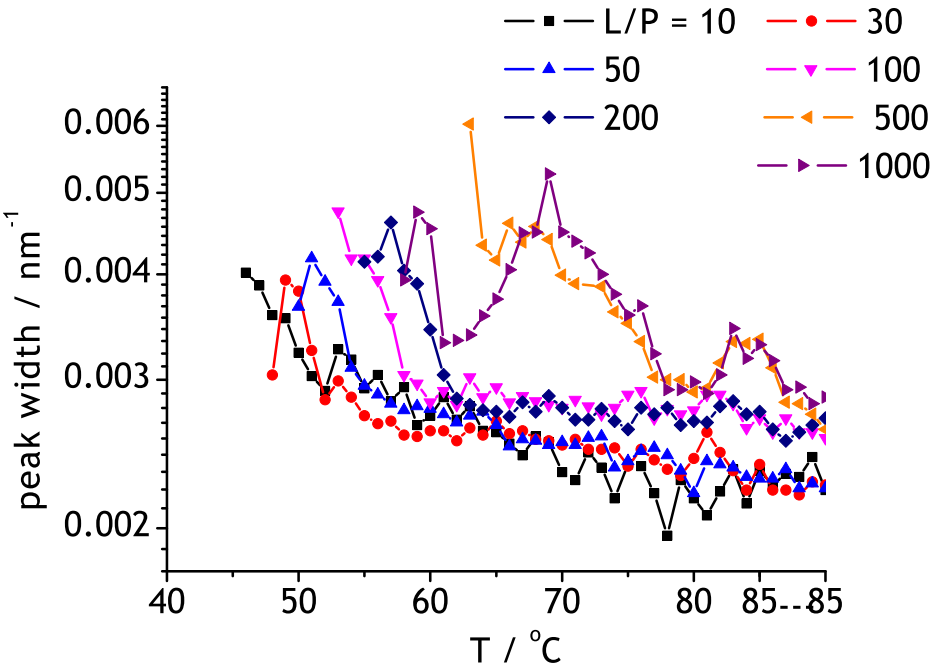

Figure 3.50: Peak width of (110) Pn3m peak during heating. The POPE to alamethicin ratios L/P are indicated. The y-axis is a logarithmic scale. The sudden increase for L/P = 500 and 1000 around 70°C occurs during the lamellar-hexagonal transition.

3.52 and 3.53. The L_α phase begins and ends at still lower temperatures with increasing alamethicin content (Fig. 3.54 and 3.55). The thermal gel to fluid transition occurs when the repulsive interactions between the lipid chains increase over a certain limit above which it is no longer possible to keep the close lipid packing characteristic of the gel phase. The increase in repulsive interactions is due to the increasing movement of the lipid chains which acquire more *gauche* isomers. Insertion of alamethicin speeds up both of these processes, by pushing away the lipid heads and creating more space for the lipid chains, allowing both lipid chain movement and the creation of

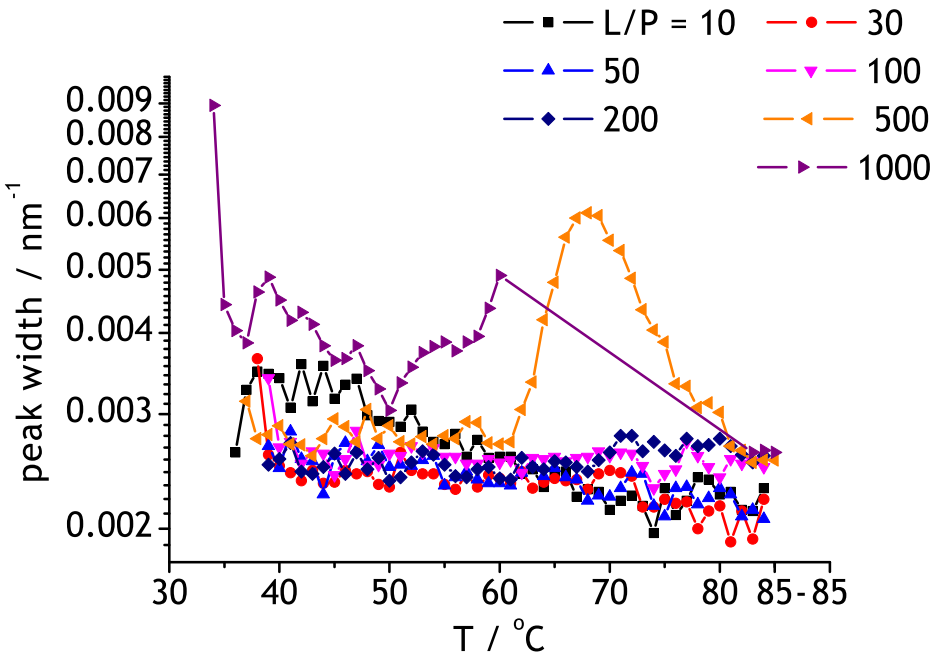

Figure 3.51: Peak width of (110) Pn3m peak during cooling. The POPE to alamethicin ratios L/P are indicated. The y-axis is a logarithmic scale. The sudden increase for L/P = 500 and 1000 around 70°C occurs during hexagonal to lamellar transition.

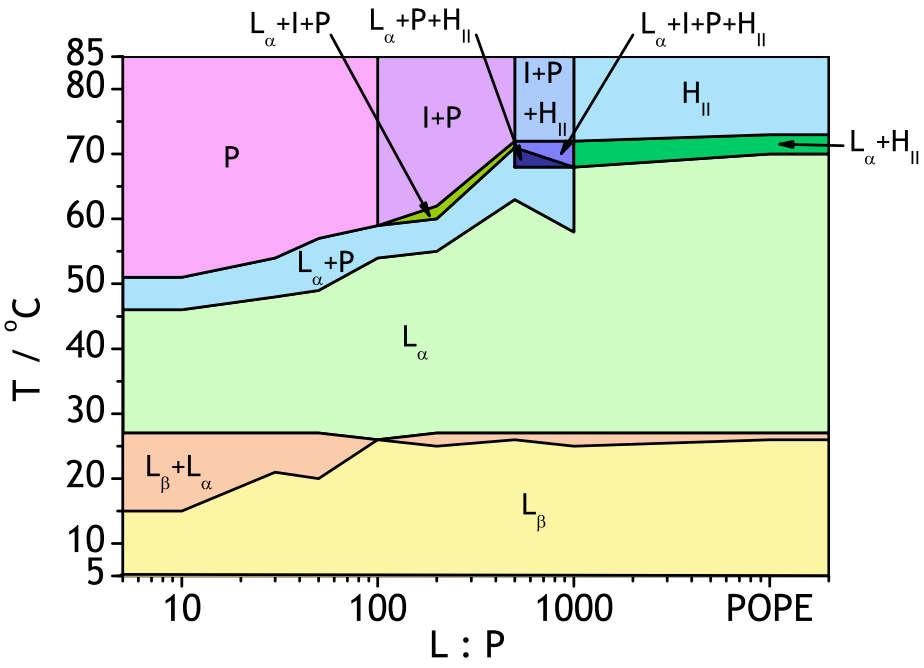

Figure 3.52: Phase diagram on heating for POPE membranes with alamethicin. P - Pn3m, I - Im3m. Other phases are labeled as usual.

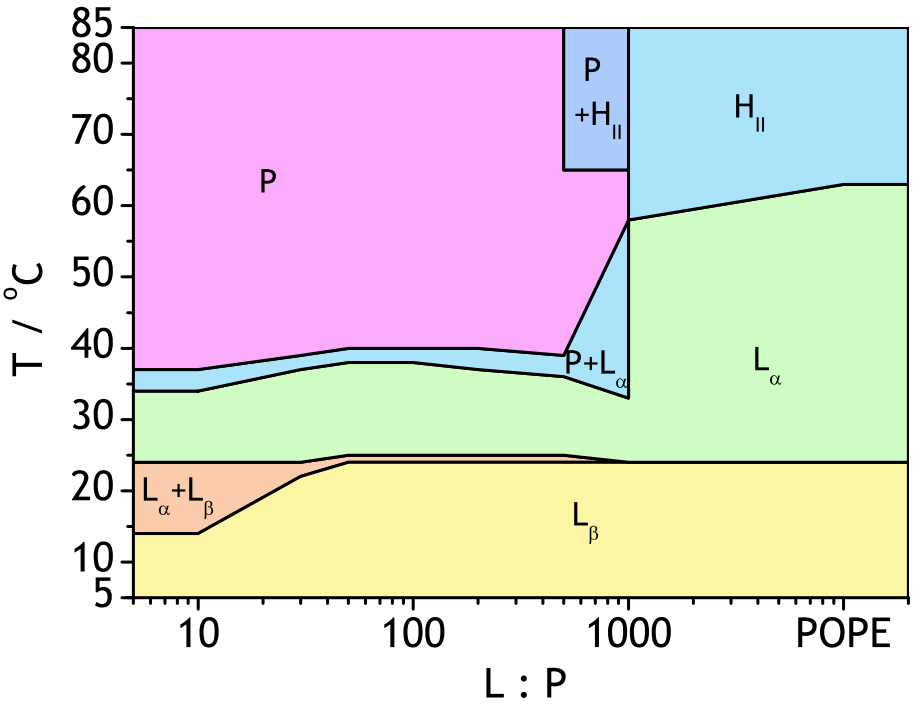

Figure 3.53: Phase diagram on cooling for POPE membranes with alamethicin. P - Pn3m, I - Im3m. Other phases are labeled as usual.

gauche bonds.

The cubic-lamellar transition begins by the growth of interlamellar attach-

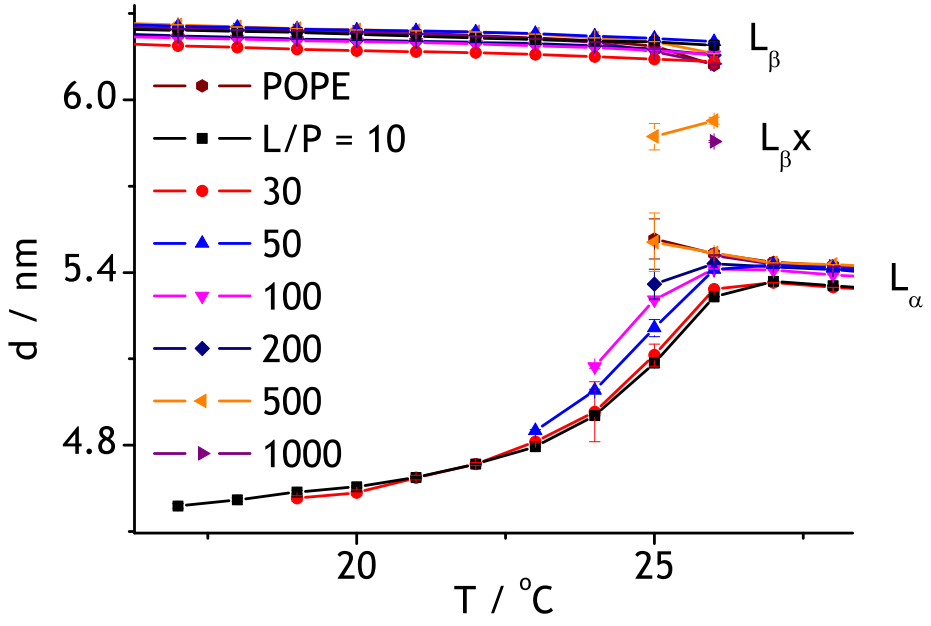

Figure 3.54: Lattice parameters of the gel and fluid phases in the POPE-alamethicin membranes during the main transition during heating. The POPE to alamethicin ratios L/P are indicated. Notice the appearance of the transient phase $L_{\beta}x$.

ments between adjacent membranes. Their formation is more probable and they are longer lived in lipids where the ratio of headgroup areas in L_α and H_{II} phases is more than 1.2 [6]. Insertion of alamethicin between the headgroups of POPE seems to increase this ratio progressively. Another point of view is the concept of intrinsic curvature introduced by Gruner [67]. The shape of the membrane is determined by the competing curvature elastic energy and the packing free energy. Substances inserted in the hydrophobic space of the membrane decrease the hydrocarbon packing free energy and so promote the formation of curved phases (hexagonal), because the competing elastic energy takes over. Insertion of substances between the headgroups

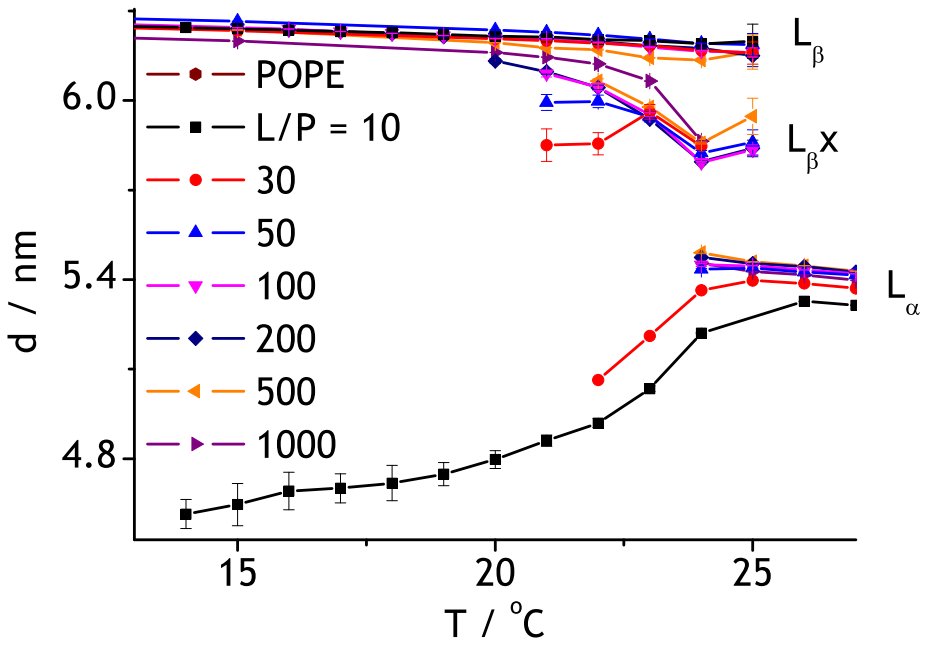

Figure 3.55: Lattice parameters of the gel and fluid phases in the POPE-alamethicin membranes during the main transition during cooling. The POPE to alamethicin ratios L/P are indicated. Notice the appearance of the transient phase $L_\beta x$.

should do the opposite, i.e. suppress the formation of curved phases. From the point of view of the curvature, the cubic phases are somewhere in the middle between the lamellar and the hexagonal phase (having an infinite and a quite small intrinsic radius of curvature, respectively) and were often observed during the transition between the two, especially in substances with an intermediate intrinsic curvature.

At the lamellar-cubic transition, the dimensions of the lamellar and the Pn3m cubic phase are always at the same ratio, with the lamellar first-order peak nearly coinciding with the (211) Pn3m peak. During cooling, these two sets of scattering planes coincide exactly. In the samples with L/P=500 and 1000, the lamellar and (211) Pn3m scattering planes coincide exactly also during heating. The growth of the hexagonal (10) scattering planes starts in coincidence with the (200) Im3m planes and ends in coincidence with the (211) Im3m planes. The same epitaxial relationships were seen in POPE membranes with melittin.

Sample labeled *ape200* was measured again after one month. Two heating and cooling cycles were performed immediately after each other. The scattering patterns were practically the same as those measured previously. The lattice parameters of all the phases increased slightly, but no profound differences were found such as in the POPE-melittin mixtures. The cubic lattice parameters are shown in Fig. 3.56. The interaction of POPE with alamethicin is considerably faster than with melittin where the equilibration into the final structure can take months.

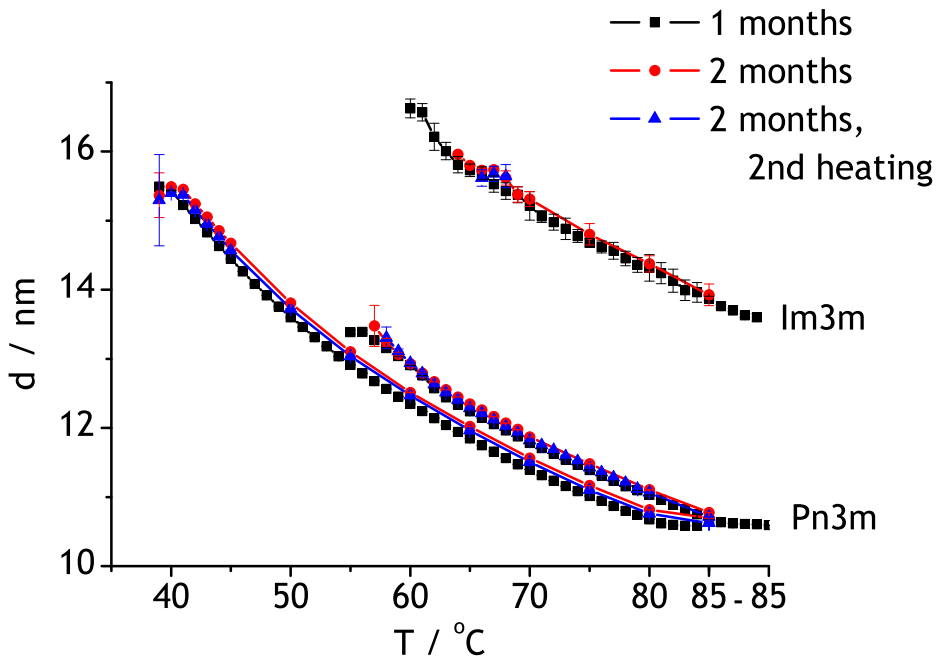

Figure 3.56: Cubic lattice parameters in sample labeled *ape200* in several measurements.

3.6 Influence of melittin on lipopolysaccharide membranes

3.6.1 LPS Re and melittin

Pure Re LPS (LPS R595 - for structure see Fig. 2.4 in Chapter 2) in water has a very rich phase diagram as described by Brandenburg *et al.* [68]. Depending on the water content, it adopts a variety of cubic or lamellar phases. In this work, the LPS membranes were prepared at water contents between 90 and 95% where a lamellar phase forms. The lattice parameter changed from 5.90 nm at 5°C to 5.09 nm at 85°C. The membranes are in the gel state until 43°C and then change into the fluid state. The transition temperature is higher that the one usually observed for LPS Re in DSC experiments. The difference should be due to the slow response of the sample to temperature changes at the employed heating rate of 1°C/min. The slow thermal response was visible during the 10-minute incubation time at 85°C when the lattice parameter was still changing.

Addition of melittin at L/P = 50 induced a phase separation of the lamellar phase into two phases with very similar bilayer spacings (Fig. 3.57 and 3.58, curve b). One phase matches the dimensions of the pure LPS phase, the other is less ordered, as deduced from the peak width, and its bilayer spacing is ∼0.7 nm thicker. The dimensions of the two phases changed simultaneously during the heating scan. There is no second WAXS peak, although the peak moved to larger s-values relative to the pure LPS peak indicating a smaller chain-to-chain spacing. The phase transition temperature did not change. On further measurements two and six weeks later, the sample contained only one lamellar phase with the bilayer spacing nearly identical to that of pure Re LPS. The equilibrium association constant for melittin and LPS is 2.85×10^6 M^{-1} [69]. The concentration of melittin in the sample was 3.69×10^{-4} M, so there should be no doubt that the majority of melittin was bound to the membranes. Although the binding of melittin to LPS was sufficient, the peptide might not be able to cross the membranes easily, especially in multilamellar vesicles. The following scenario is proposed. In the first moments of the interaction, the peptide binds to the outer membrane of the liposome. Later, it begins to cross the membrane and binds to the next layers, and so on. At the moment of the first measurement, we observed two bilayer spacings - one with bound LPS and one without. Later, after

sufficient storage time, the peptides crossed the membranes down to the innermost layers of the liposome and intercalated into the membranes. Hence, we observed only one lamellar spacing, with the peptides evenly distributed. The local peptide concentration is not that high anymore (also considering the similar dimensions of LPS and melittin molecules, this amount of melittin does not have such a strong effect), so the difference with respect to the original LPS spacing is small.
With increased melittin concentration (5 lipids per 1 peptide), the same lamellar phase is observed as at lower melittin content (the peaks marked by an arrow in Fig. 3.57 and 3.58), but an additional lamellar phase appears (two low intensity peaks marked by a bar in Fig. 3.57). The bilayer spacing of the new phase is twice as large as the spacing of the other lamellar phase (around 11 nm). The two visible peaks are the first and the third order, the second order is hidden under the first-order peak of the phase with the smaller lattice parameter. This phase disappears about 15°C below the transition temperature of LPS Re. Another sample with the same L/P ratio was prepared and measured (curves d, e in Fig. 3.57 and 3.58). It features the same two lamellar phases, but the lattice parameter of the larger phase is now around 8 nm, so their lattice parameters are at a ratio of 3:4 instead of 1:2. The smaller phase splits into two in the fluid state (curve e in Fig. 3.58) and just below 80°C a hexagonal phase develops with a lattice spacing around 7.5 nm. Also, an additional weak peak at s $\sim$0.9 nm^{-1} appears which does not belong to any of the two lamellar phases. The lamellar phase with the larger lattice spacing is probably a LPS lamellar phase, where the inserted melittin caused a reorientation of the LPS headgroups from parallel to perpendicular position with respect to the membrane.

3.6.2 LPS Ra and melittin

The scattering pattern of pure Ra LPS (LPS R60 - for structure see Fig. 2.4 in Chapter 2) shows one very broad diffuse peak that could be the envelope of several cubic peaks as in lipid A (see below) or simply a broad micellar scattering (curve a in Fig. 3.59 and 3.60). Another peak or just a shoulder is seen at low angles, as also seen in lipid A. This could be a lamellar phase with a spacing of $\sim$19 nm. The addition of melittin at L/P = 50 initially did not change the scattering pattern substantially. More measurements made after several weeks and months (curves c to e in Fig. 3.59 and 3.60) revealed an evolving lamellar phase with a lattice parameter of $\sim$9.5 nm in the gel phase

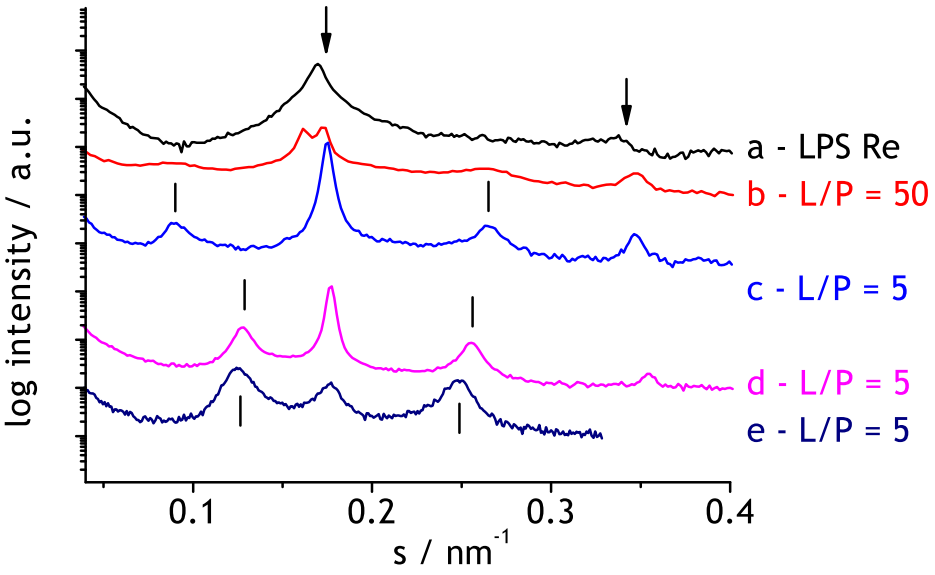

Figure 3.57: LPS Re with melittin at 5°C. a - LPS Re; b - LPS Re with melittin, L/P = 50; cde - LPS Re with melittin, L/P = 5.

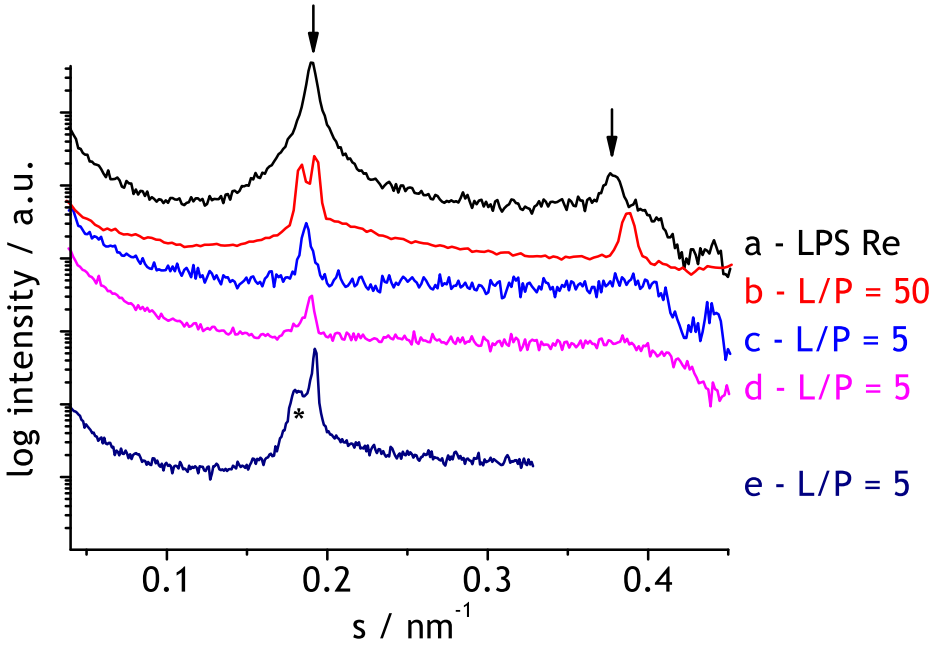

Figure 3.58: LPS Re with melittin at 65°C. a - LPS Re; b - LPS Re with melittin, L/P = 50; cde - LPS Re with melittin, L/P = 5.

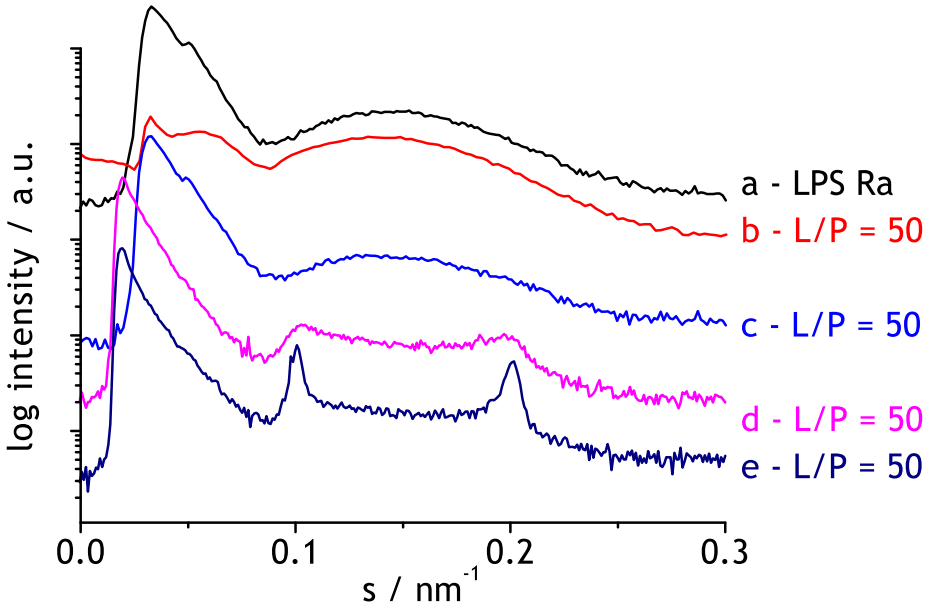

Figure 3.59: Scattering patterns of Ra LPS with melittin at L/P = 50 at 5°C.

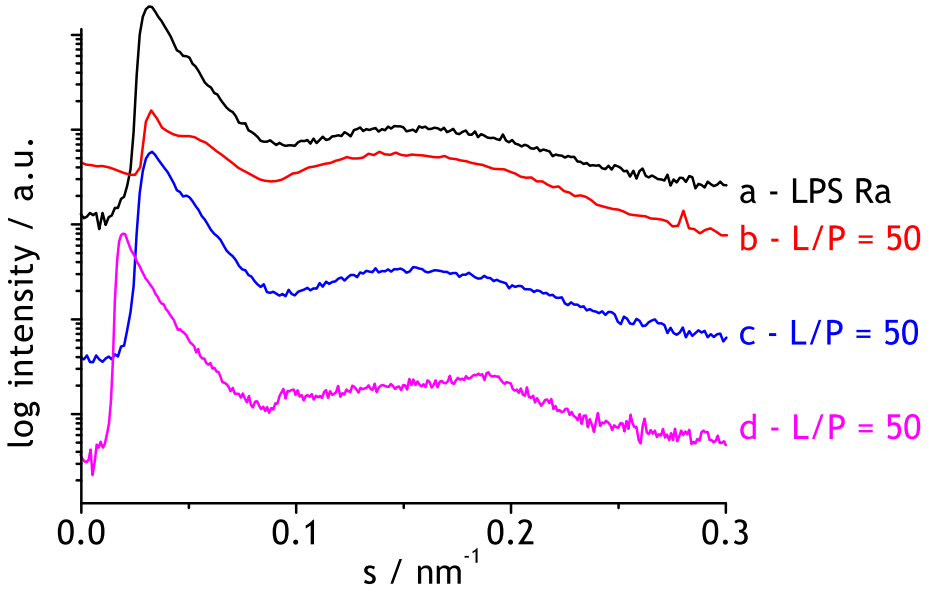

Figure 3.60: Scattering patterns of Ra LPS with melittin at L/P = 50 at 65°C.

and ∼10 nm in the fluid phase. The phase transition was at 35°C.
LPS Ra with melittin at L/P = 5 shows a variety of lamellar phases (Fig. 3.61). Although the lattice parameters are quite close to each other and the phase transition always occurs around 50°C, the sample behaved differently even one year after preparation. It is possible that the sample gets into a metastable state during long storage at low temperatures (4°C), so the thermal behaviour during the following heating may proceed in many different ways.

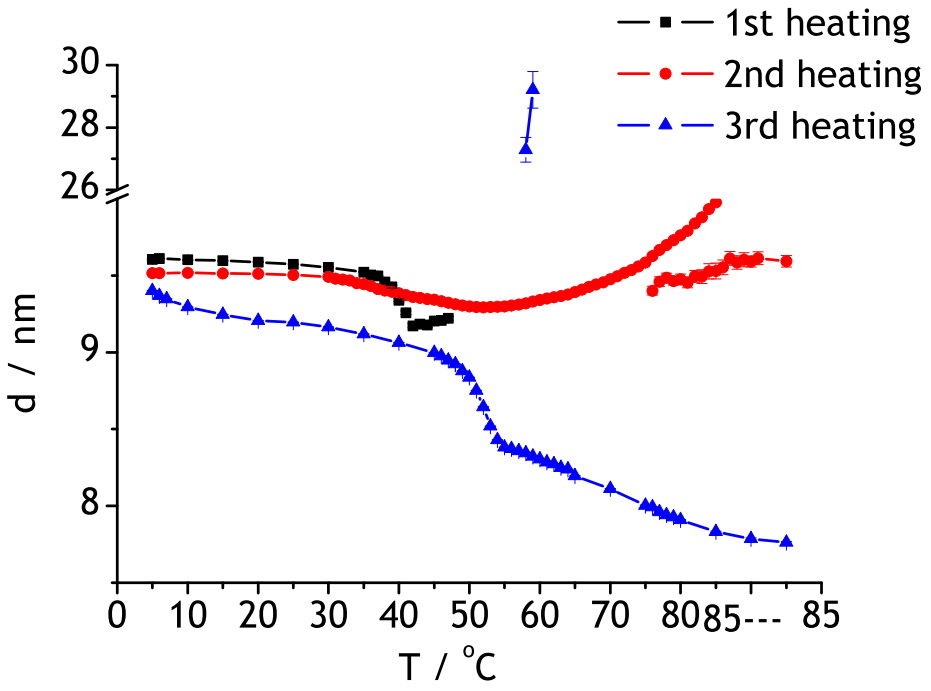

Figure 3.61: Lattice parameters of lamellar phases in LPS Ra with melittin at L/P = 5 for three different measurements.

3.6.3 Lipid A and melittin

A broad diffuse peak was observed in the scattering patterns of pure lipid A (for structure see Fig. 2.4 in Chapter 2). It is the contour peak of four

diffraction peaks characteristic of a cubic phase with the lattice parameter 11.14 nm at 5°C. According to the position of the reflections, the cubic phase could be either Pn3m or Im3m, in accordance with the former findings for lipid A [68]. Another peak positioned at ∼0.05 nm^{-1} could be the first-order peak of a lamellar phase with a bilayer spacing of 21.57 nm at 5°C (Fig. 3.62). The distance between the lipid chains in the gel phase is the same as for the LPS Re samples. In the fluid state of lipid A (above 50°C), the peaks characteristic of the cubic phase lose some intensity and the lamellar phase disappears. The addition of melittin at L/P = 50 improves the long-range organization of the cubic phase, giving rise to more discernible peaks, but without changing the dimensions significantly (curve b in Fig. 3.62). The arrangement of the lipid chains in the gel phase does not change, nor the temperature of the chain melting transition. An inverted hexagonal phase develops at 69°C with a periodicity of 6.91 nm. The (10) and (11) peaks can be seen in Fig. 3.64, curve b. A considerable amount of diffuse scattering is observed, probably resulting from the residual cubic phase. At L/P = 4, the cubic phase in the gel state is replaced by a lamellar phase, with a spacing of d = 5.46 nm at 5°C (the highest peak in Fig. 3.62, curve c). The other two diffuse peaks in Fig. 3.62 could belong to a swollen lamellar phase with a bilayer spacing of 8.50 nm at 5°C. The gel to liquid crystalline transition is at 54°C. At 57°C, a H_{II} phase develops with a periodicity of 7.46 nm (Fig. 3.63 and 3.64, curve c). The dimensions and the thermal behaviour of the hexagonal phases at L/P ratios 50 and 4 are practically the same. The difference in the lattice parameters is about 0.1 nm. When the melittin content is increased to L/P = 2, only the swollen lamellar phase is present at 5°C (Fig. 3.62, curve d). This phase persists till 29°C, above which only one diffuse peak is observed (Fig. 3.63 and 3.64, curve d). This peak arises from another lamellar phase, because its position matches the position of a gel peak seen in the sample with L/P = 4. An overview of all structures induced by melittin in lipid A membranes during the heating from 5 to 85°C is given in Fig. 3.65.

It is interesting that melittin changes the organization of LPS molecules by inducing a variety of phases, without affecting the chain spacing significantly, or only after long storage times. Melittin interacts primarily with the head groups and influences in this way the ratio of the cross sections of the head group and the chains, a parameter that determines into which phase the molecules will arrange. The energy landscape of the LPS-melittin mixtures seems to be very flat, so the path to be adopted depends on small details

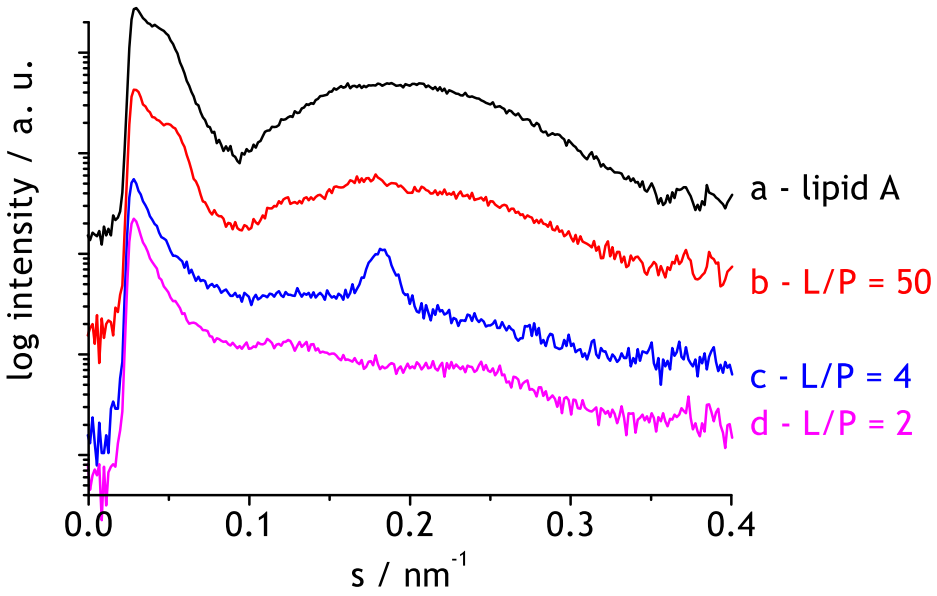

Figure 3.62: Lipid A and melittin at 5°C. a - lipid A; bcd - lipid A with melittin at L/P = 50, 4, 2.

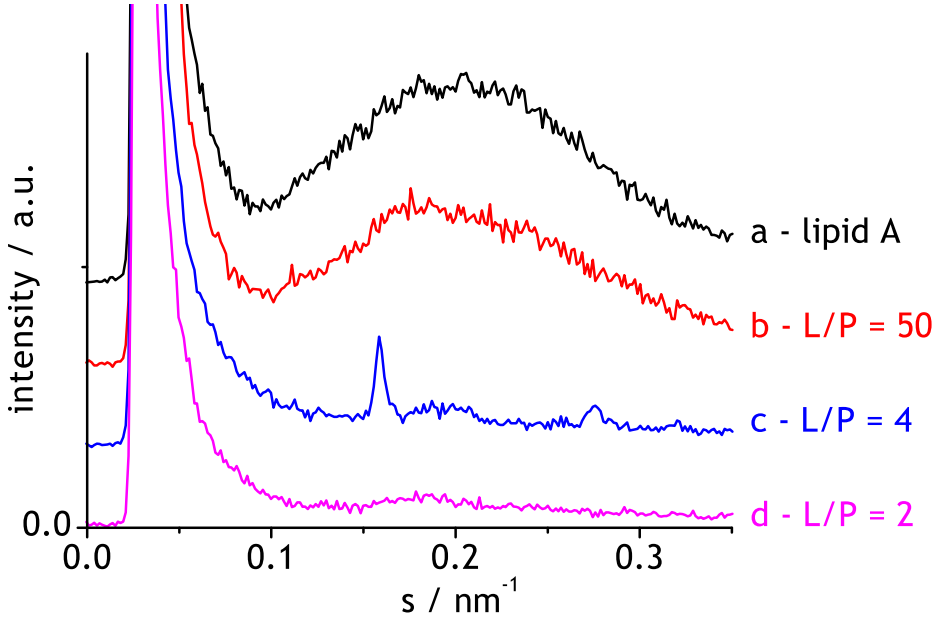

Figure 3.63: Lipid A with melittin at 65°C. a - lipid A; bcd - lipid A with melittin at L/P = 50, 4, 2.

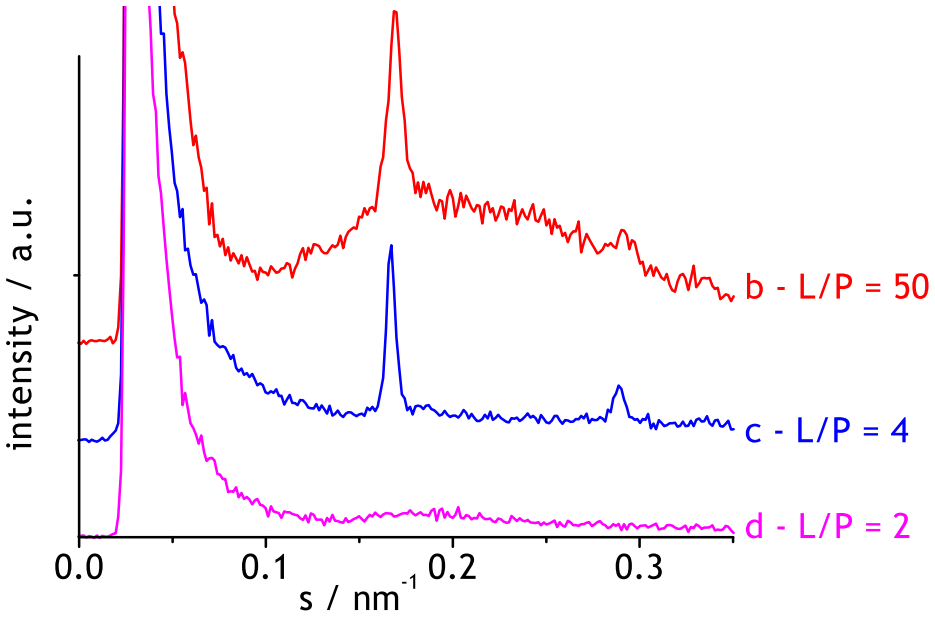

Figure 3.64: Lipid A with melittin at 80°C. bcd - lipid A with melittin at L/P = 50, 4, 2.

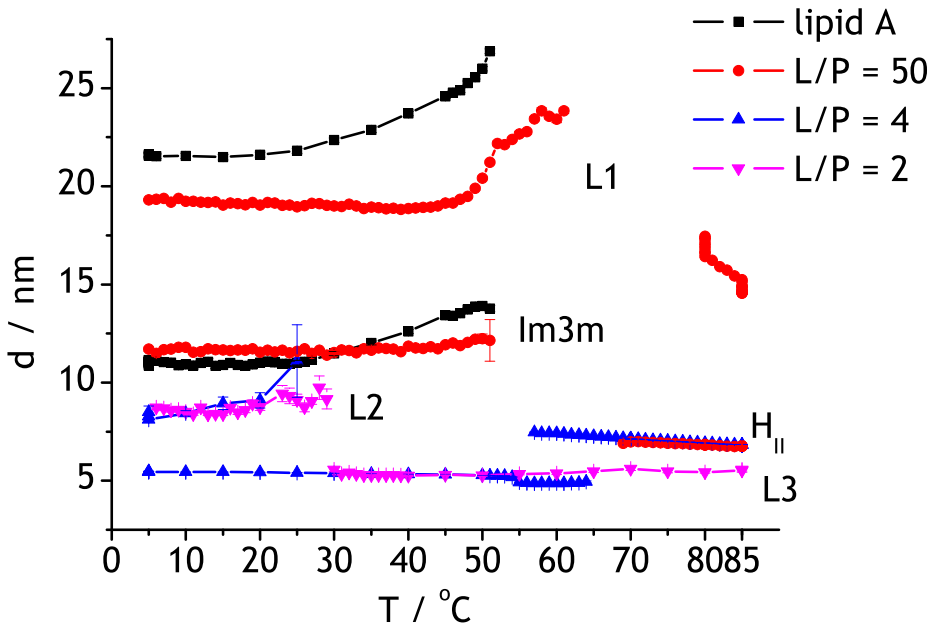

Figure 3.65: All phases that melittin induces in lipid A. L1, L2, L3 - different lamellar phases.

in the history of the sample, like storage times and temperatures or the procedure used for sample equilibration. This explains why the same sample can exhibit a variety of arrangements.

Chapter 4

Summary, conclusions and outlook

The goal of this work was to investigate the effects of the antimicrobial peptides alamethicin and melittin on zwitterionic model lipid membranes. Most antimicrobial peptides kill bacterial cells, but do not attack mammalian cells. It was proposed that the basis of the selectivity is in the different lipid composition of the cell membranes with the most important difference being the membrane charge [1]. Mammalian membranes are made up of mostly zwitterionic lipids while bacterial membranes contain a large amount of charged lipids which are supposed to facilitate the interaction with the cationic antibacterial peptides. Therefore, most studies were done on membranes composed of negatively charged lipids (typically phosphatidylglycerols) versus zwitterionic membranes (typically phosphatidylcholines). However, cell membranes contain a wide variety of lipids with different physical properties and phase behaviour.

The model membranes in this study were prepared from two zwitterionic lipids: POPC, abundant in mammalian cell membranes, or POPE, abundant in bacterial cell membranes. Both lipids have the same chain composition and differ in the headgroup. This structural difference determines their thermotropic phase behaviour with POPC forming lamellar phases and POPE lamellar phases at low and hexagonal phases at high temperatures. Another set of model membranes was prepared from specific bacterial lipids, lipopolysaccharides isolated from the bacterium *S. minnesota*.

The structures of the mixed lipid-peptide membranes were determined by X-ray diffraction during heating and cooling from 5 to 85°C and partial phase

diagrams were constructed.
The structure of lipid membranes is determined by the balance between the curvature elastic energy of the lipid monolayers and the packing properties of the lipids constituting it, given by the geometry of the molecules [6]. Addition of other molecules may affect either of these quantities. For instance, addition of hydrophobic molecules promotes hexagonal phases because they are able to relieve the packing stress of this phase by filling the hydrophobic interstices between the cylinders. With X-ray diffraction experiments on powder samples, it is possible to identify the structure of the lipid phases, but not the position of the peptides in the membrane, unless they form ordered arrays. Nonetheless, we can infer the position of the peptides in the membrane from the phase changes they induce in the given lipid.
The molecules of POPC have similar cross sections of the headgroup and the chains, so their preferred packing is in planar bilayers. Insertion of either alamethicin or melittin did not destroy the lamellar organization of POPC, although the quality of the packing decreased. Both peptides are amphipathic, so they are likely to insert into the polar-apolar interface of the bilayer, between the lipid headgroups. This increases the mean headgroup cross section compared to the mean chain cross section and consequently increases the curvature elastic energy. The mixed lipid-peptide bilayer could decrease the curvature elastic energy by curving towards the chains (positive curvature), for instance by forming micelles. It seems though that the curvature stress is not high enough to overcome the packing constraints and the lamellar structure is preserved with part of the curvature stress being relieved through bilayer undulations (Fig. 3.12). The undulations cause an increase in the lamellar lattice parameter.
The molecules of POPE have a smaller headgroup cross section than chain cross section. When molecules of POPE arrange into planar bilayers, the curvature elastic stress is higher than in the case of POPC. As the temperature increases, the difference in the cross sections increases and so does the curvature stress until the lamellar structure turns into a highly negatively curved inverted hexagonal phase. Mixed lipid-peptide membranes form cubic phases whose curvature is negative, but less than that of the hexagonal phase (Fig. 2.8 and 2.9). The peptides inserted between the headgroups decreased the difference between the mean headgroup and chain cross section and consequently the curvature stress. Melittin-induced cubic phases usually formed during heating at the lamellar to hexagonal phase transition and on cooling persisted till the onset of the gel phase. The lattice parameters

were very similar through a wide range of lipid to peptide ratios (Fig. 3.23). The onset temperature and type of the cubic phases induced by alamethicin depended on the peptide concentration. The phase diagrams of mixed POPE-alamethicin membranes are presented in Fig. 3.52 and 3.53. The dimensions and thermal behaviour of the phases in the mixed lipid-peptide membranes mutually influenced each other and a number of epitaxial relationships were observed. Such interdependence could be explained by confinement in an onion vesicle with layers formed by different lipid phases [64].
The interaction of melittin with specific bacterial lipids, the lipopolysaccharides from *S. minnesota*, was also investigated. Lipopolysaccharides form the outer layer of the outer cell membranes of Gram negative bacteria. Antimicrobial peptides need to cross this outer membrane, because cell death is caused by damage of the inner cytoplasmic membrane. Melittin can cross the LPS membranes and form a complex with released LPS, which is a prerequisite for its bactericidal activity and subsequent prevention of the toxic shock by the neutralization of the released LPS. It was not possible to construct a full phase diagram because of the irreproducibility of the measurements. More systematic and repeated measurements are necessary to achieve this goal. An overview of phases induced by melittin in the lipopolysaccharide lipid A is given in Fig. 3.65.
X-ray diffraction measurements allow to identify the structure of lipid membranes. More insight into the peptide-lipid interaction could be gained by investigation of the dynamics of the interaction by infrared spectroscopy. The changes in the spectra of the interacting species highlight the functional groups involved in the interaction. These measurements could also help to confirm the position of the peptide in the membranes, which we could only deduce from the induced lipid phases. Especially, the technique of 2D infrared spectroscopy might be very useful to follow the dynamics of the peptides.
The scattering patterns of the cubic phases have enough reflections (about 10) for the reconstruction of the electron density profiles of the membranes. The profiles could help to explain the epitaxial relationships between the lipid phases and to see how the changes in the cubic lattice parameters can be attributed to changes in the membrane thickness and the water channel diameter.

Appendix A

List of abbreviations

ATR FTIR spectroscopy - attenuated total reflection Fourier transform infrared spectroscopy
ATR IR spectroscopy - attenuated total reflection infrared spectroscopy
bc phases - bicontinuous cubic phases
DEPE - 1,2-Dielaidoyl-sn-Glycero-3-Phosphoethanolamine (structure like DOPE, but with a delta 9-*trans* double bond instead of delta 9-*cis*)
DLPC - 1,2-Dilauroyl-sn-Glycero-3-Phosphocholine
DMPC - 1,2-Dimyristoyl-sn-Glycero-3-Phosphocholine
DMPG - 1,2-Dimyristoyl-sn-Glycero-3-[Phospho-rac-(1-glycerol)] (Sodium Salt)
DOPC - 1,2-Dioleoyl-sn-Glycero-3-Phosphocholine
DOPE - 1,2-Dioleoyl-sn-Glycero-3-Phosphoethanolamine
DPhPC - 1,2-Diphytanoyl-sn-Glycero-3-Phosphocholine
DPhPE - 1,2-Diphytanoyl-sn-Glycero-3-Phosphoethanolamine
DPPC - 1,2-Dipalmitoyl-sn-Glycero-3-Phosphocholine
DPPG - 1,2-Dipalmitoyl-sn-Glycero-3-[Phospho-rac-(1-glycerol)] (Sodium Salt)
DTPC - 1,2-Di-O-Tetradecyl-sn-Glycero-3-Phosphocholine
DTPG - 1,2-Di-O-Tetradecyl-sn-Glycero-3-[Phospho-rac-(1-glycerol)] (Sodium Salt) (like DTPC, but with a glycerol headgroup)
ESR - electron spin resonance
EYPC - L-α-Phosphatidylcholine from egg yolk (mixture of PC with different chains: 16:0 - 34%, 16:1 - 2%, 18:0 - 11%, 18:1 - 32%, 18:2 - 18%, 20:4 - 3%)
FRET - Förster resonance energy transfer
IR - infrared
IRRAS - infrared reflection-absorption spectroscopy

L/P - lipid to peptide ratio
LPS - lipopolysaccharide
LUV - large unilamellar vesicles
OCD - oriented circular dichroism
OPPC - 1-Oleoyl-2-Palmitoyl-sn-Glycero-3-Phosphocholine
PC - phosphatidylcholine
PE - phosphatidyletanolamine
PG - phosphatidylglycerol
POPC - 1-Palmitoyl-2-Oleoyl-sn-Glycero-3-Phosphocholine
POPE - 1-Palmitoyl-2-Oleoyl-sn-Glycero-3-Phosphoethanolamine
POPG - 1-Palmitoyl-2-Oleoyl-sn-Glycero-3-[Phospho-rac-(1-glycerol)] (Sodium Salt)
REES spectroscopy - red-edge excitation shift spectroscopy
SAXS - small-angle X-ray scattering
WAXS - wide-angle X-ray scattering

Appendix B

Chemical structures of lipids.

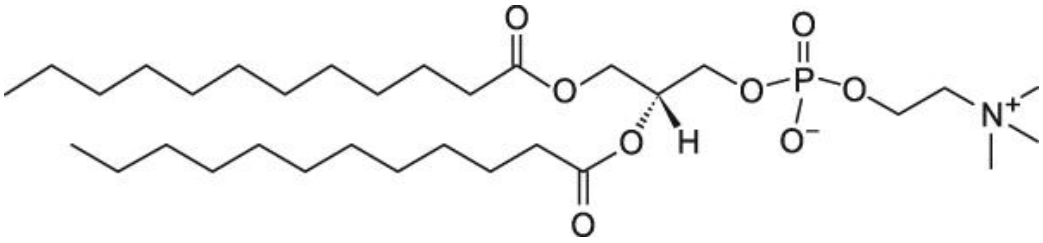

Figure B.1: DLPC - 1,2-Dilauroyl-sn-Glycero-3-Phosphocholine

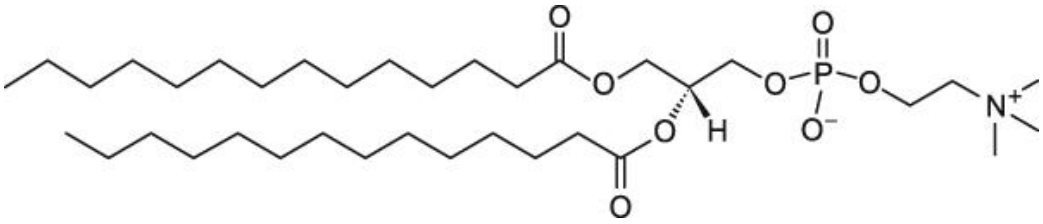

Figure B.2: DMPC - 1,2-Dimyristoyl-sn-Glycero-3-Phosphocholine

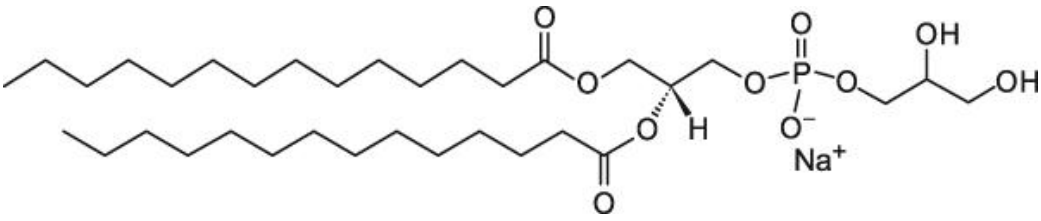

Figure B.3: DMPG - 1,2-Dimyristoyl-sn-Glycero-3-[Phospho-rac-(1-glycerol)] (Sodium Salt)

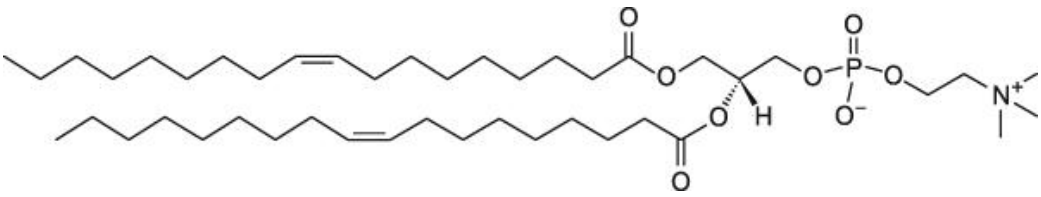

Figure B.4: DOPC - 1,2-Dioleoyl-sn-Glycero-3-Phosphocholine

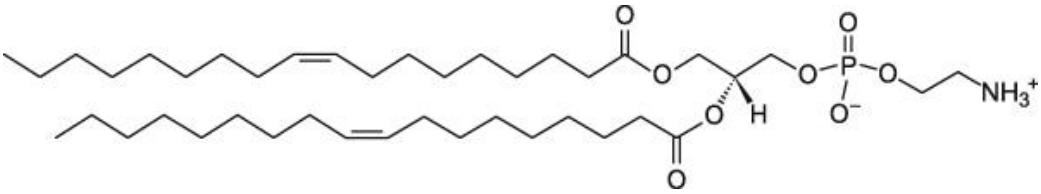

Figure B.5: DOPE - 1,2-Dioleoyl-sn-Glycero-3-Phosphoethanolamine

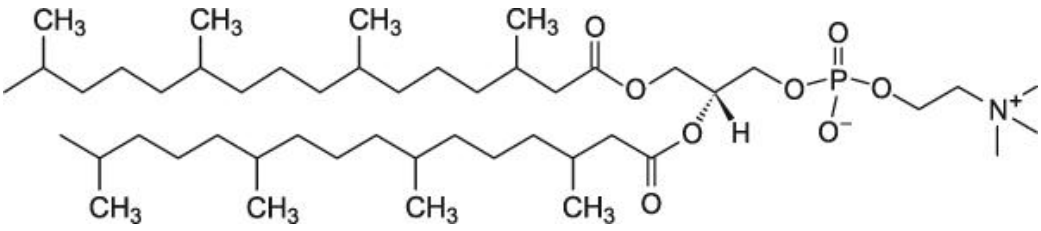

Figure B.6: DPhPC - 1,2-Diphytanoyl-sn-Glycero-3-Phosphocholine

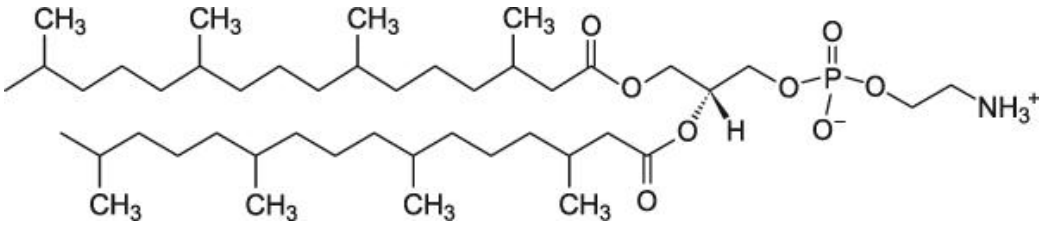

Figure B.7: DPhPE - 1,2-Diphytanoyl-sn-Glycero-3-Phosphoethanolamine

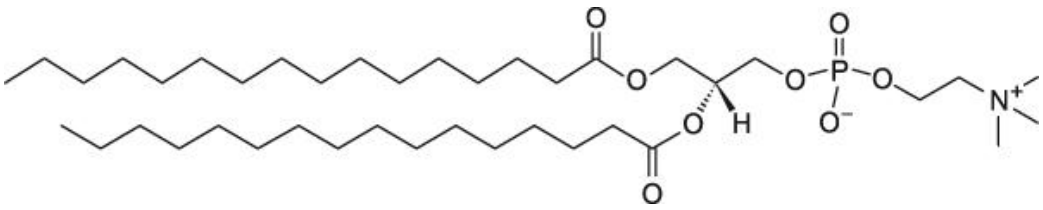

Figure B.8: DPPC - 1,2-Dipalmitoyl-sn-Glycero-3-Phosphocholine

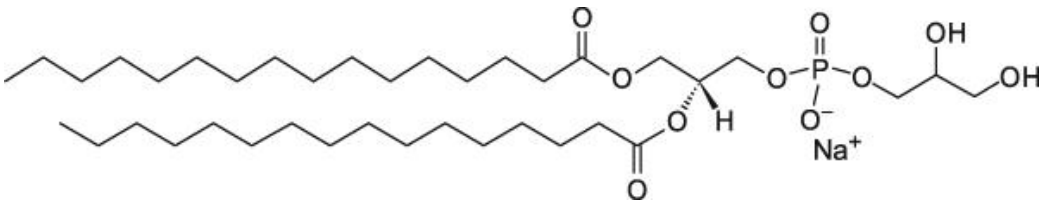

Figure B.9: DPPG - 1,2-Dipalmitoyl-sn-Glycero-3-[Phospho-rac-(1-glycerol)] (Sodium Salt)

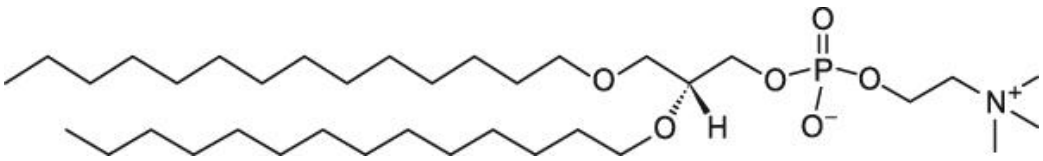

Figure B.10: DTPC - 1,2-Di-O-Tetradecyl-sn-Glycero-3-Phosphocholine

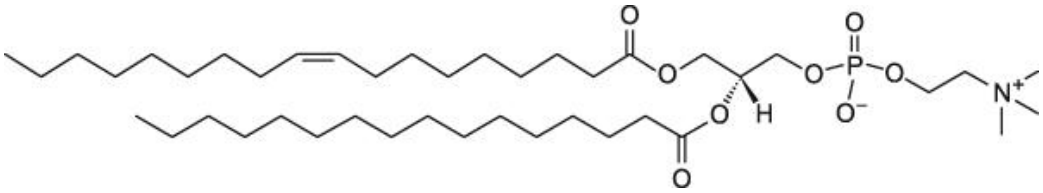

Figure B.11: OPPC - 1-Oleoyl-2-Palmitoyl-sn-Glycero-3-Phosphocholine

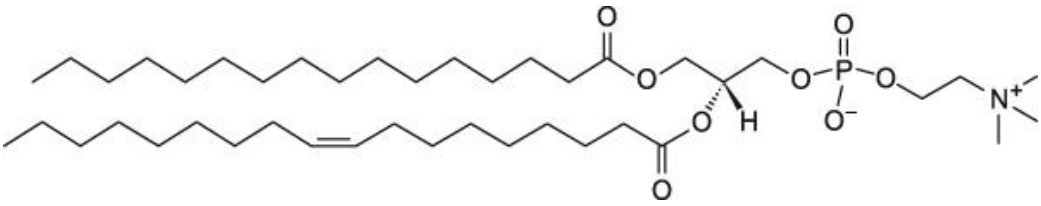

Figure B.12: POPC - 1-Palmitoyl-2-Oleoyl-sn-Glycero-3-Phosphocholine

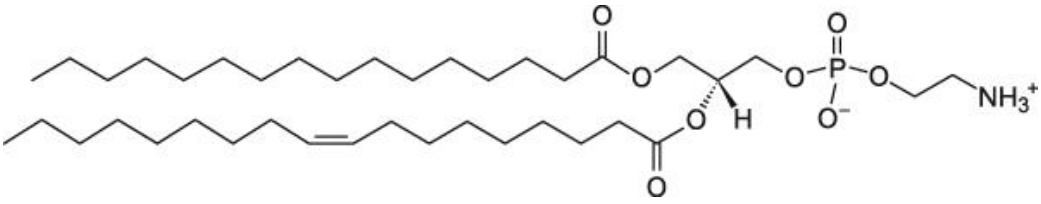

Figure B.13: POPE - 1-Palmitoyl-2-Oleoyl-sn-Glycero-3-Phosphoethanolamine

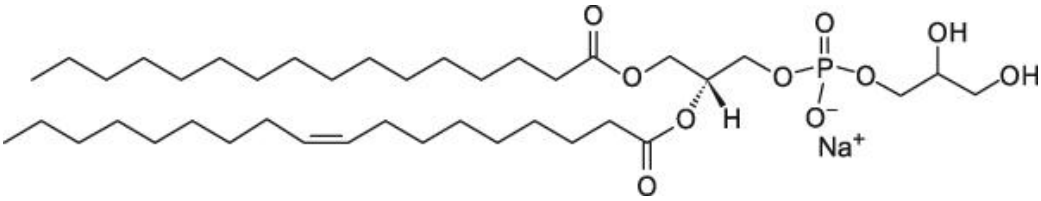

Figure B.14: POPG - 1-Palmitoyl-2-Oleoyl-sn-Glycero-3-[Phospho-rac-(1-glycerol)] (Sodium Salt)

Bibliography

[1] G. Saberwal, R. Nagaraj: *Cell-lytic and antibacterial peptides that act by perturbing the barrier function of membranes: facets of their conformational features, structure-function correlations and membrane-perturbing abilities.* Biochim. Biophys. Acta. **1031**(2), 109 (1994)
Erratum in: Biochim. Biophys. Acta. **1235**(1), 159 (1995).

[2] C.E. Dempsey: *The actions of melittin on membranes.* Biochim. Biophys. Acta. **1031**(2), 143 (1990).

[3] H. Nikaido: *Molecular basis of bacterial outer membrane permeability revisited.* Mol. Biol. Rev. **67**(4), 593 (2003).

[4] J. Andrä, M.H. Koch, R. Bartels, K. Brandenburg: *Biophysical characterization of endotoxin inactivation by NK-2, an antimicrobial peptide derived from mammalian NK-lysin.* Antimicrob. Agents Chemother. **48**(5), 1593 (2004).

[5] J.M. Seddon, R.H. Templer: Polymorphism of Lipid-Water Systems. In: *Handbook of Biological Physics*, (Hoff, A. J., series ed.), Vol. 1, *Structure and Dynamics of Membranes* (R. Lipowsky, E. Sackmann, eds.), Elsevier SPC, Amsterdam, (1995).

[6] J.M. Seddon: *Structure of the inverted hexagonal (HII) phase, and non-lamellar phase transitions of lipids.* Biochim. Biophys. Acta. **1031**(1), 1 (1990).

[7] G. Cevc, D. Marsh: *Phospholipid bilayers: Physical principles and models.* John Wiley & Sons, New York, (1987).

[8] J.F. Sadoc, J. Charvolin: *Infinite periodic minimal surfaces and their crystallography in the hyperbolic plane.* Acta Crystallogr. A. **45**, 10 (1989).

[9] N. Sitaram, R. Nagaraj: *Interaction of antimicrobial peptides with biological and model membranes: structural and charge requirements for activity.* Biochim. Biophys. Acta. **1462**, 29 (1993).

[10] E. Habermann, J. Jentsch: *Sequence analysis of melittin from tryptic and peptic degradation products.* Hoppe Seylers Z. Physiol. Chem. **348**(1), 37 (1967).

[11] T.C. Terwilliger, D. Eisenberg: *The structure of melittin. I. Structure determination and partial refinement.* J. Biol. Chem. **257**(11), 6010 (1982).

[12] T.C. Terwilliger, D. Eisenberg: *The structure of melittin. II. Interpretation of the structure.* J. Biol. Chem. **257**(11), 6016 (1982).

[13] J.L. Moreland, A. Gramada, O.V. Buzko, Q. Zhang and P.E. Bourne: *The Molecular Biology Toolkit (mbt): A Modular Platform for Developing Molecular Visualization Applications.* BMBC Bioinformatics. **6**, (2005).

[14] Y.H. Lam, S.R. Wassall, C.J. Morton, R. Smith, F. Separovic: *Solid-state NMR structure determination of melittin in a lipid environment.* Biophys. J. **81**(5), 2752 (2001).

[15] D. Allende, A. Vidal, S.A. Simon, T.J. McIntosh: *Bilayer interfacial properties modulate the binding of amphipathic peptides.* Chem. Phys. Lipids. **122**, 65 (2003).

[16] N. Asthana, S.P. Yadav, J.K. Ghosh: *Dissection of antibacterial and toxic activity of melittin: a leucine zipper motif plays a crucial role in determining its hemolytic activity but not antibacterial activity.* J. Biol. Chem. **279**(53), 55042 (2003).

[17] I. Constantinescu, M. Lafleur: *Influence of the lipid composition on the kinetics of concerted insertion and folding of melittin in bilayers.* Biochim. Biophys. Acta. **1667**, 26 (2004).

[18] H. Raghuraman, A. Chattopadhyay: *Effect of micellar charge on the conformation and dynamics of melittin.* Eur. Biophys. J. **33**, 611 (2004).

[19] T. Pott, M. Paternostre, E.J. Dufourc: *A comparative study of the action of melittin on sphingomyelin and phosphatidylcholine bilayers.* Eur. Biophys. J. **27**, 237 (1998).

[20] S. Frey, L.K. Tamm: *Orientation of melittin in phospholipid bilayers. A polarized attenuated total reflection infrared study.* Biophys. J. **60**(4), 922 (1991).

[21] T. Wieprecht, M. Beyermann, J. Seelig: *Thermodynamics of the coil-a-helix transition of amphipathic peptides in a membrane environment: the role of vesicle curvature.* Biophys. Chem. **96**, 191 (2002).

[22] J.H. Kleinschmidt, J.E. Mahaney, D.D. Thomas, D. Marsh: *Interaction of bee venom melittin with zwitterionic and negatively charged phospholipid bilayers: a spin-label electron spin resonance study.* Biophys. J. **72**, 737 (1997).

[23] C.R. Flach, F.G. Prendergast, R. Mendelsohn: *Infrared reflection-absorption of melittin interaction with phospholipid monolayers at the air/water interface.* Biophys. J. **70**, 531 (1996).

[24] J.P. Bradshaw, C.E. Dempsey, A. Watts: *A combined X-ray and neutron diffraction study of selectively deuterated melittin in phospholipid bilayers: effect of pH.* Mol. Membr. Biol. **11**, 79 (1994).

[25] F.Y. Chen, M.T. Lee, H.W. Huang: *Evidence for membrane thinning effect as the mechanism for peptide-induced pore formation.* Biophys. J. **84**, 3751 (2003).

[26] F. Lavialle, R.G. Adams, I.W. Levin: *Infrared spectroscopic study of the secondary structure of melittin in water, 2-chloroethanol, and phospholipid bilayer dispersions.* Biochemistry. **21**(10), 2305 (1982).

[27] R. Maget-Dana: *The monolayer technique: a potent tool for studying the interfacial properties of antimicrobial and membrane-lytic peptides and their interactions with lipid membranes.* Biochim. Biophys Acta. **1462**, 109 (1999).

[28] L. Yang, T.A. Harroun, T.M. Weiss, L. Ding, H.W. Huang: *Barrel-stave model or toroidal model? A case study on melittin pores.* Biophys. J. **81**, 1475 (2001).

[29] A.S. Ladokhin, S.H. White: *'Detergent-like' permeabilization of anionic lipid vesicles by melittin.* Biochim. Biophys. Acta. **1514**(2), 253 (2001).

[30] H. Raghuraman, A. Chattopadhyay: *Influence of lipid chain unsaturation on membrane-bound melittin: a fluorescence approach.* Biochim. Biophys. Acta. **1665**, 29 (2004).

[31] I. Cornut, B. Desbat, J.M. Turlet, J. Dufourcq: *In situ study by polarization modulated Fourier transform infrared spectroscopy of the structure and orientation of lipids and amphipathic peptides at the air-water interface.* Biophys. J. **70**, 305 (1996).

[32] A.M. Batenburg, B. de Kruijff: *Modulation of membrane surface curvature by peptide-lipid interactions.* Biosci. Rep. **8**(4), 299 (1988).

[33] P. Verma, D.F.H. Wallach, I.C.P. Smith: *The action of melittin on phosphatide multibilayers as studied by infrared dichroism and spin labeling. A model approach to lipid-protein interactions.* Biochim. Biophys. Acta. **345**, 129 (1974).

[34] W.S. Chelack, A. Petkau: *Distribution of alamethicin in lipid membranes and water.* J. Lipid Res. **14**, 255 (1973).

[35] B. Bechinger: *Structure and functions of channel-forming peptides: magainins, cecropins, melittin and alamethicin.* J. Membr. Biol. **156**, 197 (1997).

[36] F.Y. Chen, M.T. Lee, H.W. Huang: *Sigmoidal concentration dependence of antimicrobial peptide activities: a case study on alamethicin.* Biophys. J. **82**(2), 908 (2002).

[37] Y. Wu, K. He, S.J. Ludtke, H.W. Huang: *X-ray diffraction study of lipid bilayer membranes interacting with amphiphilic helical peptides: diphytanoyl phosphatidylcholine with alamethicin at low concentrations.* Biophys. J. **68**(6), 2361 (1995).

[38] U.P. Fringeli, M. Fringeli: *Pore formation in lipid membranes by alamethicin.* Proc. Natl. Acad. Sci. U S A. **76**(8), 3852 (1979).

[39] K. He, S.J. Ludtke, D.L. Worcester, H.W. Huang: *Neutron scattering in the plane of membranes: structure of alamethicin pores.* Biophys. J. **70**(6), 2659 (1996).

[40] S. Stankowski, G. Schwarz: *Lipid dependence of peptide-membrane interactions. Bilayer affinity and aggregation of the peptide alamethicin.* FEBS Lett. **250**(2), 556 (1989).

[41] S.L. Keller, S.M. Bezrukov, S.M. Gruner, M.W. Tate, I. Vodyanoy, V.A. Parsegian: *Probability of alamethicin conductance states varies with nonlamellar tendency of bilayer phospholipids.* Biophys. J. **65**(1), 23 (1993).

[42] S.L. Keller, S.M. Gruner, K. Gawrisch: *Small concentrations of alamethicin induce a cubic phase in bulk phosphatidylethanolamine mixtures.* Biochim. Biophys. Acta. **1278**(2), 241 (1996).

[43] S.J. Archer, J.F. Ellena, D.S. Cafiso: *Dynamics and aggregation of the peptide ion channel alamethicin. Measurements using spin-labeled peptides.* Biophys. J. **60**(2), 389 (1991).

[44] I. Vodyanoy, J.E. Hall, V. Vodyanoy: *Alamethicin adsorption to a planar lipid bilayer.* Biophys. J. **53**(5), 649 (1988).

[45] W.T. Heller, K. He, S.J. Ludtke, T.A. Harroun, H.W. Huang: *Effect of changing the size of lipid headgroup on peptide insertion into membranes.* Biophys. J. **73**(1), 239 (1997).

[46] R. Ionov, A. El-Abed, A. Angelova, M. Goldmann, P. Peretti: *Asymmetrical ion-channel model inferred from two-dimensional crystallization of a peptide antibiotic.* Biophys. J. **78**(6), 3026 (1997).

[47] V. Vitkova, P. Meleard, T. Pott, I. Bivas: *Asymmetrical ion-channel model inferred from two-dimensional crystallization of a peptide antibiotic.* Eur. Biophys. J. **35**(3), 281 (2006).

[48] M. Bak, R.P. Bywater, M. Hohwy, J.K. Thomsen, K. Adelhorst, H.J. Jakobsen, O.W. Sørensen, N.C. Nielsen: *Conformation of alamethicin in oriented phospholipid bilayers determined by ^{15}N solid-state nuclear magnetic resonance.* Biophys. J. **81**(3), 1684 (2001).

[49] A. Spaar, C. Munster, T. Salditt: *Conformation of peptides in lipid membranes studied by x-ray grazing incidence scattering.* Biophys. J. **87**(1), 396 (2004).

[50] E. Storm, H.I. Israel: *Photon cross sections from 1 keV to 100 MeV for elements Z = 1 to 100.* Nuclear Data Tables A7, 565 (1970).

[51] Y.K. Levine: *X-ray diffraction studies of membranes.* Progr. Surf. Membr. Sci. **3**, 279 (1973).

[52] J.F. Nagle, S. Tristram-Nagle: *Structure of lipid bilayers.* Biochim. Biophys. Acta. **1469**(3), 159 (2000).

[53] G. Pabst, M. Rappolt, H. Amenitsch, P. Laggner: *Structural information from multilamellar liposomes at full hydration: full q-range fitting with high quality x-ray data.* Phys. Rev. E. **62**, 4000 (2000).

[54] N. Kučerka, Y. Liu, N. Chu, H.I. Petrache, S. Tristram-Nagle, J.F. Nagle: *Structure of fully hydrated fluid phase DMPC and DLPC lipid bilayers using X-ray scattering from oriented multilamellar arrays and from unilamellar vesicles.* Biophys. J. **88**(4), 2626 (2005).

[55] R.C. Pandey, J.C. Cook, K.L. Rinehart: *High resolution and field desorption mass spectrometry studies and revised structure of alamethicin I and II.* J. Am. Chem. Soc. **99**, 9469 (1977).

[56] A.V. Botelho, T. Huber, T.P. Sakmar, M.F. Brown: *Curvature and hydrophobic forces drive oligomerization and modulate activity of rhodopsin in membranes.* Biophys. J. **91**(12), 4464 (2006).

[57] C.D. Stubbs, S.J. Slater: *The effects of non-lamellar forming lipids on membrane protein-lipid interactions.* Chem. Phys. Lipids. **81**(2), 185 (1996).

[58] A. Angelova, R. Ionov, M.H. Koch, G. Rapp: *Interaction of the peptide antibiotic alamethicin with bilayer- and non-bilayer-forming lipids: influence of increasing alamethicin concentration on the lipids supramolecular structures.* Arch. Biochem. Biophys. **378**(1), 93 (2000).

[59] N. Kučerka, S. Tristram-Nagle, J.F. Nagle: *Structure of fully hydrated fluid phase lipid bilayers with monounsaturated chains.* J. Membr. Biol. **208**(3), 193 (2005).

[60] G. Pabst, S. Danner, R. Podgornik, J. Katsaras: *Entropy-driven softening of fluid lipid bilayers by alamethicin.* Langmuir. **23**, 11705 (2007).

[61] N. Kučerka, S. Tristram-Nagle, J.F. Nagle: *Structure of fully hydrated fluid phase lipid bilayers with monounsaturated chains.* J. Membr. Biol. **208**(3), 193 (2005).

[62] C. Li, T. Salditt: *Structure of Magainin and Alamethicin in Model Membranes Studied by X-Ray Reflectivity.* Biophys. J. **91**, 3285 (2006).

[63] A.M. Squires, R.H. Templer, J.M. Seddon, J. Woenkhaus, R. Winter, T. Narayanan, S. Finet: *Kinetics and mechanism of the interconversion of inverse bicontinuous cubic mesophases.* Phys. Rev. E. **72**(1), 011502 (2005).

[64] C.E. Conn, O. Ces, X. Mulet, S. Finet, R. Winter, J.M. Seddon, R.H. Templer: *Dynamics of Structural Transformations between Lamellar and Inverse Bicontinuous Cubic Lyotropic Phases.* Phys. Rev. Lett. **96**, 108102 (2006).

[65] M. Clerc, A.M. Levelut, J.F. Sadoc: *Transitions between mesophases involving cubic phases in the surfactant-water systems. Epitaxial relations and their consequences in a geometrical framework.* J. Phys. II. **1**, 1263 (1991).

[66] P. Mariani, L.Q. Amaral, L. Saturni, H. Delacroix: *Hexagonal-cubic phase transitions in lipid containing systems: epitaxial relationships and cylinder growth.* J. Phys. II. **4**, 1393 (1994).

[67] S.M. Gruner: *Intrinsic curvature hypothesis for biomembrane lipid composition: a role for nonbilayer lipids.* Proc. Natl. Acad. Sci. U S A. **82**(11), 3665, (1985).

[68] K. Brandenburg, W. Richter, M.H. Koch, H.W. Meyer, U. Seydel: *Characterization of the nonlamellar cubic and HII structures of lipid A from Salmonella enterica serovar Minnesota by X-ray diffraction and freeze-fracture electron microscopy.* Chem. Phys. Lipids. **91**(1), 53 (1998).

[69] A. Bhunia, P.N. Domadia, S. Bhattacharjya: *Structural and thermodynamic analyses of the interaction between melittin and lipopolysaccharide.* BiochimḂiophys. Acta. **1768**(12), 3282 (2007).

[70] S. Toraya, T. Nagao, K. Norisada, S. Tuzi, H. Saitô, S. Izumi, A. Naito: *Morphological behavior of lipid bilayers induced by melittin near the phase transition temperature.* Biophys. J. **89**(5), 3214 (2005).

[71] A.M. Batenburg, J.H. van Esch, B. de Kruijff: *Melittin-induced changes of the macroscopic structure of phosphatidylethanolamines.* Biochemistry. **27**(7), 2324 (1988).

Acknowledgement

I would like to thank all those who made possible the completion of this thesis:

- Hasylab for giving me the opportunity for the PhD. study and Hasylab coworkers for a good working atmosphere

- my supervisor Sérgio Funari for guiding me through the study and many helpful discussions

- professors Edgar Weckert, Robert L. Johnson and Klaus Brandenburg for supervising the dissertation and disputation

- Klaus Brandenburg, Jörg Howe and Gerald von Busse from FZ Borstel for help with infrared measurements, providing of melittin and LPS and useful discussions

- Michael Rappolt for enlightening about cubic phases

- Chandrashehkar Kulkarni for telling me about onion vesicles

- Alke, Bernd and Wolfgang for invaluable help with Zusammenfassung

- and, in particular, my friends, my family and Manolo for all kinds of support during the PhD. years.